

Mechanisms of *Shigella flexneri* dissemination through  
double membrane vacuole escape

Erin Allison Weddle,  
Bunker Hill, WV

Master of Science in Biological and Physical Sciences, University of Virginia, 2018

Bachelor of Science in Biology, Shenandoah University, 2016

A Dissertation presented to the Graduate Faculty of the University of Virginia in  
Candidacy for the Degree of  
Doctor of Philosophy of Science in

Microbiology, Immunology, and Cancer Biology

University of Virginia  
May 2022

## Abstract

*Shigella flexneri* is an important human pathogen that causes the severe diarrheal disease, bacillary dysentery and accounts for 270 million and nearly 200,000 deaths per year. *S. flexneri* invades colonic epithelial cells and hijacks the host actin cytoskeleton to move in the cytosol of infected cells and disseminate to neighboring cells through a process called cell-to-cell spread. The bacterial type three-secretion system (T3SS) is required for cell-to-cell spread and escape from double membrane vacuoles (DMVs) in the adjacent cell. Before my thesis work, very little was known about the mechanisms that facilitate DMV escape. My thesis work has uncovered multiple factors, both host and bacterial, that contribute to *S. flexneri* DMV escape. We characterized two T3SS effectors, IcsB (Chapter 2) and IpgB1 (Chapter 3), during cell-to-cell spread. IcsB, via its acyltransferase activity, is required for efficient DMV escape and cell-to-cell spread through an unknown mechanism that does not involve host autophagy, a process that IcsB was proposed to modulate. IpgB1, via its guanine nucleotide exchange factor (GEF) activity, facilitates cell-to-cell spread through its target small GTPase, Rac1, to antagonize RhoA-mediated restriction of DMV escape. We also found a novel host factor, lysophospholipase 2 (LYPLA2) that plays a role in DMV escape (Chapter 4) during cell-to-cell spread. LYPLA2 hydrolyzes long chain fatty acids from membrane lysophospholipids and membrane-

anchored proteins. My work has provided characterization of the first bacterial and host factors required for efficient DMV escape during *S. flexneri* cell-to-cell spread and offers novel insights into the mechanisms of *S. flexneri* pathogenesis.

## **Acknowledgements**

Thank you to Dr. Hervé Agaisse for his mentorship and guidance throughout my doctoral research. I greatly appreciate his patience and dedication to my training and development as an independent scientist, as well as his enthusiasm and optimism for science. Thank you to all the members of the Agaisse and Derré labs, both present and former, for their support, ideas, camaraderie, and delicious baked goods over the years! Special thanks to my wonderful thesis committee, Dr. Amy Bouton, Dr. Isabelle Derré, Dr. Sarah Ewald, Dr. Jim Casanova, and Dr. Hervé Agaisse for the enjoyable discussions and wonderful ideas that helped shape my thesis work.

I would not have been able to succeed in graduate school without the support of my fellow graduate students and lab mates, who have become some of my closest friends. Thank you for all the lunch breaks, coffee breaks, and game nights! I also want to acknowledge my parents, husband, and the rest of my wonderful family who listened to countless hours of science talk and encouraged me along the way. Finally, thank you to my beloved dogs and horses, who have been the best listeners of all.

## Table of Contents

1. CHAPTER 1: INTRODUCTION	1
1.1 INTRODUCTION TO SHIGELLA	1
1.1.1 MODELS FOR STUDYING <i>S. FLEXNERI</i> PATHOGENESIS	2
1.1.2 CELLULAR/MOLECULAR PATHOGENESIS	3
1.1.2.1 INVASION OF COLONIC EPITHELIAL CELLS	4
1.1.2.2 PRIMARY VACUOLE ESCAPE	6
1.1.2.3 ACTIN-BASED MOTILITY	8
1.1.2.4 CELL-TO-CELL SPREAD	9
1.1.2.4.1 PROTRUSION FORMATION	12
1.1.2.4.2 PROTRUSION RESOLUTION/VLP FORMATION	13
1.1.2.4.3 VLP RESOLUTION/DMV FORMATION	14
1.1.2.4.4 DMV ESCAPE	14
1.1.2.5 AVOIDANCE OF AUTOPHAGY DURING INFECTION	18
1.2 DISSERTATION GOALS	19
2. CHAPTER 2: THE ROLE OF THE TYPE THREE SECRETION SYSTEM EFFECTOR ICSB AND LC3-DEPENDENT AUTOPHAGY IN <i>S. FLEXNERI</i> DISSEMINATION	20
2.1 SUMMARY	21
2.2 INTRODUCTION	22
2.3 MATERIALS AND METHODS	25
2.3.1 CELL LINES AND BACTERIAL STRAINS	25
2.3.2 DNA CONSTRUCTS AND TRANSFECTION	25
2.3.3 BACTERIAL INFECTION	26
2.3.4 SIRNA AND WESTERN BLOT	26
2.3.5 SIZE OF INFECTION FOCI	27
2.3.6 LIVE IMAGING	27
2.4 RESULTS	28
2.4.1 ICSB PROMOTES <i>S. FLEXNERI</i> SPREAD FROM CELL TO CELL	28
2.4.2 ICSB PROMOTES CELL-TO-CELL SPREAD THROUGH ESCAPE FROM DMVS	32
2.4.3 THE AUTOPHAGY MARKER LC3 IS EXCLUSIVELY RECRUITED TO DMVS	38
2.4.4 LC3 IS RECRUITED EQUALLY TO THE DMVS CONTAINING WILD TYPE BACTERIA OR THE <i>ICSB</i> MUTANT	45
2.4.5 THE <i>ICSB</i> MUTANT FAILS TO ESCAPE FROM LC3 <sup>+</sup> AS WELL AS LC3 <sup>-</sup> DMVS	46

2.4.6 ICSB PROMOTES PROMPT ESCAPE FROM DMVS	46
2.4.7 LC3 CORRELATES WITH, BUT IS NOT THE CAUSE OF VACUOLE ESCAPE FAILURE	50
2.4.8 LC3-DEPENDENT AUTOPHAGY DOES NOT INHIBIT <i>S. FLEXNERI</i> SPREAD FROM CELL TO CELL	53
2.5 DISCUSSION	57
3. CHAPTER 3: THE TYPE THREE SECRETION SYSTEM EFFECTOR IPGB1 PROMOTES <i>S. FLEXNERI</i> CELL-TO-CELL SPREAD THROUGH DOUBLE MEMBRANE VACUOLE ESCAPE	62
<hr/>	
3.1 SUMMARY	63
3.2 INTRODUCTION	64
3.3 MATERIALS AND METHODS	66
3.3.1 CELL LINES AND BACTERIAL STRAINS	66
3.3.2 DNA CONSTRUCTS AND CELL TRANSFECTION	67
3.3.3 BACTERIAL INFECTION	68
3.3.4 SIRNA TRANSFECTION	68
3.3.5 WESTERN BLOTTING	69
3.3.6 ANTIBODIES	70
3.3.7 IMMUNOFLUORESCENCE	70
3.3.8 SIZE OF INFECTION FOCI	71
3.3.9 LIVE IMAGING	72
3.3.10 <i>IN VIVO S. FLEXNERI</i> INFECTION	73
3.3.11 HISTOLOGY	73
3.3.12 IMMUNOFLUORESCENCE ON COLON SECTIONS	74
3.4 RESULTS	76
3.4.1 IPGB1 IS REQUIRED FOR EFFICIENT INVASION IN HT-29 CELLS	76
3.4.2 IPGB1 IS REQUIRED FOR EFFICIENT DISSEMINATION IN HT-29 CELLS	80
3.4.3 IPGB1 IS REQUIRED FOR PROMPT AND EFFICIENT DMV ESCAPE	82
3.4.4 THE <i>IPGB1</i> MUTANT DISPLAYS A PROTRUSION BRANCHING PHENOTYPE	86
3.4.5 RAC1 PROMOTES CELL-TO-CELL SPREAD	89
3.4.6 RAC1 PROMOTES DMV ESCAPE	92
3.4.7 RHOA DEPLETION RESCUES THE <i>IPGB1</i> CELL-TO-CELL SPREAD DEFECT	96
3.4.8 RHOA RESTRICTS DMV ESCAPE	101

3.4.9 IPGB1 ENHANCES RAC1 RECRUITMENT AND ANTAGONIZES RHOA RECRUITMENT TO DMVS	105
3.4.10 RHOA DOES NOT PROMOTE ACTIN POLYMERIZATION AROUND DMVS	110
3.4.11 IPGB1 CONTRIBUTES TO <i>S. FLEXNERI</i> INVASION AND CELL-TO-CELL SPREAD <i>IN VIVO</i>	112
3.4.12 IPGB1 CONTRIBUTES TO <i>S. FLEXNERI</i> PATHOGENESIS	114
3.5 DISCUSSION	116
3.5.1 HOW DOES IPGB1 ANTAGONIZE THE RECRUITMENT OF RHOA?	116
3.5.2 HOW DOES RHOA RESTRICT DMV ESCAPE?	118
3.5.3 HOW DOES IPGB1 CONTRIBUTE TO PATHOGENESIS?	120
4. CHAPTER 4: THE HOST LYSOPHOSPHOLIPASE II AS A NOVEL CONTRIBUTOR TO <i>S. FLEXNERI</i> CELL-TO-CELL SPREAD	123
<hr/>	
4.1 SUMMARY	124
4.2 INTRODUCTION	124
4.3 MATERIALS AND METHODS	126
4.3.1 CELL LINES AND BACTERIAL STRAINS	126
4.3.2 BACTERIAL INFECTION	127
4.3.3 SIRNA TRANSFECTION	127
4.3.4 ANTIBODIES	127
4.3.5 SIZE OF INFECTION FOCI	128
4.3.6 LIVE IMAGING	128
4.4 RESULTS	129
4.4.1 LYPLA2/APT2 FACILITATES <i>S. FLEXNERI</i> CELL-TO-CELL SPREAD	129
4.4.2 LYPLA2/APT2 PROMOTES <i>S. FLEXNERI</i> DMV ESCAPE	134
4.5 DISCUSSION	137
5. CHAPTER 5: PERSPECTIVES AND FUTURE DIRECTIONS	141
<hr/>	
5.1 SUMMARY OF WORK	142
5.2 DMV ESCAPE AS A T3SS EFFECTOR-DRIVEN PROCESS	144
5.2.1 WHAT IS THE MECHANISM OF ICSB-DEPENDENT DMV ESCAPE?	144
5.2.2 WHAT IS THE MECHANISM OF IPGB1-DEPENDENT DMV ESCAPE?	147
5.2.3 HOW ARE ICSB AND IPGB1 LOCALIZED DURING INFECTION?	148
5.3 HOST FACTORS AS CONTRIBUTORS TO <i>S. FLEXNERI</i> DMV ESCAPE	149
5.3.1 HOST MEMBRANE TRAFFICKING AS A REGULATOR OF VACUOLE ESCAPE	149

<b>5.3.1.1 MODULATION OF HOST MEMBRANE TRAFFICKING TO REMAIN INSIDE VACUOLE</b>	<b>150</b>
<b>5.3.1.2 MODULATION OF HOST MEMBRANE TRAFFICKING AND VACUOLE ESCAPE</b>	<b>154</b>
<b>5.3.2 LYPLA2, A HOST LIPID-MODIFYING ENZYME EXPLOITED FOR DMV ESCAPE?</b>	<b>157</b>
<b>5.4 HOW ARE THE INNER AND OUTER MEMBRANES DISSOLVED?</b>	<b>158</b>
<b>5.5 NOVEL TARGETS FOR THERAPEUTIC INTERVENTIONS</b>	<b>161</b>
<b>5.6 CONCLUSIONS AND SIGNIFICANCE OF WORK</b>	<b>162</b>
<u>APPENDIX 1: PRIMERS AND TEMPLATES USED IN THIS STUDY</u>	<u>164</u>
<u>REFERENCES</u>	<u>167</u>

## List of Figures and Tables

Figure 1.1: <i>S. flexneri</i> cell-to-cell spread in colonic epithelial cells.....	10
Table 1.1: Bacterial and host factors involved during each step of cell-to-cell spread.....	11
Figure 1.2: Topologies of inner and outer membranes of double membrane vacuole.....	16
Figure 2.1: The <i>icsB</i> mutant is as invasive as wild type bacteria.....	30
Figure 2.2: The <i>icsB</i> mutant displays a spreading defect.....	31
Figure 2.3: Tracking individual bacteria using time-lapse microscopy of HT-29 cells expressing plasma membrane-targeted YFP and infected with CFP-expressing.....	34
Figure 2.4: The <i>icsB</i> mutant displays a DMV escape defect.....	36
Figure 2.5: Tracking analysis of <i>S. flexneri</i> during cell-to-cell spread.....	37
Figure 2.6: Tracking LC3 recruitment using HT-29 cells expressing LC3-mCherry and plasma membrane-targeted YFP, and infected with CFP-expressing <i>S. flexneri</i> .....	40
Figure 2.7: LC3 is recruited equally to double membrane vacuoles containing wild type or <i>icsB</i> mutant bacteria.....	42
Figure 2.8: Tracking analysis of LC3 recruitment to DMVs during cell-to-cell spread.....	44
Figure 2.9: The <i>icsB</i> mutant is not delayed in protrusions or VLPs.....	48
Figure 2.10: IcsB promotes prompt escape from DMVs.....	49
Figure 2.11: Positive correlation between the time until escape and the time until LC3 recruitment.....	52
Figure 2.12: Autophagy does not inhibit <i>S. flexneri</i> spread from cell to cell.....	55
Figure 2.13: LC3 does not inhibit <i>S. flexneri</i> spread from cell to cell.....	56
Figure 3.1: IpgB1 is required for efficient invasion and cell-to-cell spread in HT-29 cells.....	78
Figure 3.2: IpgB2 is not required for invasion or cell-to-cell spread in HT-29 cells.....	79
Figure 3.3: The phenotypes of <i>ipgB1/ipgB2</i> and <i>icsB/ipgB1</i> double mutants.....	81
Figure 3.4: IpgB1 is required for efficient DMV escape.....	84
Figure 3.5: The protrusion branching phenotype.....	87
Figure 3.6: Rac1 signaling is required for efficient cell-to-cell spread.....	90
Figure 3.7: Rac1 depletion decreases DMV escape.....	94
Table 3.1: Rho family siRNA screen.....	98
Figure 3.8: RhoA depletion restores <i>ipgB1</i> cell-to-cell spread.....	100

Figure 3.9: RhoA depletion restores <i>ipgB1</i> DMV escape.....	103
Figure 3.10: IpgB1 enhances Rac1 and antagonizes RhoA recruitment to DMVs.....	107
Figure 3.11: IpgB1 modulates levels of Rac1 and RhoA DMVs.....	109
Figure 3.12: IpgB1 does not affect actin accumulation around DMVs.....	111
Figure 3.13: IpgB1 contributes to <i>S. flexneri</i> invasion and cell-to-cell spread <i>in vivo</i> .....	113
Figure 3.14: IpgB1 contributes to <i>S. flexneri</i> pathogenesis.....	115
Figure 3.15: Model for the role of IpgB1 in DMV escape during <i>S. flexneri</i> cell-to-cell spread.....	122
Figure 4.1: Rho family-related siRNA screen.....	132
Figure 4.2: LYPLA2 depletion reduces cell-to-cell spread.....	133
Figure 4.3: LYPLA2/APT2 is required for efficient DMV escape.....	135
Figure 4.4: The activities of LYPLA2/APT2 (LYPLA2 activity).....	140
Figure 5.1: Current Model of DMV escape.....	143
Table 5.1: Mechanisms of membrane trafficking modulation by vacuole-residing bacterial pathogens.....	150

## List of Abbreviations

3-MA, 3-methyladenine  
ABM, actin-based motility  
ANOVA, analysis of variance  
APT, acyl-protein thioesterase  
ARP2/3, actin related protein 2/3 complex  
Baf-A1, Bafilomycin A1  
CCV, *Coxiella*-containing vacuole  
CFL1, cofilin 1  
CFP, cyan fluorescent protein  
CFU, colony-forming unit  
CLEM, correlative light electron microscopy  
DMV, double membrane vacuole  
DTT, dithiothreitol  
ECL, enhanced chemiluminescence  
EEA1, early endosome antigen 1  
EM, electron microscopy  
FBS, fetal bovine serum  
FFA, free fatty acid  
GAP, GTPase activating protein  
GEF, guanine nucleotide exchange factor  
GEF, guanine nucleotide exchange factor  
HRP, horseradish peroxidase  
IAM, infection-associated macropinosome  
IF, immunofluorescence  
ILK, integrin-linked kinase  
IPTG, isopropyl  $\beta$ -D-1 thiogalactopyranoside  
LB, lysogeny broth  
LC3, microtubule-associated protein light chain 3  
LCV, *Legionella*-containing vacuole  
LLO, Listeriolysin O  
LYPLA, lysophospholipase  
LysoPLs, lysophospholipids  
Mb-YFP, membrane-YFP  
MCV, *Mycobacteria*-containing vacuole  
Mpl, metalloprotease  
N-WASP (aka WASL), neural Wiskott-Aldrich syndrome protein  
ORF, open reading frame  
PBS, phosphate buffered saline

PFN1, profilin 1  
PI3P, phosphatidylinositol 3-phosphate  
PIK3C2A, class II phosphatidylinositol 3-phosphate kinase  
PlcA, phospholipase C A  
PlcB, phospholipase C B  
SCV, *Salmonella*-containing vacuole  
SDS-PAGE  
siRNA, small interfering RNA  
T3SS, type three secretion system  
TBK1, TANK-binding kinase 1  
TBS, tris-buffered saline  
TSB, tryptic soy broth  
VLP, vacuole-like protrusion  
WASL (aka N-WASP), Wiskott-Aldrich syndrome protein-like  
WB, western blot  
WIP, WASP-interacting protein  
WT, wild type  
YFP, yellow fluorescent protein

## 1. Introduction

### 1.1 Introduction to *Shigella*

Bacteria belonging to the genus *Shigella* are gram negative, non-spore-forming, facultative anaerobic rod shaped bacteria that are closely related to *Escherichia coli*. *Shigella spp.* cause severe diarrheal disease in primates known as bacillary dysentery, or Shigellosis (1). *Shigella* is an important human pathogen, causing 270 million cases and 200,000 deaths globally each year, with the majority of this burden falling on low-income countries in Africa and Asia (2). Nearly one third of the total deaths occur in young children under the age of five and *Shigella* was found to be one of the most prevalent etiologies of diarrhea for children in this age group (3–5). There is no natural reservoir for *Shigella* and the primary mode of transmission is person-to-person. *Shigella* is spread via the fecal-oral route and has a very low infectious dose, with as few as 10-100 bacteria being sufficient to cause disease (6).

There are four species of *Shigella*: *S. flexneri*, which is the most prevalent and widespread strain that is endemic in low and middle-income countries, *S. sonnei*, which causes the majority of the cases in high-income countries, *S. dysenteriae* (especially serotype 1), which is historically associated with high-fatality epidemics, but relatively uncommon now, and *S. boydii*, which remains relatively uncommon (6). Treatment of *Shigella* is usually in the form of supportive care, but use of antibiotics can shorten the duration of symptoms and

reduce transmission. First-line therapy consists of oral ciprofloxacin and azithromycin, with second choice options being cefixime or ceftriaxone. However, there has recently been a startling increase in resistance to multiple antibiotics among *Shigella* strains (6–8), emphasizing the need for novel therapeutics. Currently, there is no vaccine against *Shigella* infection, although there is serotype-specific natural immunity following infection (9). As *S. flexneri* is the most widespread and prevalent species, it is also the most studied and well-characterized species in terms of cellular and molecular pathogenesis and the topic of this thesis.

### **1.1.1 Models for studying *S. flexneri* pathogenesis**

Early studies in human volunteers determined that *S. flexneri* is very infectious pathogen with a high attack rate following low-dose inoculation (10–12). Studies performed in non-human primates revealed that *S. flexneri* invades and resides within colonic epithelial cells (13). Oral infection of mice does not lead to productive infection (14). To study inflammatory response to *S. flexneri* in the absence of a small animal model, non-intestinal models such as the guinea pig eye and the mouse lung have been used (15, 16). The inflammatory response to intestinal infection has also been studied by injecting *S. flexneri* into the ileal loop of adult rabbits (17–19). Rectal inoculation of guinea pigs led to liquid stools

and weight loss, but the massive ulceration of the colon and bloody diarrhea seen in infected humans was not recapitulated in this model (20). Similar results were observed more recently using NlrC4<sup>-/-</sup> mice as a model of *S. flexneri* infection, although the immuno-compromised status of the mice could affect the infection outcome (21). Most promisingly, our lab and others have shown that infection of infant rabbits recapitulates the symptoms of shigellosis and serves as a suitable model of *S. flexneri* infection (22, 23).

Given that studies in non-human primates uncovered that *S. flexneri* was an intracellular pathogen, tissue culture systems emerged as a viable model with the discovery that *S. flexneri* could invade and replicate within cultured cells (24). This led to the expansion of studies using *in vitro* cell culture systems to study the cellular pathogenesis of *S. flexneri* and its interactions with host cells.

### 1.1.2 Cellular/molecular pathogenesis

*S. flexneri* contains a chromosome of approximately 4.6 Mb and a 220 kb large virulence plasmid, which encodes one of its most important virulence factors: the Mxi-Spa type three secretion system (T3SS) (25–27). The *S. flexneri* T3SS is a needle-like apparatus that spans both bacterial membranes and also penetrates the host cell membrane to allow for the delivery of bacterial effector proteins into the cytosol of host cells. The large virulence plasmid encodes the

structural components of the T3SS as well as about 25 effectors, which function throughout its infection process (27, 28).

#### **1.1.2.1 Invasion of colonic epithelial cells**

Following ingestion, *S. flexneri* travels through the intestinal tract until it reaches the colon, the site of colonization. Relatively little is known about the mechanisms that allow the bacteria to overcome the hostile environments of the human digestive system and reach the colon. *S. flexneri* produces an extracellular serine protease called Pic, which possesses mucinolytic activity *in vitro* and could play a role in the bacteria traversing the mucus layer in the colon to access the colonic epithelial cells (29–31).

*S. flexneri* crosses the epithelium to gain access to the basolateral side of the cells. It was shown using the rabbit ileal loop model that the activity of antigen sampling M cells in the small intestine facilitates the invasion of the epithelium (32). However, the human colon, which is the physiological site of *S. flexneri* infection, is devoid of M cells. Furthermore, evidence exists from tissue culture of colonic epithelial cells that *S. flexneri* is able to invade at the apical surface of the cell as well as remodel tight junctions, both of which could provide access to the basolateral surface (33, 34). The exact mechanism of how the bacteria cross the epithelium to invade at the basolateral side remains unknown.

In HeLa cells, *S. flexneri* enters cells via the trigger mechanism of entry, which has been fairly well studied (35). It is noteworthy that entry into polarized epithelial cells occurs at the basolateral surface and the mechanism has not been well characterized. The translocases IpaB and IpaC are inserted into the host cell membrane and form the pore, or translocon, of the T3SS (36). Interestingly, IpaC interacts with the host intermediate filament vimentin and keratin 18, which results in a conformational change of the translocon that is required to stabilize docking of *S. flexneri* to host cells (37). Following translocon insertion and stable docking, the opening of the translocon is facilitated by a conformational change induced by host cell actin polymerization and translocation of early effectors can proceed (37–40).

Among the early effectors are IpgB1 and IpgB2, which are bacterial guanine nucleotide exchange factors (GEFs) that belong to a family of homologous proteins that are defined by a conserved WxxxE motif (41). IpgB1 and IpgB2 activate the Rho GTPases Rac1 and RhoA, respectively, and are required for the actin polymerization that leads to membrane ruffling for bacterial entry (42–44). It has been shown that the T3SS effectors IpaA, which depolymerizes actin, and IpgD, a phosphoinositide 4-phosphatase, could have roles during invasion (45, 46); however, clear evidence of this in polarized, colonic epithelial cells remains to be shown.

### 1.1.2.2 Primary Vacuole Escape

Following invasion, bacteria are enveloped in a single membrane vacuole (primary vacuole). Escape from the primary vacuole depends on the *Shigella* T3SS. The T3SS translocases, IpaB and IpaC, are required for vacuolar escape (47). Interestingly, unlike *Listeria monocytogenes*, a cytosolic pathogen that escapes the primary vacuole through the activity of two bacterial phospholipases and a pore-forming toxin Listeriolysin O (LLO)(48), *S. flexneri* does not produce any specific proteins that challenge the integrity of the membrane. This suggests that *S. flexneri* could require on host cell factor(s), and the consequential damage and destabilization caused by the formation of T3SS translocon, for vacuole escape.

Following vacuole escape, vacuole membrane remnants are recognized by the host cell autophagic machinery and are subsequently degraded (49). Furthermore, the autophagy machinery has been implicated in the repair of damaged endosomal membranes (50), suggesting that membrane repair by host factors could prevent vacuole destabilization escape. Along these lines, the autophagy marker LC3 is recruited to bacteria in primary vacuoles as well as double membrane vacuoles following cell-to-cell spread and this seems to be associated with less destabilization (51). Furthermore, bacteria lacking the T3SS effectors IcsB and VirA were found to be more frequently associated with LC3, suggesting *S. flexneri* could be subverting the recruitment of the autophagy

proteins (51). These data suggest a potential link between subversion of membrane repair by the autophagy machinery and vacuole destabilization, which could potentially be modulated by bacterial effectors; however, the mechanism of this process remains unclear.

In the context of vacuole-residing bacterial pathogens, pathogen-containing vacuoles can be enveloped in and stabilized by structures formed by host cytoskeletal components, such as actin (52, 53). It is thus tempting to speculate whether cytosolic pathogens such as *S. flexneri* prevent such actin-dependent stabilization. Actin networks around the primary vacuoles have been observed during *S. flexneri* infection and have been referred to as “actin cages” (54); however, it remains unclear if there is a role for actin cages in inhibiting vacuole escape. Furthermore, *de novo* actin polymerization around the primary vacuole following uptake results in a thick and dynamic actin structure coined the “actin cocoon” (55). Canonical actin-related host factors, such as CDC42, TOCA-1, WIP, N-WASP, ARP2/3, cofilin, coronin, and cortactin are recruited to the actin cocoon. The subversion of these host factors and the dynamics of the actin cocoon may be regulated by T3SS effectors, including IpgD, IpgB1, and IcsB. Formation of the actin cocoon is associated with delayed vacuole rupture; however, it seems to be important for the complete disassembly of vacuolar membrane remnants and subsequent infection steps (55). Therefore, the role of

actin in the prevention of *S. flexneri* primary vacuole destabilization remains elusive.

### 1.1.2.3 Actin-based motility

Following invasion, *S. flexneri* hijacks the host cell actin cytoskeleton to propel itself throughout the cytosol in the process called actin-based motility (ABM)(Figure 1.1, step 1). ABM is achieved through expression of the autotransporter protein IcsA (VirG) on the surface at the pole of the bacteria (56, 57). IcsA recruits host actin nucleation-promoting factor Neural Wiskott-Aldrich syndrome protein (N-WASP) to the bacterial pole. N-WASP then recruits and activates a host actin nucleator complex, the ARP2/3 complex, which leads to robust actin polymerization at the bacterial pole and the formation of characteristic “actin tails” (58–60). Complete N-WASP activation by *S. flexneri* is a complex process that also depends on the host protein TOCA-1, regulation of tyrosine phosphorylation by the tyrosine kinases Btk and Abl, and additional cytoskeleton regulators, such as profilin and WIPF2 (61–65). Additionally, the *S. flexneri* protease IcsP contributes to the polar localization of IcsA (66) and thus, formation of the actin tail at one pole resulting in the directional propulsion of the bacteria.

#### 1.1.2.4 Cell to cell spread

The ability of *S. flexneri* to harness ABM to spread from the primary infected cell to neighboring cells through cell-to-cell spread enables its dissemination through the host epithelium (Figure 1.1). The importance of cell-to-cell spread for *S. flexneri* pathogenesis was recently demonstrated, as a fully invasive, yet spreading deficient mutant was essentially avirulent in an infant rabbit model of bacillary dysentery (23). The mechanisms that support ABM are fairly well understood; however, ABM alone is not sufficient for cell-to-cell spread. Molecular and cellular factors, both host and bacterial, that facilitate cell-to-cell spread remain less characterized. This section will discuss the sequential steps of cell-to-cell spread: protrusion formation, protrusion resolution/vacuole-like protrusion (VLP) formation, VLP resolution/double membrane vacuole (DMV) formation, and DMV escape. A summary of host and bacterial factors currently known to be involved during each step can be found in table 1.1

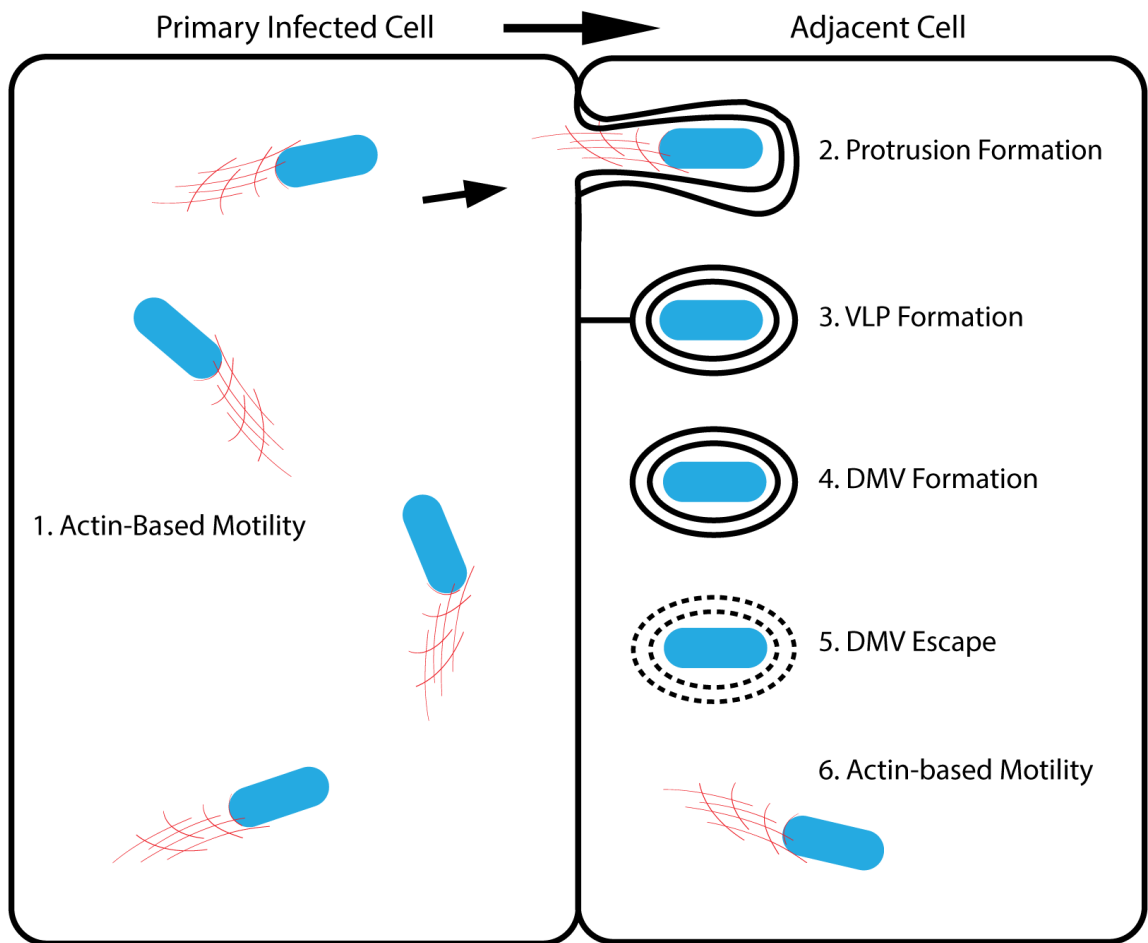


**Figure 1.1: *S. flexneri* cell-to-cell spread in colonic epithelial cells** Schematic depicting the sequential steps of intercellular spread: 1. Actin-based motility (ABM) 2. Protrusion formation 3. Vacuole-like protrusion (VLP) formation 4. Double membrane vacuole (DMV) formation 5. Double membrane vacuole (DMV) escape 6. Actin-based motility (ABM) in adjacent cell.

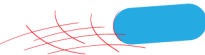
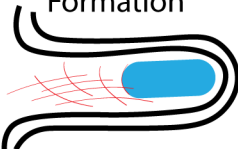
Vacuole Escape	Bacterial Factors	Host Factors
	IpaB IpaC IpgD	Exocyst Complex Sorting Nexins EEA1 Rab 4, Rab5, Rab11
Actin-Based Motility 	IcsA IcsP	Arp2/3 N-WASP TOCA-1 Btk Abl Profilin WIPF2
Protrusion Formation 	IcsA	Arp2/3 N-WASP mDia1/2 Myosin-X
VLP Formation 	Type III Secretion System IpgD	STK11 PIK2C2A
DMV Formation 	?	?
Double Membrane Vacuole Escape 	Type III Secretion System IcsB? VirA?	?

Table 1.1: Bacterial and host factors involved during each step of cell-to-cell spread

#### 1.1.2.4.1 Protrusion Formation

As motile bacteria encounter cell-cell junctions, they push against the plasma membrane, protruding into the adjacent cell (Figure 1.1, step 2).

Interestingly, protrusion formation seems to occur preferentially at tricellular junctions where three cells meet and requires the cadherin-dependent integrity of cell-cell junctions (67). In addition to cell-cell junctions, *S. flexneri* also actively maintains epithelial cell adhesion and prevents rounding by producing the T3SS effector OspE, which binds integrin-linked kinase (ILK) to stabilize epithelial cell focal adhesions (68, 69). It is presumed that, similar to cytosolic ABM, IcsA and N-WASP/ARP2/3 are responsible for actin polymerization in *S. flexneri* protrusions leading to protrusion elongation. In addition to ARP2/3, the host formins mDia1/2 localize to protrusions and are required for proper protrusion formation (70, 71). Myosin-X also localizes to protrusions and was proposed to facilitate protrusion formation by bridging actin filaments and the plasma membrane (72). To promote the efficient formation of membrane protrusion, *S. flexneri* reduces intercellular tension through the production of IpaC, which binds to host  $\beta$ -catenin (73).

#### 1.1.2.4.2 Protrusion Resolution/VLP Formation

The resolution of membrane protrusions into double membrane vacuoles (DMVs) occurs through the formation of an intermediate compartment termed the vacuole-like protrusion (VLP)(Figure 1.1, Step 3). Like DMVs, VLPs are comprised of two continuous membranes from the primary infected cell and the adjacent cell, respectively. However, they remain attached to the primary infected cell by a membrane tether, which arises from the collapse of the protrusion neck, presumably due to the disassembly of the underlying actin cytoskeleton network (74). The transition from protrusion to VLP relies on local host tyrosine kinase signaling, which is maintained by the serine/threonine kinase STK11 (75). The host class II phosphatidylinositol-3 kinase (PIK3C2A), which is required for phosphatidylinositol-3-phosphate (PI3P) production in protrusions, also promotes protrusion resolution into VLPs (74).

Several studies have demonstrated that bacterial T3SS is required for the resolution of protrusions into VLPs (47, 76), highlighting that ABM alone is not sufficient for cell-to-cell spread in epithelial cells. The T3SS effector IpgD, via its phosphatidylinositol 4-phosphatase activity, also contributes specifically to protrusion resolution through regulation of phosphatidylinositol-4,5-phosphate levels, which control *de novo* cortical actin formation in protrusions (77).

Additional factors contributing to protrusion resolution/VLP formation remain to be determined.

#### **1.1.2.4.3 VLP resolution/DMV Formation**

The transition from VLP to DMV is marked by the loss of the membrane tether to the primary cell (74)(Figure 1.1, Step 4). It is not yet understood how the membranous tether is cleared. Host protein dynamin 2, which is involved in membrane scission, localizes to areas of protrusion engulfment and is required for cell-to-cell spread (67). Depletion of additional host factors involved in the endocytic pathway (clathrin, Epsin-1) also reduced cell-to-cell spread (67, 74); however, whether they contribute to VLP resolution remains unknown.

#### **1.1.2.4.4 DMV escape**

Resolution of VLPs leads to the formation of secondary, double membrane vacuoles (DMVs), in which the inner membrane is derived from the primary infected cell and the outer membrane is derived from the newly infected secondary cell. The membranes comprising DMVs that form during cell-to-cell spread have opposite topologies (Figure 1.2). The inner membrane results from an exocytosis-like process whereby the bacteria exit the primary cell. Consequently, the cytoplasm-facing, inner leaflet (Figure 1.2, orange) of the

membrane ends up on the inside of the vacuole and the outer leaflet (Figure 1.2, blue) faces the spaces between the two membranes. In contrast, the outer membrane results from an endocytosis-like process whereby the bacteria enter the secondary cells. In this case, the inner leaflet (Figure 1.2, orange) of the second membrane is on the outside of the DMV, facing the cytosol of the secondary cell and the outer leaflet (Figure 1.2, blue) faces the space between the two membranes. Whether the differing topologies of the inner and outer membranes of the DMV influence the process of DMV escape remains to be investigated.

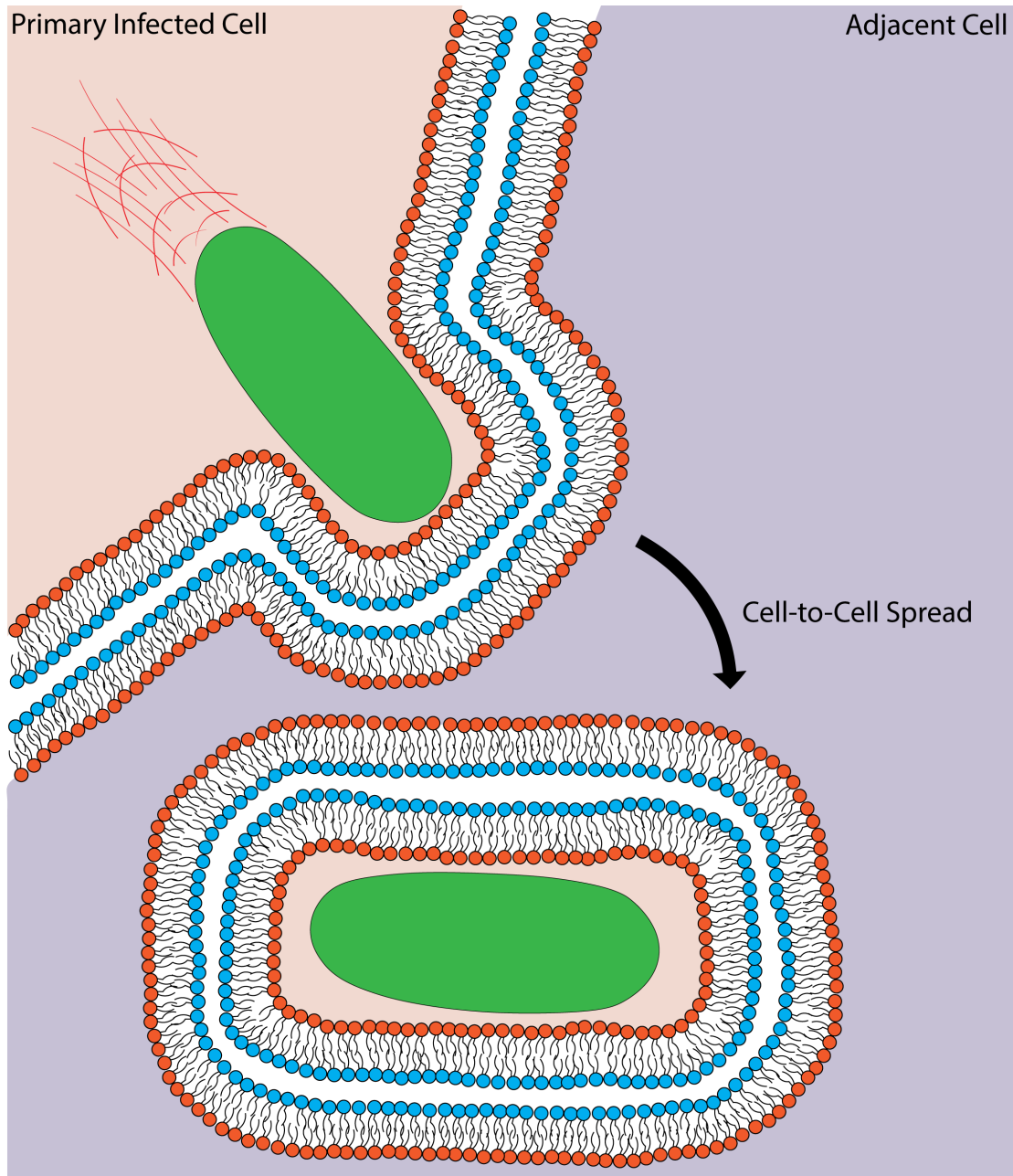


**Figure 1.2: Topologies of inner and outer membranes of double membrane vacuole**  
 Orange phospholipids indicate cytoplasmic facing leaflet of membrane and blue phospholipids indicate extracellular facing leaflet.

Prior to my thesis work, very little was known about the mechanisms that support *S. flexneri* DMV escape (Figure 1.1, step 5). However, the process of DMV escape has been fairly well characterized for *Listeria*, as it requires the same molecular players as primary vacuole escape. It has been demonstrated that, in addition to primary vacuole escape, the *Listeria* broad range phospholipase, PlcB, is required for DMV escape (48, 78, 79). Additionally, pH-dependent activation of PlcB by a bacterial metalloprotease (Mpl) in the slightly acidic environment of DMVs contributes to *Listeria* DMV escape (80, 81). Furthermore, LLO is critical for DMV escape, as bacterial mutants lacking LLO remained trapped in DMVs in adjacent cells following cell-to-cell spread (78). Interestingly, an electron microscopy study revealed that, following cell-to-cell spread of *Listeria* in macrophages, mutants conditionally deficient in LLO expression remained trapped in vacuoles comprised of either a single or a double membrane, while mutants lacking PlcA, PlcB and LLO expression were found trapped within vacuoles comprised of two membranes (82). This suggested that the activities of the phospholipases could disrupt the inner membrane of the DMV, even in the absence of LLO, but LLO was required for disruption of the outer membrane. The differential requirement for dissolution of the inner versus outer membrane could be in part due to the opposite topologies or differing molecular composition of the membranes, although this remains to be explored.

Unlike *Listeria*, *S. flexneri* lacks phospholipases and obvious proteins that would challenge the integrity of the vacuole membrane. Previous studies using inducible systems identified a role for the T3SS in *S. flexneri* DMV escape following cell-to-cell spread (47, 76). It was also revealed that *Shigella* mutants lacking both T3SS effectors IcsB and VirA accumulate in vacuoles during cell-to-cell spread, suggesting they could play a role in DMV escape (51). However, their specific roles and mechanisms require further exploration. Additional roles of *Shigella* T3SS effectors and host factors that contribute to DMV escape remain uncharacterized.

#### **1.1.2.5 Avoidance of autophagy during infection of colonic epithelial cells**

During cell-to-cell spread within the epithelium, *S. flexneri* is able to avoid some aspect of the host immune response, such as antibody-mediated immunity. However, the intracellular environment innately possesses several systems for protection against pathogens, which have been extensively reviewed elsewhere (83). One such host cell defense systems is autophagy, an elegant cascade that leads to the sequestration and eventual lysosomal degradation of cytoplasmic cargo. *S. flexneri* was first reported to be targeted by autophagy while in the cytosol displaying ABM (84). A later study showed that the host autophagy machinery targets membrane-bound bacteria either following invasion or cell-to-

cell spread (51). The work presented in chapter 2 of this thesis provides novel insights into the controversy of which compartment(s) are targeted by autophagy and the functional implications during *S. flexneri* cell-to-cell spread.

## 1.2 Dissertation goals

The process of cell-to-cell spread is essential for *S. flexneri* pathogenesis. The mechanisms supporting actin-based motility are relatively well understood. However, less is known about the bacterial and host factors required for the subsequent steps of the spreading process, including double membrane vacuole escape. The bacterial type-three secretion system is known to be required for DMV escape. We hypothesized that specific T3SS effector(s) would be involved in DMV escape. The goals of this work are to address this hypothesis by assessing the roles of candidate T3SS effectors IcsB (Chapter 2), IpgB1, and IpgB2 (Chapter 3) during *S. flexneri* infection. These novel insights would not only further our understanding of *S. flexneri* pathogenesis, but also provide additional clarification on the mechanisms that support vacuole stability versus vacuolar escape of intracellular pathogens.

## **2. Chapter 2: The role of type three secretion system effector protein IcsB and LC3-dependent autophagy in *Shigella flexneri* dissemination**

This chapter is a modified version of the previously published article: Weddle E, Agaisse H. "Spatial, Temporal, and Functional Assessment of LC3-Dependent Autophagy in *Shigella flexneri* Dissemination." *Infection and Immunity*. 86(8) 2018 July. doi: 10.1128/IAI.00134-18.

Experimental Contributions: Weddle E designed and performed all experiments, wrote the manuscript, and created all figures, under the guidance and supervision of Agaisse, H.

## 2.1 Summary

*Shigella flexneri* disseminates within the colonic mucosa by displaying actin-based motility in the cytosol of epithelial cells. Motile bacteria form membrane protrusions that project into adjacent cells and resolve into double membrane vacuoles (DMVs), from which the bacteria escape, thereby achieving cell-to-cell spread. During dissemination, *S. flexneri* is targeted by LC3 dependent autophagy, a host cell defense mechanism against intracellular pathogens. The *S. flexneri* type III secretion effector IcsB was initially proposed to counteract the recruitment of the LC3-dependent autophagy machinery to cytosolic bacteria. However, a recent study proposed that LC3 was recruited to bacteria in DMVs formed during cell-to-cell spread. To resolve the controversy and clarify the role of autophagy in *S. flexneri* infection, we tracked dissemination using live confocal microscopy and determined the spatial and temporal recruitment of LC3 to bacteria. This approach demonstrated that (1) LC3 was exclusively recruited to wild type or *icsB* bacteria located in DMVs, and (2) the *icsB* mutant was defective in cell to cell spread due to failure to escape LC3-positive as well as LC3-negative DMVs. Failure of *S. flexneri* to escape DMVs correlated with late LC3 recruitment, suggesting that LC3 recruitment is the consequence and not the cause of DMV escape failure. Inhibition of autophagy had no positive impact on the spreading of wild type or *icsB* mutant bacteria. Our results unambiguously

demonstrate that IcsB is required for DMV escape during cell-to-cell spread, regardless of LC3 recruitment, and do not support the previously proposed notion that autophagy counters *S. flexneri* dissemination.

## 2.2 Introduction

Autophagy is a cellular process that is responsible for the degradation and recycling of cellular debris and damaged organelles. Ubiquitination and recognition by adaptor proteins, such as p62, TANK binding kinase 1 (TBK1), and NDP52 can selectively target cargos for autophagy and recruit the autophagy machinery (85–88). Several members of the ATG family of proteins are involved in formation of an isolation membrane around cytosolic cargo forming an autophagosome (89). One of these proteins, ATG8/LC3, is conjugated to phosphatidylethanolamine and localizes to the isolation membrane (90), where it controls its expansion around cytosolic cargo (91). This autophagosome matures along the endo/lysosomal pathway and eventually fuses with a lysosome, resulting in degradation of the cargo.

Canonical and non-canonical autophagy pathways are increasingly recognized as host cell defense mechanisms against intracellular infection. LC3-associated isolation membranes are recruited to and entrap cytosolic bacteria in a specialized form of autophagy called xenophagy (92). Alternatively, LC3 can be

recruited to a pathogen-containing vacuole in non-canonical pathways that do not require all of the classical autophagy proteins (93–95). Many intracellular bacteria, including *L. pneumophila*, *S. enterica* and *L. monocytogenes*, have been shown to be targeted by autophagy. Pathogens such as *L. pneumophila* and *S. enterica* are recognized by the autophagy machinery while residing in vacuoles (96, 97). Cytosolic pathogens such as *L. monocytogenes*, which quickly escape from primary vacuoles formed upon invasion, are detected by autophagy either in vacuoles prior to escape or in the cytosol after escape (95).

*S. flexneri* is also targeted by autophagy during intracellular infection. The LC3-dependent autophagy machinery was first shown to target *S. flexneri* in the cytosol as a result of the surface expression of IcsA (84). IcsA was proposed to bind autophagy-related protein 5 (ATG5) and thus trigger autophagic recognition of cytosolic bacteria. The *S. flexneri* protein IcsB, which was first identified as a type three secreted effector protein required for intercellular spread (98, 99), was proposed to prevent recognition of cytosolic bacteria by binding to IcsA and masking it from ATG5 (84). More recently, it was proposed that LC3 is not recruited to cytosolic bacteria, but to bacteria located in vacuoles (51). In this study, the authors capitalized on a transcriptional reporter of the activity of the T3SS and the secreted translocator IpaB for identifying bacteria in membrane-bound compartments during intercellular infection. By combining

these markers with LC3 labeling, the authors concluded that LC3 was recruited to bacteria located in the double membrane vacuoles formed during *S. flexneri* spread from cell to cell. This approach also confirmed that the *icsB* mutant was more frequently associated with LC3, suggesting that IcsB is required for escaping LC3-positive vacuoles. Although the study clearly demonstrated that LC3 was recruited to actively secreting *S. flexneri*, the approach did not allow for the unambiguous identification of features of cell-to-cell spread, including protrusions, VLPs, and vacuoles.

Here, we have used time-lapse confocal microscopy in cells expressing plasma membrane targeted YFP to track the dissemination of individual CFP-expressing bacteria and the simultaneous recruitment of mCherry-LC3. We provide the unambiguous demonstration that LC3 is recruited to *S. flexneri* when located in the double membrane vacuoles that derive from membrane protrusions formed during dissemination. Importantly, our approach uncovered that IcsB contributes to DMV escape, regardless of LC3 recruitment. Additionally, we revealed a positive correlation between the time until LC3 recruitment and the time until vacuole escape. Finally, we demonstrated that inhibiting autophagy did not rescue the spreading defect in cells infected with the *icsB* mutant. Moreover, inhibition of autophagy impaired cell-to-cell spread of wild-type bacteria. Collectively, these results do not support

the notion that the LC3-dependent autophagy machinery acts as host cell defense mechanism against *S. flexneri* during cell-to-cell spread.

## 2.3 Materials and Methods

### 2.3.1 Cell lines and bacterial strains

HT-29 cells (ATCC HTB-38) were cultured at 37°C with 5% CO<sub>2</sub> in McCoy's 5A medium (Gibco) supplemented with 10% heat-inactivated fetal bovine serum (FBS) (Invitrogen). The wild-type *Shigella flexneri* strain used in this study is serotype 2a 2457T (24). The *icsB* strain of *S. flexneri* was generated by allelic exchange resulting in replacement of the *icsB* open reading frame (ORF) in the *Shigella* large virulence plasmid by the coding region of a kanamycin resistance cassette. The *icsB* strain was complemented by expressing wild-type *icsB* from the arabinose-inducible pBAD promoter in vector pBAD18 (ATCC #87393).

### 2.3.2 DNA constructs and cell transfection

HT-29 cell lines stably expressing yellow fluorescent protein (YFP) membrane markers were generated using the pMX-Mb-YFP vector (74). MAPLC3B was cloned into the XhoI and NotI sites of the pMX\_mCherry vector. The corresponding lentiviruses were generated in 293T cells cotransfected with

the packaging constructs pCMV $\Delta$ 8.2 $\Delta$ vpr (HIV helix packaging system) and pMD2.G (a vesicular stomatitis virus glycoprotein) as previously described (100).

### 2.3.3 Bacterial infection

*S. flexneri* was grown overnight in LB broth at 30°C with agitation. The bacteria were diluted 1:100 and grown to exponential phase for approximately 3 h at 37°C with agitation. Cells were infected with *S. flexneri* expressing CFP under the control of an isopropyl- $\beta$ -D-thiogalactopyranoside (IPTG)-inducible promoter. Infection was initiated by centrifuging the plate at 1,000 rpm for 5 min, and internalization of the bacteria was allowed to proceed for 1 h at 37°C before gentamicin (50 M final concentration) and IPTG (4 mM final concentration) was added to kill the extracellular bacteria and induce CFP expression, respectively. For time-lapse microscopy, imaging began 2 hours post-infection. For *S. flexneri* focus size analysis, infected cells were incubated at 37°C for 16 hours.

### 2.3.4 siRNA and western blot

Cells were transfected by reverse transfection with Dharmafect1 and a pool of small interfering RNAs (siRNAs) (D1, D2, D3, and D4; 12.5 nM each, 50 nM total final concentration) targeting LC3B or siRNA buffer alone (mock) and

incubated for 96 h in a 384-well format. Knockdown efficiency was determined by western blot for LC3B (Nanotools 0231-100/LC3-5F10 used at 1:100). Western blot quantification was performed using Fiji.

### **2.3.5 Size of infection foci**

The size of infection foci formed in plasma membrane-YFP-expressing HT-29 cells and infected with the listed CFP-expressing *S. flexneri* strains was determined in a 96-well plate format (catalog no. 3904; Corning). After fixation with 4% paraformaldehyde, the plates were imaged using the ImageXpress Micro imaging system (Molecular Devices). Margins of individual foci were determined manually and image analysis for focus size (area) was performed with the ImageXpress imaging software (Molecular Devices) as previously described (75). Image analyses were conducted on at least 50 infection foci in each independent experiment.

### **2.3.6 Live imaging**

Bacterial dissemination was monitored using time-lapse confocal microscopy. Plasma membrane-YFP-expressing HT-29 cells were grown in McCoy's medium in eight-well chambers (Lab-Tek II [catalog no. 155409; Thermo Fisher Scientific]) at 37°C in 5% CO<sub>2</sub>. Cells were infected with the listed CFP-expressing *S. flexneri*

strains and imaged with a Leica DMI 8 spinning-disc confocal microscope driven by the iQ software (Andor). Z-stacks were captured 2 hours post-infection every 2 min for 6 hr. The corresponding movies were generated with the Imaris software (Bitplane). Protrusions were defined as plasma membrane extensions that formed as a result of bacteria reaching the cell cortex and projecting into adjacent cells. Vacuole-like protrusions (VLPs) were defined as an intermediate compartment between protrusions and vacuoles, characterized by a continuous membrane lining around the bacteria and a membranous tether. Double membrane vacuoles (DMVs) were defined as membrane-bound compartments that derived from VLPs after resolution of the membranous tether. As opposed to VLPs, DMVs were therefore no longer connected to the primary infected cell. Free (cytosolic) bacteria were defined as bacteria that were previously observed in vacuoles but were no longer surrounded by a continuous lining of the plasma membrane.

## **2.4 Results**

### **2.4.1 IcsB promotes *S. flexneri* spread from cell to cell**

To study the role of IcsB in *S. flexneri* dissemination, we generated a mutant lacking *icsB*. To determine if the *icsB* mutant displayed an invasion and/or primary vacuole escape defect, we performed a gentamicin protection

assay comparing the isogenic wild type 2457T strain and the *icsB* mutant. The *icsB* mutant showed no significant difference compared to wild type in colony-forming units (CFUs) 1 hour post invasion (Figure 2.1A), or in infection foci numbers 8 hours post invasion (Figure 2.1B), indicating that the *icsB* mutant was as invasive as the wild-type strain. We have previously established the intestinal HT-29 cell line as a model system for studying the dissemination of *S. flexneri* in epithelial cells (62, 75), which leads to the formation of large infection foci sixteen hours post infection (Figure 2.2, WT). We compared the area of the foci formed in cells infected with wild type bacteria (Figure 2.2, WT) and the *icsB* mutant (Figure 2.2, *icsB*). While the wild type strain formed large foci, the *icsB* mutant formed significantly smaller foci. Using computer-assisted image analysis, we measured the area of individual infection foci. The average foci size formed in cells infected with the *icsB* mutant was significantly smaller than wild type, revealing a 65% decrease in spreading (Figure 2.2, WT vs. *icsB*). The complemented strain (*icsB/picsB*) formed infection foci with average size similar to wild type (Figure 2.2, *icsB/picsB*, +Arabinose), indicating that the spreading defect of the *icsB* mutant strain was rescued by expression of IcsB. These results indicate that the expression of the T3SS effector protein IcsB is not required for invasion and primary vacuole escape, but promotes efficient spread from cell to cell in intestinal epithelial cells.

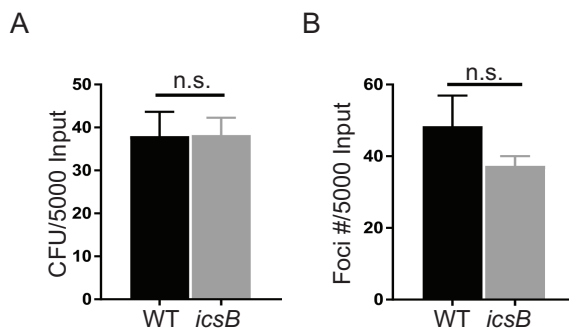


**Figure 2.1: The *icsB* mutant is as invasive as wild type bacteria** Gentamycin protection assay was performed in HT-29 cells. CFUs were determined 2 hours post-infection (**A**) or foci number were analyzed 8 hours post infection (**B**) and normalized to CFUs per inoculum. Mean of three independent experiments is shown. Error bars represent standard error of mean of three independent experiments; n.s., not significant; unpaired t-test.

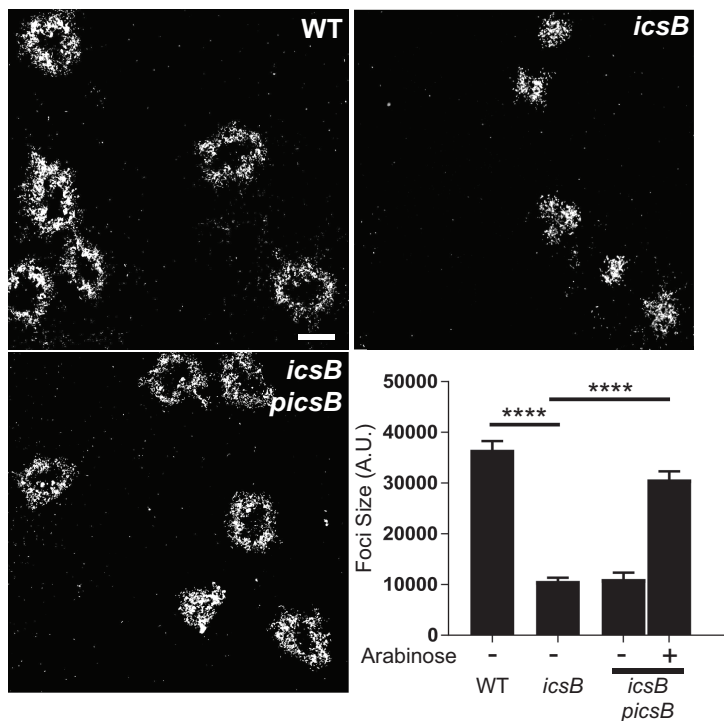


**Figure 2.2: The *icsB* mutant displays a spreading defect** Representative images of HT-29 cells infected with CFP-expressing WT, *icsB*, or *icsB/picsB* *S. flexneri*. Scale bar, 200  $\mu$ m. Graph shows quantification of area of infection focus for WT, *icsB*, and *icsB/picsB*. The expression of *icsB* is under the control of an arabinose inducible promoter. Uninduced (-) and 1% arabinose (+) induced conditions are shown. Arabinose was added 1 hour post-infection. 50 foci per strain/condition were measured in each experiment. Error bars represent standard error of mean of three independent experiments; \*\*\*\*,  $p < 0.0001$ ; one-way ANOVA with multiple comparisons.

### 2.4.2 IcsB promotes cell-to-cell spread through escape from DMVs

To determine the stage of dissemination at which the *icsB* mutant was defective, we used time-lapse confocal microscopy to track the progression and timing of cell-to-cell spread (74, 76). We infected HT-29 cells expressing plasma membrane-targeted YFP with wild type or *icsB* mutant strains expressing IPTG-inducible CFP to track motile, cytosolic bacteria forming membrane protrusions that projected into neighboring cells, which was followed by the collapse of the protrusion neck into VLPs (74) (Figure 2.3A, DMV Escape Success). VLPs then resolved into double membrane vacuoles (DMVs) from which the bacteria subsequently escaped. In some instances, the bacteria failed to escape from DMVs and remained trapped until the end of the movie (Figure 2.3B, DMV Escape Failure). In Figure 2.4, we show the representative tracking of 40 wild type (Figure 2.4A, Wild Type) and 40 *icsB* (Figure 2.4A, *icsB*) bacteria from a single experiment. Dark blue shading at the beginning of each track indicates the bacteria in the primary infected cell cytosol. Light blue shading indicates the bacteria in protrusions, purple indicates the bacteria in a VLP, yellow shading refers to a bacteria in a DMV, and green shading indicates that the YFP-membrane was no longer visible and the bacteria have regained actin-based motility, showing that it was free in the cytosol of the adjacent cell. Tracking results showed that 76% of wild type bacteria that formed protrusions were

successful in spreading to the adjacent cell (Figure 2.4B, Wild Type, green, DMV escape). Twenty-four percent of the bacteria that formed protrusions failed to spread to the adjacent cell. Thirteen percent failed in protrusions that ultimately collapsed, bringing the pathogen back to the primary infected cell (Figure 2.4B, Wild Type, dark blue, protrusion failure) and 11% failed to escape from DMVs (Figure 2.4B, Wild Type, yellow, DMV escape failure).

In contrast with wild type bacteria, tracking analysis revealed that 37% of the *icsB* mutant strain that formed protrusions successfully spread to the adjacent cell (Figure 2.4B, *icsB*, green, DMV escape). Similar to wild type, a small percentage of bacteria failed in protrusions that collapsed, bringing the pathogen back to the primary infected cell (Figure 2.4B, *icsB*, dark blue, protrusion failure). In contrast with wild type bacteria for which only a minority of spreading bacteria failed to escape vacuoles (11%), the majority of the *icsB* bacteria (53%) failed to escape DMVs and remained trapped in a membrane bound compartment (Figure 2.4B, *icsB*, yellow, DMV escape failure). A total of 147 wild type and 147 *icsB* bacteria were tracked for at least 3 hours in three independent experiments. We found similar values among our three independent experiments (Figure 2.5). Taken together, these results indicate that the T3SS effector protein IcsB promotes cell-to-cell spread through escape from double membrane vacuoles.

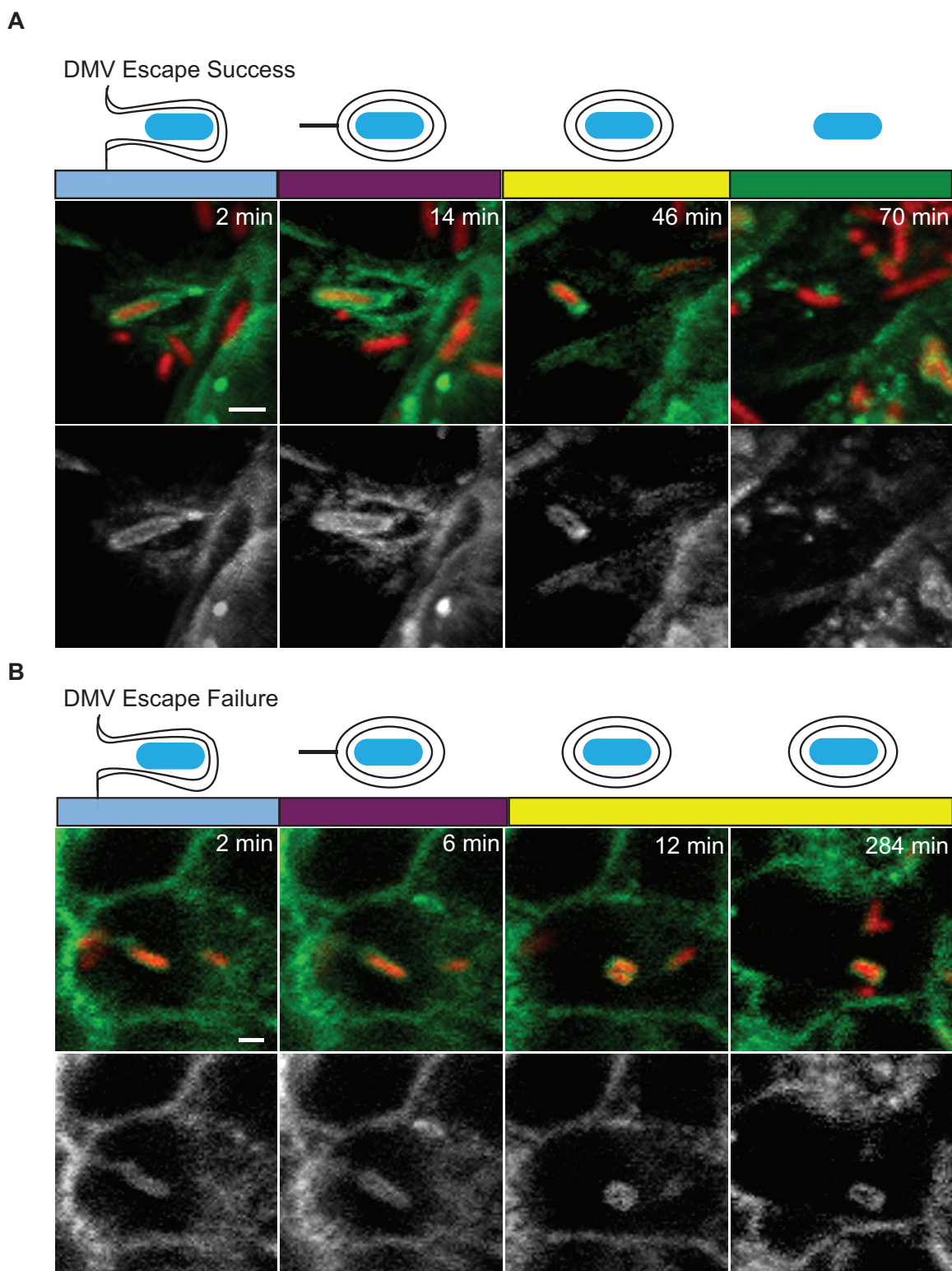


**Figure 2.3: Tracking individual bacteria using time-lapse microscopy of HT-29 cells expressing plasma membrane-targeted YFP and infected with CFP-expressing *S. flexneri*. (A, B) Representative images showing the progression of a single bacterium**

over time. For each panel, the top image shows a merged image of bacteria (red, pseudo-color) and plasma membrane (green, pseudo-color) and the bottom images show plasma membrane only. The schematic at the top of each panel shows stage and corresponding color code of spread progression as used in figure 3 **(A)** Successful progression of a bacterium from the primary cell cytoplasm into a membrane protrusion (2 min, Protrusion) that resolves into a vacuole-like protrusion (14 min, VLP), then a double membrane vacuole (46 min, DMV) from which the bacterium escape and gains access to the cytoplasm of the adjacent cell (70 min, Free bacteria). **(B)** Unsuccessful progression of a bacterium from the primary cell cytoplasm into a membrane protrusion (2 min, Protrusion) that resolves into a vacuole-like protrusion (6 min, VLP) and then a double membrane vacuole (12 min, DMV) and remains trapped in the DMV (284 min, DMV). Green, plasma membrane; Red, Shigella. Scale bar, 2  $\mu\text{m}$ .

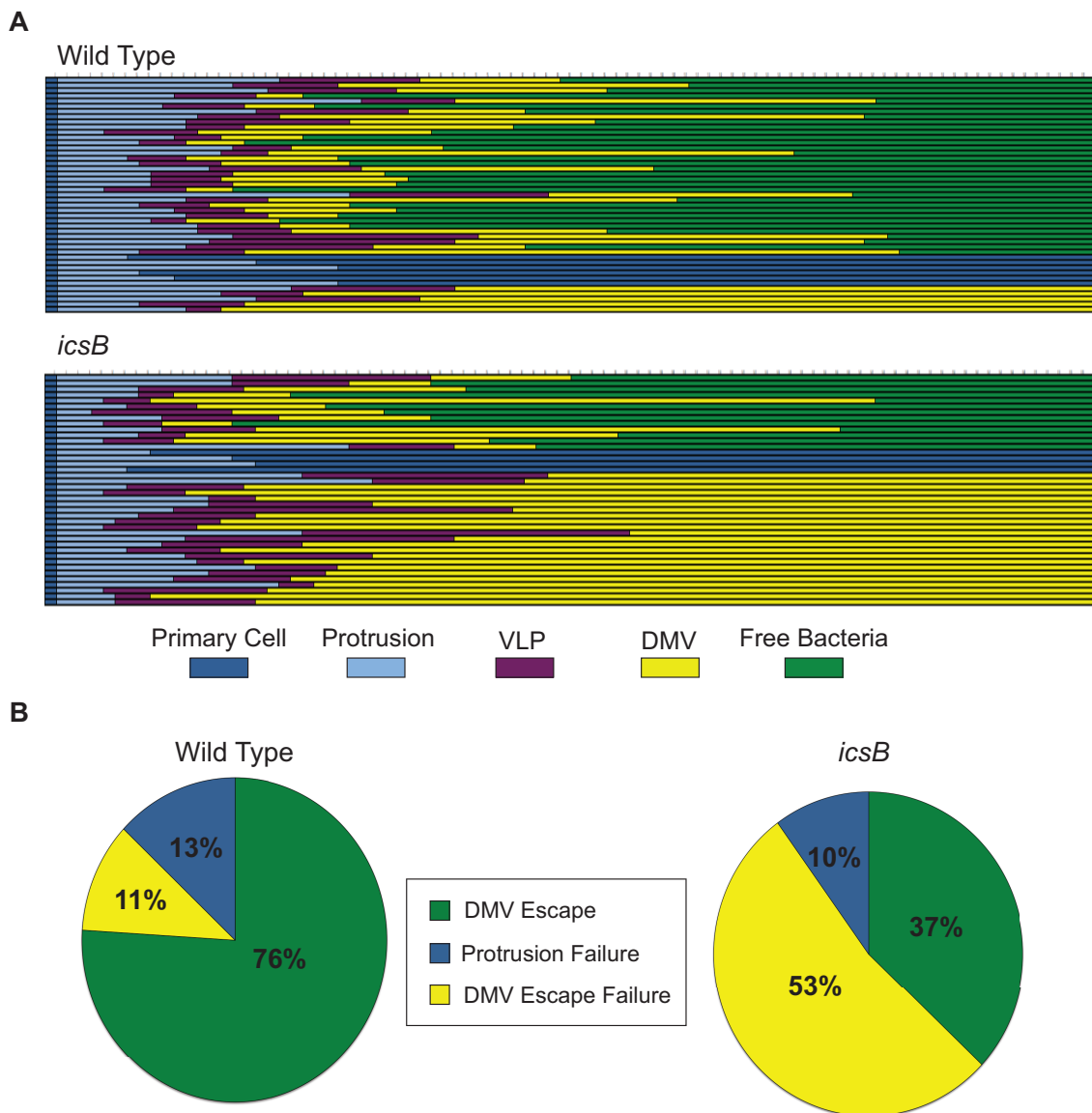


**Figure 2.4: The *icsB* mutant displays a DMV escape defect** (A) Representative tracking analysis of WT (top) or *icsB* (bottom) bacteria in HT-29 cells. Each line represents tracking of one bacterium for 180 minutes. The progression of the dissemination process was depicted using the following color key: Primary cell, dark blue; Protrusion, light blue; VLP, purple; Double membrane vacuole, yellow; Free bacteria in adjacent cell, green. Forty bacteria were tracked in 8 independent infection foci per strain. (B) Graphs showing the relative proportion of fates of tracked bacteria in 3A for wild type (left) or *icsB* (right). Protrusion failure back to primary cell, dark blue; double membrane vacuole escape failure, yellow; double membrane vacuole escape, green.

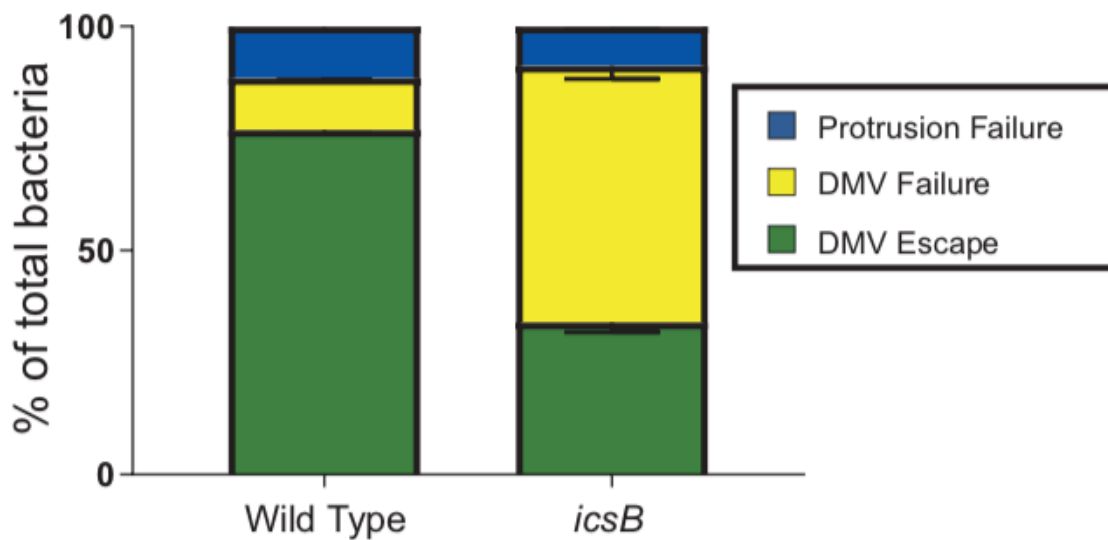


**Figure 2.5: Tracking analysis of *S. flexneri* during cell-to-cell spread** Graph showing the relative proportion of fates of tracked bacteria for wild type (left) or *icsB* (right). Protrusion failure back to primary cell, dark blue; double membrane vacuole escape failure, yellow; double membrane vacuole escape, green; Error bars represent standard error of the mean of three independent experiments. At least 40 bacteria per strain were tracked in each experiment.

### 2.4.3 The autophagy marker LC3 is exclusively recruited to DMVs

IcsB has been previously suggested to counteract the recruitment of the LC3 marker to cytosolic bacteria (84). However, a recent report suggested instead that IcsB was required for escaping LC3-positive DMVs (51). In order to clarify the spatial and temporal recruitment of LC3 to *S. flexneri* during cell-to-cell spread, we used HT-29 cell lines that express mCherry-LC3 in combination with plasma membrane targeted-YFP. The distinction between LC3-negative (LC3<sup>-</sup>) bacteria (Figure 2.6A, LC3<sup>-</sup> DMV) and LC3-positive (LC3<sup>+</sup>) bacteria (Figure 6A, LC3<sup>+</sup> DMV) was made based on the recruitment of mCherry-LC3 around CFP-expressing bacteria (Figure 2.6A, LC3<sup>+</sup> DMV, mCherry-LC3). We first used the approach to quantify the ratio of LC3<sup>+</sup> bacteria per total number of bacteria in infected cells. As previously described (51, 84), we observed an increase in LC3<sup>+</sup> bacteria in cells infected with *icsB* (Figure 2.6B). We next used time-lapse confocal microscopy to track the progression of individual bacteria and simultaneously the recruitment of mCherry-LC3. Figure 2.7 shows the representative tracking of 40 wild type (Figure 2.7A, wild type) and 40 *icsB* (Figure 2.7A, *icsB*) bacteria from a single experiment. Dark blue shading at the beginning of each track represents the location of the bacterium in the primary infected cell cytosol. Light blue shading indicates the bacterium in protrusions, purple indicates the bacterium in a VLP, and yellow shading refers to a

bacterium in a DMV. Red shading denotes a bacterium in a DMV to which LC3 has been recruited. Green shading indicates that the YFP membrane was no longer visible and the bacterium has regained actin-based motility, showing that it was free in the cytosol of the adjacent cell. A total of 147 wild type and 147 *icsB* bacteria were tracked for at least 3 hours in three independent experiments. We found similar values among our three independent experiments (Figure 2.8). In all cases of LC3 recruitment to CFP-positive bacteria (N=57), back-tracking of the bacteria revealed that LC3 was recruited to plasma membrane-YFP positive DMVs that derived from plasma membrane-YFP positive protrusions formed during cell-to-cell spread. LC3 was never recruited to plasma membrane-YFP positive protrusions or VLPs, or to plasma membrane-YFP negative (cytosolic) bacteria. These experiments provide the unambiguous demonstration that the LC3 autophagy marker is only recruited to *S. flexneri* when bacteria are located in plasma membrane vacuoles that derive from the membrane protrusions formed during cell-to-cell spread, i.e. DMVs.

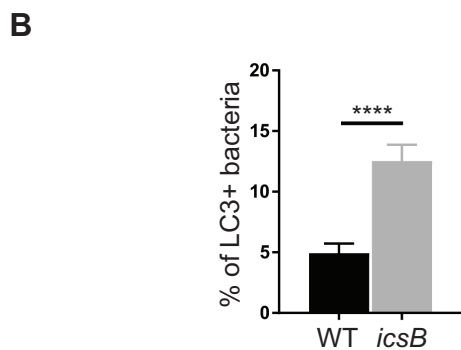
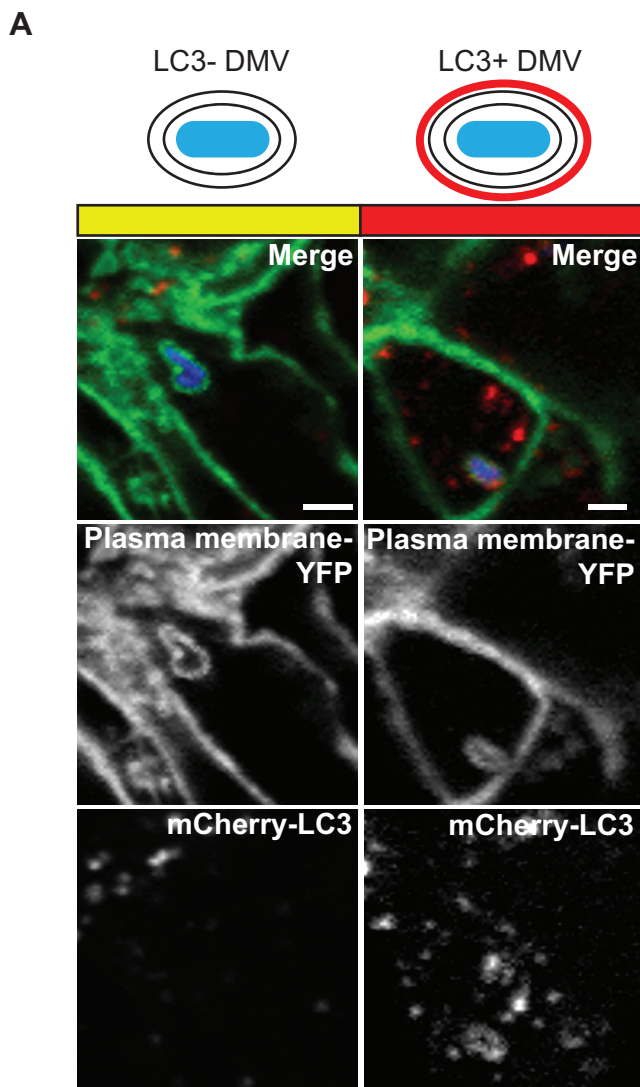


**Figure 2.6: Tracking LC3 recruitment using HT-29 cells expressing LC3-mCherry and plasma membrane-targeted YFP, and infected with CFP-expressing *S. flexneri* (A)** Representative images of cells expressing LC3-mCherry and plasma membrane targeted YFP infected with CFP-expressing *S. flexneri*. Panels on the left show example where LC3-mCherry is not recruited to DMV (LC3<sup>-</sup> DMV, yellow bar) and right panels show example where LC3-mCherry is recruited to DMV (LC3<sup>+</sup> DMV, red bar). Scale bar, 2 $\mu$ m

**(B)** Graph shows percentage of wild type (black) or *icsB* (gray) bacteria associated with LC3 4 hours post-infection. Error bars represent standard error of the mean of three independent experiments. Total bacteria from 8 infection foci per strain were counted in each experiment. \*\*\*\*,  $p < 0.0001$ ; unpaired t-test.

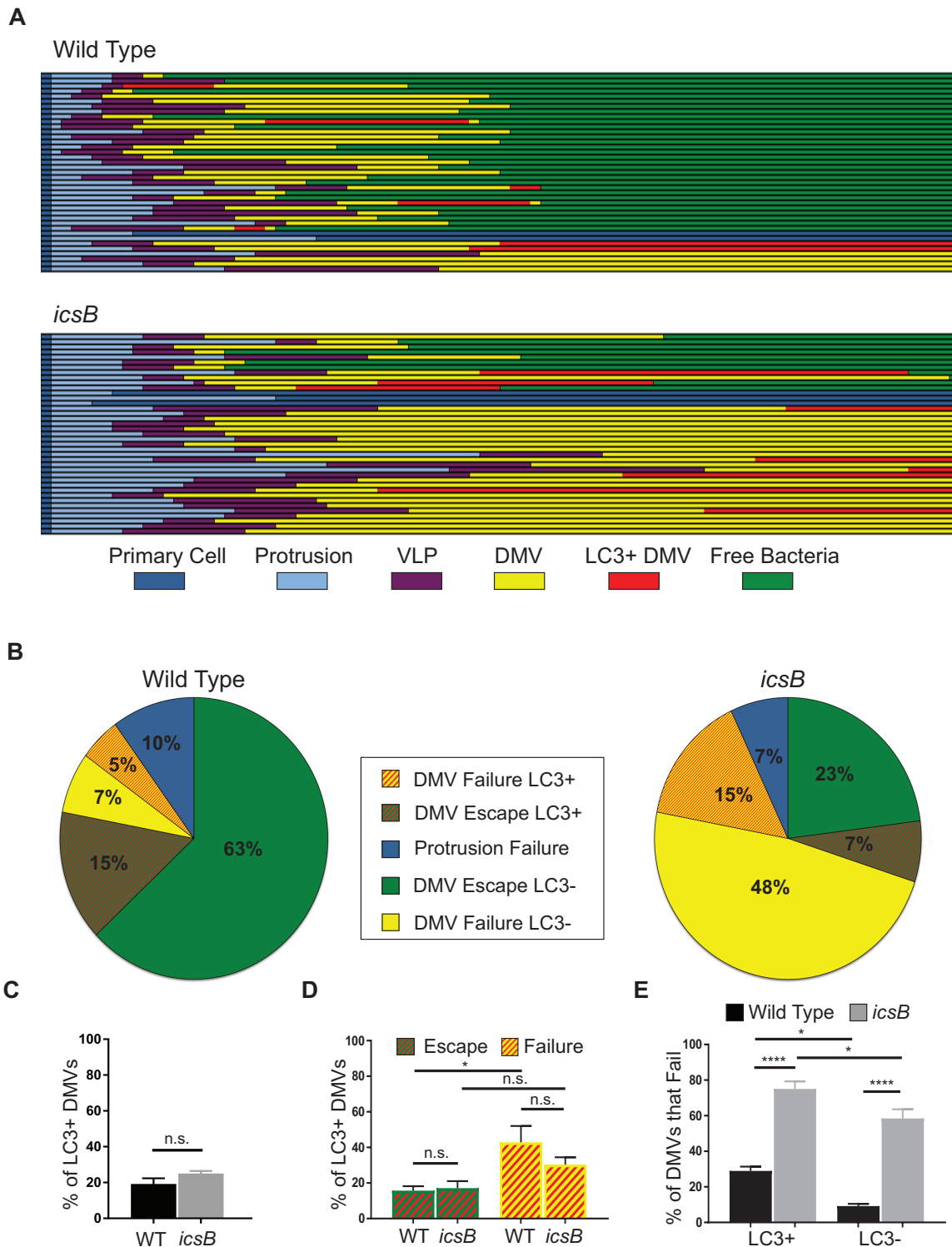


**Figure 2.7: LC3 is recruited equally to double membrane vacuoles containing wild type or *icsB* mutant bacteria (A)** Representative tracking analysis of dissemination and LC3 recruitment for wild type (top) or *icsB* (bottom) bacteria. Each line represents tracking of one bacterium for 180 minutes. The progression of the dissemination process was depicted using the following color key: Primary cell, dark blue; Protrusion, light

blue; VLP, purple; LC3<sup>-</sup>DMV, yellow; LC3<sup>+</sup>DMV, red; Free bacteria in adjacent cell, green. **(B)** Graphs showing the relative proportion of fates of tracked bacteria in 5A for wild type (left) or *icsB* (right). Protrusion failure back to primary cell, dark blue; LC3<sup>-</sup> double membrane vacuole escape failure, yellow; LC3<sup>+</sup> double membrane vacuole escape failure, yellow with red stripes; LC3<sup>-</sup> double membrane vacuole escape, green; LC3<sup>+</sup> double membrane vacuole escape, green with red stripes. **(C)** Graph depicting the percentage of DMVs that recruited LC3 for wild type or *icsB* **(D)** Graph depicting the percentage of DMVs that recruited LC3 for wild type or *icsB* grouped according to DMV escape (green and red) or DMV escape failure (yellow and red) **(E)** Graph depicting the percentage of DMVs escape failure among wild type or *icsB* bacteria grouped according to LC3<sup>+</sup> or LC3<sup>-</sup> DMVs. **(C-E)** At least 40 bacteria were tracked per experiment. Error bars indicate standard error of the mean of three independent experiments. n.s., not significant; \*,  $p < 0.05$ ; \*\*\*,  $p < 0.0001$ ; unpaired t-test or one-way ANOVA with multiple comparisons.

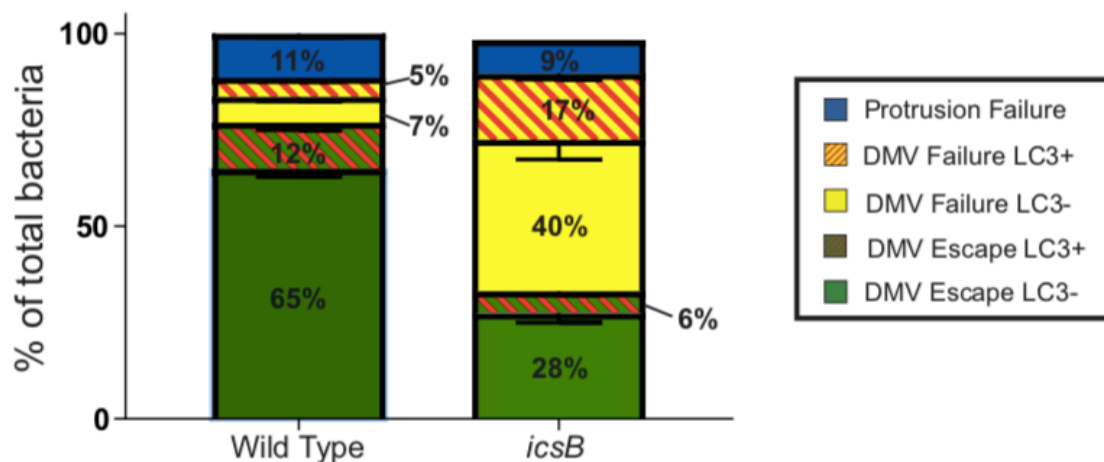


**Figure 2.8: Tracking analysis of LC3 recruitment to DMVs during cell-to-cell spread**  
 Graph showing the relative proportion of fates of tracked bacteria for wild type (left) or *icsB* (right). Protrusion failure back to primary cell, dark blue; LC3- double membrane vacuole escape failure, yellow; LC3+ double membrane vacuole escape failure, yellow with red stripes; LC3- double membrane vacuole escape, green; LC3+ double membrane vacuole escape, green with red stripes. Error bars represent standard error of the mean of three independent experiments. At least 40 bacteria per strain were tracked in each experiment.

#### **2.4.4 LC3 is recruited equally to the DMVs containing wild type bacteria or the *icsB* mutant**

The increased numbers of LC3<sup>+</sup> bacteria in cells infected with the *icsB* mutant (51, 84) (Figure 2.6B) may reflect a potential role for IcsB in counteracting the recruitment of the LC3-dependent autophagy machinery to DMVs.

Alternatively, wild type bacteria and the *icsB* mutant could recruit LC3 equally in the course of cell-to-cell spread, but vacuole escape failure of the *icsB* mutant may lead to an accumulation of LC3<sup>+</sup> vacuoles over time in cells infected with the *icsB* mutant, and therefore show an increased numbers of LC3<sup>+</sup> bacteria in infected cells. To determine whether DMVs harboring the *icsB* mutant recruited LC3 more frequently than wild-type, we tracked individual DMVs that derived from protrusion during cell to cell spread, and determined the percentage of DMVs that became LC3-positive. We found no significant difference in the percentage of DMVs that recruited LC3 in cells infected with wild type or the *icsB* mutant (Figure 2.7C, Wild Type vs. *icsB*). We further examined whether comparing bacteria in groups according to their success or failure to escape DMVs may reveal differences in LC3 recruitment. However, we found no difference in LC3 recruitment between the wild type strain and the *icsB* mutant strain among bacteria that escaped DMVs (Figure 2.7D, Wild Type vs. *icsB*, Escape, green and red bars), or failed to escape DMVs (Figure 2.7D, Wild Type

vs. *icsB*, Failure, yellow and red bars). Thus, LC3 is not recruited more frequently to the *icsB* mutant relative to the number of bacteria in DMVs, and the increased numbers of LC3<sup>+</sup> bacteria in cells infected with the *icsB* mutant is a consequence of the increased numbers of DMVs due to vacuole escape failure.

#### **2.4.5 The *icsB* mutant fails to escape from LC3<sup>+</sup> as well as LC3<sup>-</sup> DMVs**

Since IcsB has been previously implicated in escape from LC3<sup>+</sup> vacuoles (51), we investigated whether there was a difference in DMV escape failure between the wild type strain and the *icsB* mutant strain depending on their location in LC3<sup>-</sup> or LC3<sup>+</sup> DMVs. As previously shown (51), the *icsB* mutant strain was significantly impaired in escape from LC3<sup>+</sup> DMVs compared to the wild type strain (Figure 2.7E, LC3<sup>+</sup>, Wild Type vs. *icsB*). However, the *icsB* mutant was equivalently defective in escaping from LC3<sup>-</sup> DMVs compared to the wild type strain (Figure 2.7E, LC3<sup>-</sup>, Wild Type vs. *icsB*). These results show that the *icsB* mutant is significantly impaired in escape from DMVs, regardless of LC3 recruitment.

#### **2.4.6 IcsB promotes prompt escape from DMVs**

We also analyzed a potential role for IcsB in the dissemination of bacteria that successfully escaped DMVs. We observed a modest increase in the time

spent in protrusions by the *icsB* mutant compared to wild type bacteria (Figure 2.9A), and no significant increase in the time spent in VLPs (Figure 2.9B). However, the time spent in DMVs before escape was significantly increased in cells infected with the *icsB* mutant compared to wild type bacteria (65 minutes vs. 40 min; Figure 2.10A), showing that IcsB is required for prompt escape from DMVs. We next investigated the impact of LC3 recruitment on the time until DMV escape. The results revealed a significant delay in DMV escape of wild type bacteria from LC3<sup>+</sup> DMVs (Figure 2.10B, LC3<sup>+</sup>, wild type, black) compared to LC3<sup>-</sup> DMVs (Figure 2.10B, LC3<sup>-</sup>, wild type, black). The same trend was observed for the *icsB* mutant, although the difference was not statistically significant. Importantly, there was a significant increase in time until escape between wild type and the *icsB* bacteria that resided in LC3<sup>-</sup> DMVs (Figure 2.10B, LC3<sup>-</sup>, Wild type vs. *icsB*). Collectively, the results indicate that the *icsB* mutant displays delayed vacuole escape (Figure 2.10) or fails to escape (Figure 2.7), even in absence of LC3 recruitment to DMVs. These results are therefore not in agreement with the notion that the role of IcsB is to counteract LC3 recruitment to DMVs.

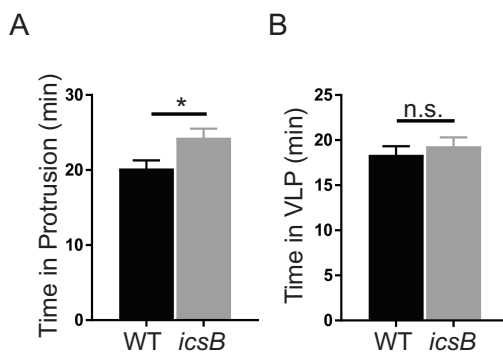


**Figure 2.9: The *icsB* mutant is not delayed in protrusions or VLPs** Graph shows average time in protrusions (A) or vacuole-like protrusions (B) of wild type or *icsB* bacteria. Data from three independent experiments is shown. Error bars indicate standard error of the mean. n.s., not significant; \*,  $p < 0.05$ ; unpaired t-test.

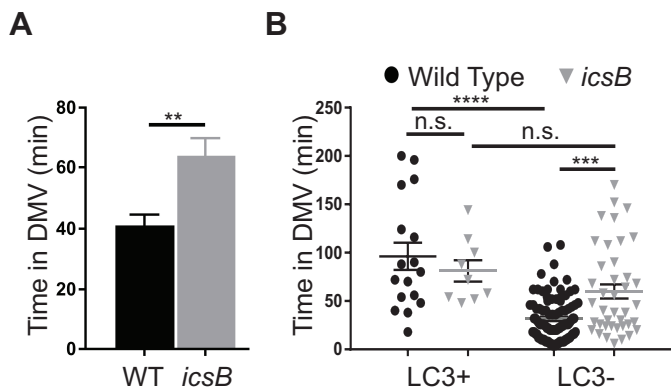


**Figure 2.10: IcsB promotes prompt escape from DMVs (A)** Graph shows the time spent by bacteria in DMVs before escape for wild type and *icsB*. **(B)** Graph shows the time spent by bacteria in DMVs before escape for wild type and *icsB* grouped according to LC3<sup>+</sup> or LC3<sup>-</sup>. Data from three independent experiments is shown. Error bars indicate standard error of the mean of three independent experiments. n.s., not significant; \*\*, p<0.005; \*\*\*, p<0.001; \*\*\*\*, p<0.0001; unpaired t-test or one-way ANOVA with multiple comparisons.

#### **2.4.7 LC3 recruitment correlates with, but is not the cause of vacuole escape failure**

The recruitment of LC3 to *S. flexneri* has been proposed to reflect the role of the LC3-dependent machinery as host cell defense mechanism. Accordingly, we found that LC3 recruitment correlated with escape failure as reflected by the observed increase in LC3 DMVs among wild type bacteria that failed to escape (Figure 2.7D) and the observed increase in vacuole escape failure among wild type bacteria that resided in LC3<sup>+</sup> DMVs (Figure 2.7E). In addition, we found that LC3 recruitment correlated with increased time spent in vacuole until escape of wild type bacteria (Figure 2.10B). To further investigate the exact role of LC3 recruitment, we determined the time until LC3 recruitment to DMV in groups of bacteria according to their success or failure to escape DMVs. Surprisingly, among the bacteria that recruited LC3 to DMVs, both wild type and *icsB* bacteria that successfully escaped DMVs recruited LC3 more rapidly than bacteria that failed to escape DMVs (Figure 2.11A, escape vs. fail to escape). Moreover, among bacteria that successfully escaped vacuoles, we found a positive correlation between the time of LC3 recruitment and the time until escape (Figure 2.11B). Thus, early LC3 recruitment correlates with prompt escape, and late LC3 recruitment correlates with delayed escape, or escape failure. These results strongly suggest that, when recruited to DMVs from which bacteria fail to

escape, LC3 recruitment is the consequence and not the cause of vacuole escape failure.

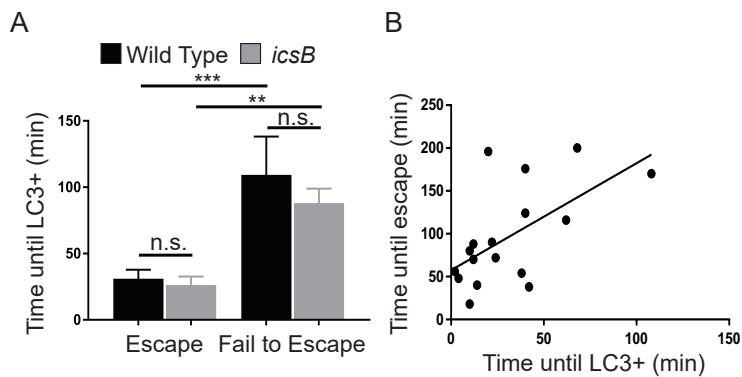


**Figure 2.11: Positive correlation between the time until escape and the time until LC3 recruitment (A)** Graph shows average time in DMV before LC3 recruitment for wild type or *icsB* bacteria grouped according to vacuole escape success or failure. Error bars indicate standard error of the mean from three independent experiments. n.s., not significant; \*,  $p < 0.05$ ; \*\*,  $p < 0.005$ ; one-way ANOVA with multiple comparisons. **(B)** Graph shows time until DMV escape vs. time until LC3 recruitment for wild type bacteria. Data from three independent experiments is shown. Pearson  $r = 0.597$ ; correlation significant,  $p < 0.05$ .

#### 2.4.8 LC3-dependent autophagy does not inhibit *S. flexneri* spread from cell to cell

To further investigate the role of the LC3-dependent autophagy machinery in *S. flexneri* spread from cell to cell, we inhibited steps of autophagy with Bafilomycin A1 (Baf-A1), chloroquine, NH<sub>4</sub>Cl or 3-MA treatments. Baf-A1 interferes with autophagy by preventing the fusion of autophagosomes with lysosomes. We found no difference in the size of the foci formed by the *icsB* mutant in cells treated with DMSO or Baf-A1 (Figure 2.12A, *icsB*, DMSO vs. Baf-A1), indicating that Baf-A1 does not rescue the spreading defect displayed by the *icsB* mutant. We noticed, however, that the foci formed by the wild type strain in the presence of Baf-A1 were significantly smaller compared to DMSO treatment (Figure 2.12A, WT, DMSO vs. Baf-A1, 35% decrease). Additionally, treatment with Baf-A1 also affected the size of the infection foci formed by the complemented *icsB* mutant (Figure 2.12A, *icsB p<sub>icsB</sub>*, DMSO vs. Baf-A1, 50% decrease). We found similar results when cells were treated with the acidification inhibitors chloroquine (Figure 2.12B) and NH<sub>4</sub>Cl (Figure 2.12C), or when treated with the specific PI3KC3 inhibitor, 3-MA (Figure 2.12D). To specifically assess the role of LC3 in dissemination, we measured the effect of LC3-depletion by siRNA on *S. flexneri* dissemination. We found no significant differences in the sizes of foci formed by wild type, *icsB* mutants, or the

complemented *icsB* mutants in mock treated cells and LC3-depleted cells (Figure 2.13). Taken together, our results indicate that inhibition of LC3 by siRNA or chemical inhibition of important steps of autophagy has no positive impact on the spreading efficiency of wild type or *icsB* mutant bacteria, suggesting that the LC3-dependent autophagy machinery does not interfere with *S. flexneri* dissemination.

In summary, this study demonstrates that (i) IcsB is required for DMV escape, (ii) the autophagy marker LC3 is exclusively recruited to DMVs, (iii) IcsB does not counter LC3 recruitment to DMVs, (iv) the recruitment of LC3 to DMVs is not the cause, but the consequence of vacuole escape failure, and (vi) the LC3-dependent autophagy machinery does not restrain *S. flexneri* spread from cell to cell.

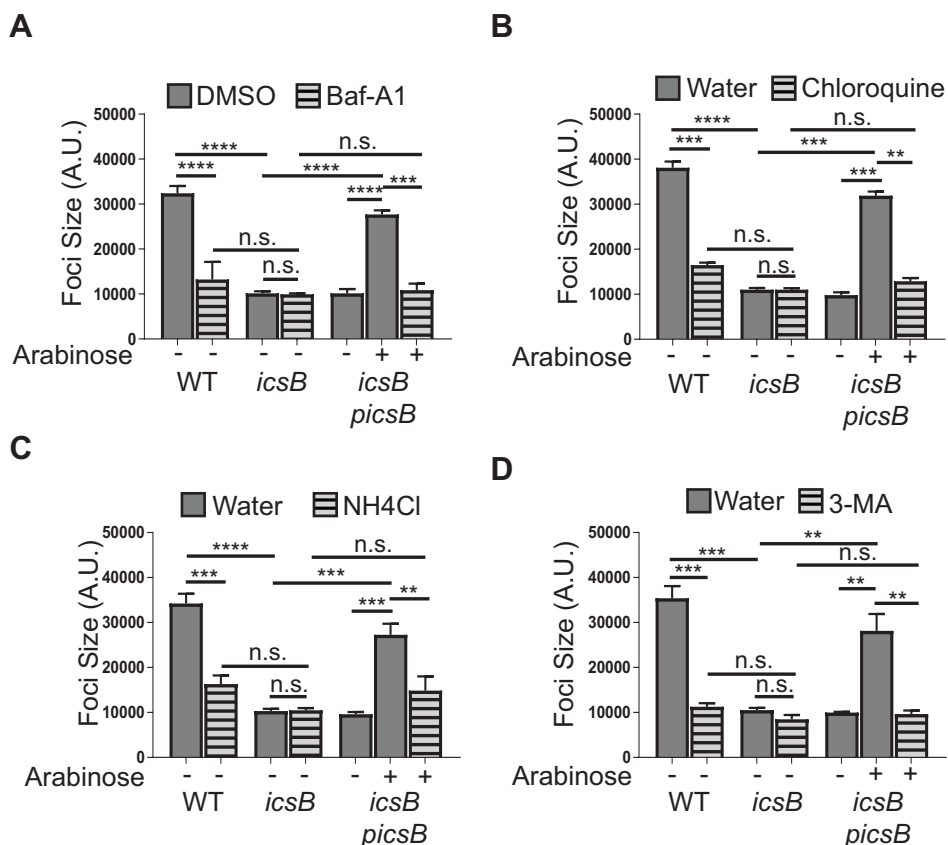


### Figure 2.12: Autophagy does not inhibit *S. flexneri* spread from cell to cell

Quantification of area of infection focus of wild type, *icsB*, or *icsB/picsB* in HT-29 cells treated with 200nM Bafilomycin A1 (A) 10 $\mu$ M Chloroquine (B) 10mM NH<sub>4</sub>Cl (C) or 6.7 mM 3-methyladenine. *picsB* is under the control of an arabinose inducible promoter. Uninduced and 1% arabinose induced conditions are shown. Arabinose and inhibitors were added 1 hour post-infection. Computer-assisted image analysis was used to measure foci size. 50 foci per experiment were measured. Error bars represent standard error of mean of three independent experiments; n.s., not significant; \*\*, p<0.005; \*\*\*, p<0.001; \*\*\*\*, p<0.0001; one-way ANOVA with multiple comparisons.

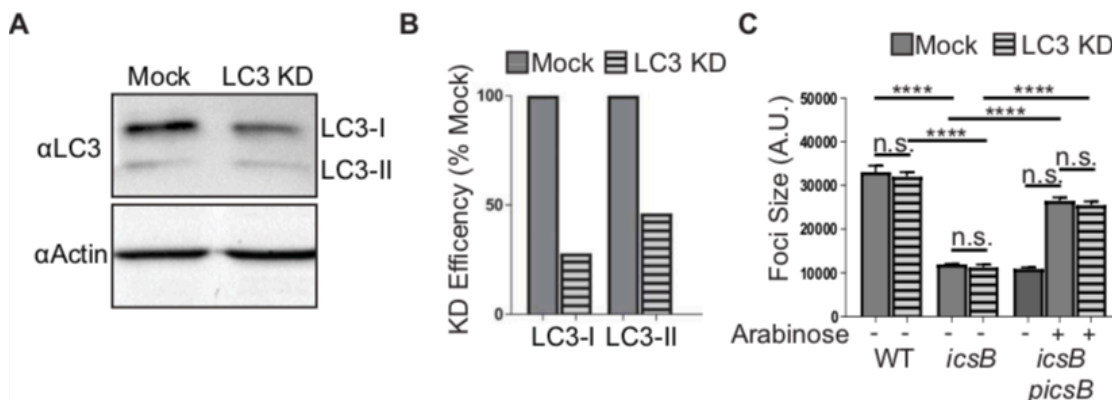


**Figure 2.13: LC3 does not inhibit *S. flexneri* spread from cell to cell** (A) Western blot of HT-29 cell lysates after treatment with transfection reagent alone (Mock) or a pool of four siRNA duplexes targeting LC3. Blots were probed for LC3 or actin control. (B) Quantification of knockdown efficiency relative to mock treatment and normalized to actin loading control (C) Quantification of area of infection focus of wild type, *icsB*, or *icsB/picsB* in HT-29 cells treated with mock or siRNA targeting LC3. *picsB* is under the control of an arabinose inducible promoter. Uninduced and 1% arabinose induced conditions are shown. Arabinose was added 1 hour post-infection. Computer-assisted image analysis was used to measure foci size. For each experiment, 50 infection foci were measured. Error bars represent standard error of mean of three independent experiments; n.s., not significant; \*\*\*\*,  $p < 0.0001$ ; one-way ANOVA with multiple comparisons.

## 2.5 Discussion

The homeostatic cellular process of autophagy plays an important role in host defense against infection with numerous intracellular pathogens. In particular, recruitment of the LC3-dependent autophagy machinery to intracellular bacteria has been proposed to act as host cell defense against the intracellular human pathogen *Shigella flexneri* (101). However, a controversy recently emerged in the field regarding the sub-cellular compartment where this defense mechanism takes place. In a first study conducted by Sasakawa and colleagues, it was proposed that the autophagy marker LC3 was recruited to cytosolic bacteria (84). However, in a later study conducted by Parsot and colleagues, LC3 was shown to be recruited to bacteria displaying an actively secreting T3SS, which are located in membrane-bound compartments (51). Here, we used live microscopy to track *S. flexneri* during the dissemination process and provided the unambiguous demonstration that LC3 is uniquely recruited to bacteria when located in the double membrane vacuoles that derive from the membrane protrusions formed during cell-to-cell spread.

Previous reports uncovered that bacteria lacking the type three secreted effector IcsB were more frequently associated with LC3. IcsB was therefore proposed to counter the entrapment of *S. flexneri* in LC3-positive compartments targeted for degradation (51, 84, 102). IcsB was first proposed to prevent the

autophagic recognition of cytosolic *S. flexneri* by blocking recognition of the autotransporter IcsA by Atg5 (84). More recently, IcsB was proposed to enable escape from LC3-positive membrane compartments through an unknown mechanism (51). Here, we demonstrate that IcsB is required for efficient DMV escape during cell-to-cell spread. However, our results uncover that the role of IcsB in vacuole escape is not related to counteracting LC3 recruitment, as our tracking experiments visualizing the plasma membrane revealed that *icsB* bacteria were trapped in LC3-positive as well as LC3-negative DMVs. To our knowledge, this is the first demonstration that IcsB facilitates DMV escape through a mechanism that is unrelated to counteracting the LC3-dependent autophagy machinery. IcsB is also the first type three effector protein to be identified to specifically contribute to escape from the double membrane vacuoles formed during cell-to-cell spread. Bioinformatics have predicted that IcsB could function as a protease or an acyltransferase (103). IcsB could thus degrade or modify vacuolar component(s), thereby challenging the integrity of the DMV membrane and promoting bacterial escape. Future studies will uncover the mechanism supporting DMV escape and the exact function of IcsB in this process.

We note that a small proportion of *icsB* bacteria were delayed in vacuole escape, but still able to successfully escape DMVs, indicating the existence of an

IcsB-independent mechanism contributing to DMV escape. This pathway may involve additional type three effector proteins. Similar to bacteria lacking *icsB*, bacteria lacking *virA* were more frequently associated with LC3-positive vacuoles (51), suggesting that, in addition to IcsB, VirA could also contribute to vacuole escape. While VirA was shown to have a GAP activity *in vitro* (104), its exact role in vacuole escape is unknown. Interestingly, the type three effector protein IpgD was shown to be required for prompt escape from primary vacuoles upon invasion, and may also be a candidate effector protein involved in DMV escape during cell-to-cell spread (105).

Surprisingly, our data uncovered that early recruitment of LC3 to the *Shigella*-containing vacuoles formed during cell-to-cell spread correlated with prompt escape of bacteria from DMVs. LC3-dependent autophagy has been shown to contribute to endosomal membrane integrity in the context of other intracellular pathogens (50, 106, 107). Interestingly, the LC3-dependent autophagy machinery was shown to be recruited to the *Salmonella*-containing vacuoles (SCVs) early during infection, in a manner dependent on the integrity of the type three secretion system (50). It was proposed that the membrane damages inflicted by the *Salmonella* type three-secretion system lead to LC3 recruitment to SCVs, reflecting a role for the autophagy machinery in repairing damaged membrane. It is therefore tempting to speculate that the early

recruitment of LC3 to *S. flexneri* containing vacuoles is a consequence of the activity of the T3SS, which is required for DMV escape (76). Consistently, LC3 has been shown to be recruited to actively secreting *S. flexneri* during infection (51). DMV escape may thus be viewed as a consequence of failure of the autophagy machinery to repair the T3SS-damaged membrane. Whether the bacteria are actively engaged in that process remains to be determined.

While our work strongly suggests that the role of IcsB is not to counteract LC3 recruitment to DMVs, it also indicates that the recruitment of the LC3-dependent autophagy machinery does not restrain dissemination of wild type bacteria. Importantly, our tracking experiments not only revealed that early LC3 recruitment predicted vacuole escape success, but also demonstrated that vacuole escape failure correlated with late LC3 recruitment. These results clearly show that LC3 recruitment is not the cause but the consequence of vacuole escape failure. We therefore speculate that, in case of failure, prolonged residency of bacteria in vacuoles, perhaps due to deficient type three secretion, ultimately leads to DMV fusion with autophagosomes/lysosomes. It is noteworthy that these instances of LC3 recruitment represent a very small proportion of spreading bacteria. Neither drug-mediated inhibition of steps involved in autophagy nor genetic interference of LC3 enhanced the spreading efficiency of wild type or *icsB* bacteria, supporting the notion that LC3-

dependent autophagy does not significantly interfere with *S. flexneri* dissemination. In fact, chemical inhibition of autophagic effects had a negative impact on cell-to-cell spread of wild type bacteria, potentially indicating a previously unappreciated role for autophagosome formation in particular, or vacuolar acidification in general, in *S. flexneri* dissemination, through an unknown mechanism.

### **3. Chapter 3: The type three secretion system effector protein IpgB1 promotes *S. flexneri* cell-to-cell spread through double-membrane vacuole escape**

This chapter is a modified version of the previously published article: Weddle EA, Köseoğlu VK, DeVasure BA, Agaisse HF. “The type three secretion system effector protein IpgB1 promotes *S. flexneri* cell-to-cell spread through double-membrane vacuole escape” PLOS Pathogens. 18(2): e1010380. 2022 February. doi: 10.1371/journal.ppat.1010380

Experimental Contributions: Weddle, EA designed and performed all tissue culture experiments, analyzed all data, wrote and edited the manuscript, and created all figures. Köseoğlu, VK and Agaisse, HF conducted rabbit experiments and prepared tissues for imaging. DeVasure, BA stained and imaged rabbit tissue sections. Agaisse, HF supported all aspects of the work.

### 3.1 Summary

*S. flexneri* is an important human pathogen that causes bacillary dysentery. During infection, *S. flexneri* invades colonic epithelial cells, hijacks the host cell cytoskeleton to move in the cytosol of infected cells, and spreads from cell to cell through formation of membrane protrusions that project into adjacent cells and resolve into double membrane vacuoles (DMVs). *S. flexneri* cell-to-cell spread requires the integrity of the bacterial type three secretion system (T3SS). However, the exact role of the T3SS effector proteins in the dissemination process remains poorly understood. Here, we investigated the role of the T3SS effector protein IpgB1 in *S. flexneri* dissemination. IpgB1 was previously characterized as a guanine nucleotide exchange factor (GEF) that contributes to invasion. In addition to the invasion defect, we showed that the *ipgB1* mutant formed smaller infection foci in HT-29 cells. Complementation of this phenotype required the GEF activity of IpgB1. Using live confocal microscopy, we showed that the *ipgB1* mutant is specifically impaired in DMV escape. Depletion of Rac1, the host cell target of IpgB1 during invasion, as well as pharmacological inhibition of Rac1 signaling, reduced cell-to-cell spread and DMV escape. In a targeted siRNA screen, we uncovered that RhoA depletion restored *ipgB1* cell-to-cell spread and DMV escape, revealing a critical role for the IpgB1-Rac1 axis in antagonizing RhoA-mediated restriction of DMV escape. Using an infant rabbit model of

shigellosis, we showed that the *ipgB1* mutant formed fewer and smaller infection foci in colons of infected animals, which correlated with attenuated symptoms of disease, including epithelial fenestration and bloody diarrhea. Our results demonstrate that, in addition to its role during invasion, IpgB1 modulates Rho family small GTPase signaling to promote cell-to-cell spread, DMV escape, and *S. flexneri* pathogenesis.

### 3.2 Introduction

The hallmark of *S. flexneri* infection is invasion of colonic epithelial cells and intercellular dissemination, leading to destruction of the mucosa and bloody diarrhea (23, 24). The process of intercellular dissemination is critical for *S. flexneri* pathogenesis (23), emphasizing the importance of understanding the cellular and molecular mechanisms that support this process.

*S. flexneri* encodes a type three secretion system (T3SS) and an arsenal of approximately twenty-five T3SS effector proteins, which manipulate host cell processes during infection. *S. flexneri* uses its T3SS to induce its uptake into nonphagocytic epithelial cells and to escape from primary vacuoles following uptake (108). In the cytosol, *S. flexneri* hijacks the host actin cytoskeleton through expression of the autotransporter protein IcsA, leading to bacterial actin-based motility (ABM) (109). As bacteria collide with cell junctions, they deform the

plasma membrane and protrude into neighboring cells. Membrane protrusions are then resolved into vacuole-like protrusions (VLPs) that resolve into double-membrane vacuoles (DMVs) in neighboring cells. The bacteria then escape from DMVs and resume ABM and cell-to-cell spread (76, 110, 111). The T3SS is required for cell-to-cell spread and more recently, the T3SS effector IcsB, an N $\epsilon$ -fatty acyltransferase, was shown to be required specifically for DMV escape during dissemination (51, 111, 112). IcsB is not the only factor facilitating DMV escape, as a proportion of *icsB* bacteria still manage to escape from DMVs, albeit a delayed process (111). Mutants that are T3SS deficient, completely fail to escape from DMVs, suggesting that additional effectors may be involved in DMV escape. However, the roles of additional effector(s) in the dissemination remain elusive.

As the process of intercellular dissemination relies on bacterial manipulation of host cytoskeleton and membrane, we became interested in T3SS effectors IpgB1 and IpgB2, two bacterial guanine nucleotide exchange factors (GEFs) that regulate Rho family small GTPases (113). Both IpgB1 and IpgB2 are members of a protein family of bacterial effectors defined by a conserved tryptophan-xxx-glutamic acid (WxxxE) motif. Functional and structural insights revealed that IpgB1 and IpgB2 are in fact bacterial GEFs and provided a mechanism for specificity and activation of Rac1 and RhoA by IpgB1 and IpgB2,

respectively (41, 114). IpgB1 and IpgB2 were investigated for their roles in *S. flexneri* invasion (42–44). An IpgB1 mutant was less invasive in HeLa cells and overexpression of IpgB1 led to Rac1-dependent membrane ruffling (42, 44), while IpgB2 was not required for invasion or spreading in HeLa cells (43, 71).

Here, we demonstrate that, in addition to its role during invasion, IpgB1 modulates Rho family small GTPase signaling to promote cell-to-cell spread through DMV escape, with consequences on the severity of *S. flexneri* pathogenesis.

### 3.3 Material and Methods

#### 3.3.1 Cell lines and bacterial strains

HT-29 cells (ATCC HTB-38) were cultured at 37°C with 5% CO<sub>2</sub> in McCoy's 5A medium (Gibco) supplemented with 10% heat-inactivated fetal bovine serum (FBS) (Invitrogen). The wild-type *Shigella flexneri* strain used in this study is serotype 2a 2457T (24). The *ipgB1* and *ipgB2* strains of *S. flexneri* were generated by allelic exchange resulting in replacement of the open reading frame (ORF) in the *S. flexneri* large virulence plasmid by the coding region of a kanamycin or chloramphenicol resistance cassettes, respectively. The *ipgB1; ipgB2* double mutant was created by replacing the *ipgB1* ORF with a kanamycin resistance cassette and replacing the *ipgB2* ORF with a chloramphenicol

resistance cassette. The *icsB*; *ipgB1* mutant was created by replacing the *icsB* ORF, *ipgB1* ORF, and the intervening region containing *ipgA* (chaperone for IcsB) with a kanamycin resistance cassette. The *ipgB1* mutant was complemented by expressing *ipgB1* from the arabinose-inducible pBAD promoter in vector pBAD18 (ATCC 87393). The catalytically dead allele of IpgB1 (E80A) (115) was generated by overlap PCR. Primers used for creating the *ipgB1* and *ipgB2* mutants and for cloning are listed in Appendix 1.

### 3.3.2 DNA constructs and cell transfection

The HT-29 cell line stably expressing yellow fluorescent protein (YFP) membrane markers was generated using the pMX-MbYFP vector (74, 111). RhoA siRNA Duplex 2-resistant RhoA was created by overlap PCR and cloned into the XhoI and NotI sites of the pMX\_mCherry vector, resulting in the generation of a N-terminal mCherry fusion protein (mCherry-siResistant RhoA). The corresponding lentiviruses were generated in 293T cells co-transfected with the packaging constructs pCMV $\Delta$ 8.2 $\Delta$ vpr (HIV helix packaging system) and pMD2.G (a vesicular stomatitis virus glycoprotein) as previously described (100).

### 3.3.3 Bacterial Infection

*S. flexneri* was grown overnight in LB broth at 30°C with agitation. The bacteria were diluted 1:100 and grown to exponential phase for approximately 3 hr at 37°C with agitation. Cells were infected with *S. flexneri* expressing CFP under the control of an isopropyl- $\beta$ -D-thiogalactopyranoside (IPTG)-inducible promoter. Infection was initiated by centrifuging the plate at 1,000 rpm for 5 min, and internalization of the bacteria was allowed to proceed for 1 hr at 37°C before gentamicin (50  $\mu$ g/ml) and IPTG (10 mM final concentration) were added to kill the extracellular bacteria and induce CFP expression, respectively. For EHT 1864 Rac1 inhibitor (Target Mol T6483) experiments, EHT 1864 or mock (H2O) was added (final concentration 20 $\mu$ M) at 1 hr postinfection for the remainder of the infection. For time-lapse microscopy, imaging began 2 hr postinfection. For *S. flexneri* focus size analysis, infected cells were incubated at 37°C for 16 hr. For gentamicin protection assays, infected cells were lysed and lysates plated for CFU at 2 hr. For foci number enumeration, infected cells were incubated at 37°C for 8 hr.

### 3.3.4 siRNA Transfection

Cells were transfected by reverse transfection with four Dharmafect1 individual small interfering RNAs (siRNAs) (50 nM total final concentration)

targeting Rac1, RhoA, or siRNA buffer alone (mock) 96 h in a 96-well plate format (Corning 3904). Knockdown efficiency was determined by Western blotting. Cells were infected or collected for western blot analysis on day four of knockdown.

### **3.3.5 Western Blotting**

Cells were directly lysed in 2x Laemmli buffer with 10mM DTT and separated by SDS-PAGE. Proteins were transferred onto nitrocellulose membranes and the membranes were incubated for 1 hr at room temperature with gentle shaking in blocking buffer (5% skim milk in 1X TBS with 0.05% Tween). The membranes were probed with primary antibodies diluted in blocking buffer overnight at 4°C with shaking. Secondary antibodies (HRP-conjugated) were diluted in blocking buffer and incubated with membranes for 1 hr room temperature with gentle shaking. ECL Standard Western blotting detection reagents (Amersham) were used to detect HRP-conjugated secondary antibodies on a BioRad ChemiDoc imaging system. Western blot quantification was performed using Fiji.

### 3.3.6 Antibodies

The following antibodies were used for western blot (WB) and/or immunofluorescence (IF): mouse monoclonal anti-RhoA (Santa Cruz sc-418; WB 1:200, IF 1:50), mouse monoclonal anti-Rac1 (Cytoskeleton ARC03; WB 1:500), mouse monoclonal anti-Rac1 (BD Biosciences 610650; IF 1:50), rabbit polyclonal anti-Actin (Sigma WB 1:10,000), HRP-conjugated goat anti-rabbit IgG (Jackson WB 1:10,000), HRP-conjugated goat anti-mouse IgG (Jackson WB 1:10,000), AlexaFluor 594-conjugated goat anti-mouse IgG (Molecular Probes IF 1:1000). For actin visualization, AlexaFluor 594-conjugated Phalloidin (Invitrogen A12381 IF 1:1000) was used.

### 3.3.7 Immunofluorescence

Monolayers of HT-29 cells were grown on collagen-coated (Sigma C3867, 1:100) glass coverslips and infected with *S. flexneri* for 5 hr, then fixed with 4% paraformaldehyde in 1x PBS for 20 minutes at room temperature and washed three times with 1x PBS. Coverslips were incubated with primary antibody diluted in 0.1% triton X-100 in 1x PBS overnight at 4°C in humidity chamber. Coverslips were then washed with 1x PBS and incubated in secondary antibody diluted in 0.1% triton X-100 in 1x PBS for 1 hr at room temperature. For phalloidin staining, coverslips were incubated with phalloidin conjugated to

AlexaFluor 594 (Invitrogen A12381) diluted in 0.1% triton X-100 in 1x PBS for 2 hr at room temperature. Coverslips were washed with PBS and then mounted with DABCO. Confocal imaging was performed using an Andor iXon ULTRA 888BV EMCCD camera and a Yokogawa CSU-W1 confocal scanner unit attached to a Leica DMI8 microscope. Z slices were captured in 1  $\mu\text{m}$  increments spanning the entire cell.

### 3.3.8 Size of infection foci

The size of infection foci formed in HT-29 cells and infected with CFP-expressing *S. flexneri* strains was determined in a 96-well plate format. After fixation with 4% paraformaldehyde for 20 minutes at room temperature, the plates were imaged using the ImageXpress Micro imaging system (Molecular Devices). Margins of individual foci were defined manually, and image analysis for foci size (area) was performed using the region measurement function in the ImageXpress imaging software (Molecular Devices) as previously described (111). Unless otherwise specified, image analyses were conducted on at least 50 infection foci in each biological replicate (n) and for at least three biological replicates (N).

### 3.3.9 Live Imaging

Bacterial dissemination was monitored using time-lapse confocal microscopy. Plasma membrane YFP-expressing HT-29 cells were grown in collagen-coated (Sigma C3867, 1:100) eight-well chambers (Lab-Tek II (Thermo Fisher Scientific catalog no. 155409) at 37°C in 5% CO<sub>2</sub>. Cells were infected with CFP-expressing *S. flexneri* strains and centrifuged at 800 rpm for 4 min. Bacteria were then allowed to invade for 1 hr before gentamicin (50 µg/ml) and IPTG (10 mM final concentration) were added to kill the extracellular bacteria and induce CFP expression, respectively. Starting 2 hrs postinfection, cells were imaged with a Leica DMI 8 spinning-disc confocal microscope driven by the iQ software (Andor). Z-stacks were captured every 2 min for 6 hrs. The corresponding movies were generated with Imaris software (Bitplane). For tracking analysis, protrusions were defined as plasma membrane extensions that formed as a result of bacteria reaching the cell cortex and projecting into adjacent cells. Vacuole-like protrusions (VLPs) were defined as an intermediate compartment between protrusions and vacuoles, characterized by a continuous membrane lining around the bacteria and a membranous tether. Double-membrane vacuoles (DMVs) were defined as membrane-bound compartments that derived from VLPs after resolution of the membranous tether. As opposed to VLPs, DMVs were therefore no longer connected to the primary infected cell. Free (cytosolic)

bacteria were defined as bacteria that were previously observed in vacuoles but were no longer surrounded by a continuous lining of the plasma membrane and have regained actin-based motility.

### **3.3.10 *In vivo S. flexneri* infection**

Animal studies were conducted using our previously described infant rabbit model of *S. flexneri* infection (23). Newborn New Zealand White rabbits were isolated after birth and kept at 30 °C, with regular feedings from tranquilized does. Infant rabbits were infected at 10-15 days old. *S. flexneri* was grown overnight at 37 °C on a rotating wheel in 5 ml tryptic soy broth (TSB) per animal. Prior to infection, the bacteria were pelleted and resuspended in PBS. Kits were anesthetized with 5% isoflurane and rectally inoculated with 200 µl of bacterial suspension (~10<sup>9</sup> CFUs per animal). Animals were monitored twice daily for clinical signs of illness.

### **3.3.11 Histology**

For clinical scoring of infection (blood, diarrhea, and fenestration), animals were euthanized by CO<sub>2</sub> inhalation and the distal colon was harvested at 24 hrs postinfection. Scoring of blood and diarrhea were performed blindly at the time of tissue harvest based on color and wetness of hind limb fur stain. Blood and

dysentery scores were determined based on the presence and severity of blood and diarrhea on the hind limb fur and were scored as (1) genitals only, (2) genitals and belly and (3) genitals, belly and legs. For determination of foci number (invasion) and foci size (cell-to-cell spread) *in vivo*, colons were harvested at 4 hr and 8 hr postinfection, respectively. The distal colons were rinsed in PBS and flushed with modified Bouin's fixative, then cut open longitudinally and displayed in cassettes as swiss-rolls. Cassettes were then immersed in neutral-buffered formalin. The tissue was preserved in 70% EtOH before loading onto a tissue processor for dehydration and paraffin infiltration. After manual embedding into a paraffin block, paraffin sections were cut at 5  $\mu$ m on a Leica microtome. Paraffin sections were stained with hematoxylin and eosin and imaged using ScanScope Slide Scanner (Leica Biosystems). Epithelial fenestration was measured along entire colon using the Aperio software and % fenestration (length of colon with fenestrated epithelium/total length of colon x 100) was calculated for each colon.

### **3.3.12 Immunofluorescence on colon sections**

Paraffin sections on slides were deparaffinized and re-hydrated as previously described (23). Antigen retrieval in pre-heated citric acid based buffer (1:100 in H<sub>2</sub>O, Vector Laboratories, H-3300) was performed in a pressure cooker

(Instant Pot) for 1 min on the high pressure setting, followed by a “quick release.” Slides were rinsed three times with PBS, then permeabilized in 0.1% Triton in PBS for 10 minutes at room temperature and blocked in 5% bovine serum albumin and 2% normal goat serum in PBS for 1 hr at room temperature. Primary antibodies (mouse anti-E-cadherin, BD Biosciences 610181, 1:100; rabbit anti-*Shigella*, ViroStat 0901, 1:100) were diluted in blocking buffer and incubated overnight at 4 °C in humidity chamber. Slides were washed three times with PBS, the secondary antibodies (goat anti-mouse IgG Alexa Fluor 514, Thermo Fisher, 1:500; goat anti-rabbit IgG Alexa Fluor Pacific Blue, Thermo Fisher, 1:500) were diluted in blocking buffer and incubated for 2 hrs at room temperature. Coverslips were mounted using 1 drop of ProLong Gold Antifade (Thermo Fisher) per swiss roll and imaged with a Nikon TE2000 microscope equipped for automated multi-color imaging including motorized stage and filter wheels, a Hamamatsu Orca ER Digital CCD Camera and piezo-driven 10x and 60x objectives. The images were processed with the MetaMorph software (Molecular Devices, Inc.). For foci number analysis, the number of foci per colon was enumerated along the entire distal colon for each animal. Foci sizes were measured using the region measurement tool of the MetaMorph software as described above.

### 3.4 Results

#### 3.4.1 IpgB1 is required for efficient invasion in HT-29 cells

To investigate the roles of IpgB1 and IpgB2 during *S. flexneri* infection, we created mutants lacking either *ipgB1* or *ipgB2* (hereby referred to as *ipgB1* and *ipgB2*) in the *S. flexneri* 2457T background by replacing the open reading frame with a kanamycin or chloramphenicol resistance cassette, respectively. We used a gentamicin protection assay in HT-29 cells to determine the roles of IpgB1 and IpgB2 during invasion of polarized colonic epithelial cells. Consistent with previously published results (42), we found that *ipgB1* produced fewer CFU at 2 hr postinfection (Figure 3.1A, WT vs. *ipgB1*) and fewer infection foci at 8 hr postinfection (Figure 3.1B, WT vs. *ipgB1*) compared to wild type bacteria. Importantly, we were able to restore the invasion defect of the *ipgB1* mutant by expression of IpgB1 *in trans* (Figure 3.1, *ipgB1 pipgB1*). To confirm the role of the previously-established GEF activity of IpgB1 during invasion (114), we generated a catalytically inactive allele of IpgB1 by mutating glutamic acid at residue 80 to alanine (E80A) (114, 115). We found that the E80A allele did not complement the invasion defect of the *ipgB1* mutant (Figure 3.1, *ipgB1 pE80A*). Mutants lacking *ipgB2* were fully invasive, producing similar number of CFUs (Figure 3.2A, WT vs. *ipgB2*) and infection foci compared to wild type bacteria (Figure 3.2B, WT vs.

*ipgB2*). Taken together, these results show that IpgB1, but not IpgB2, functions as a GEF to facilitate invasion in HT-29 cells.

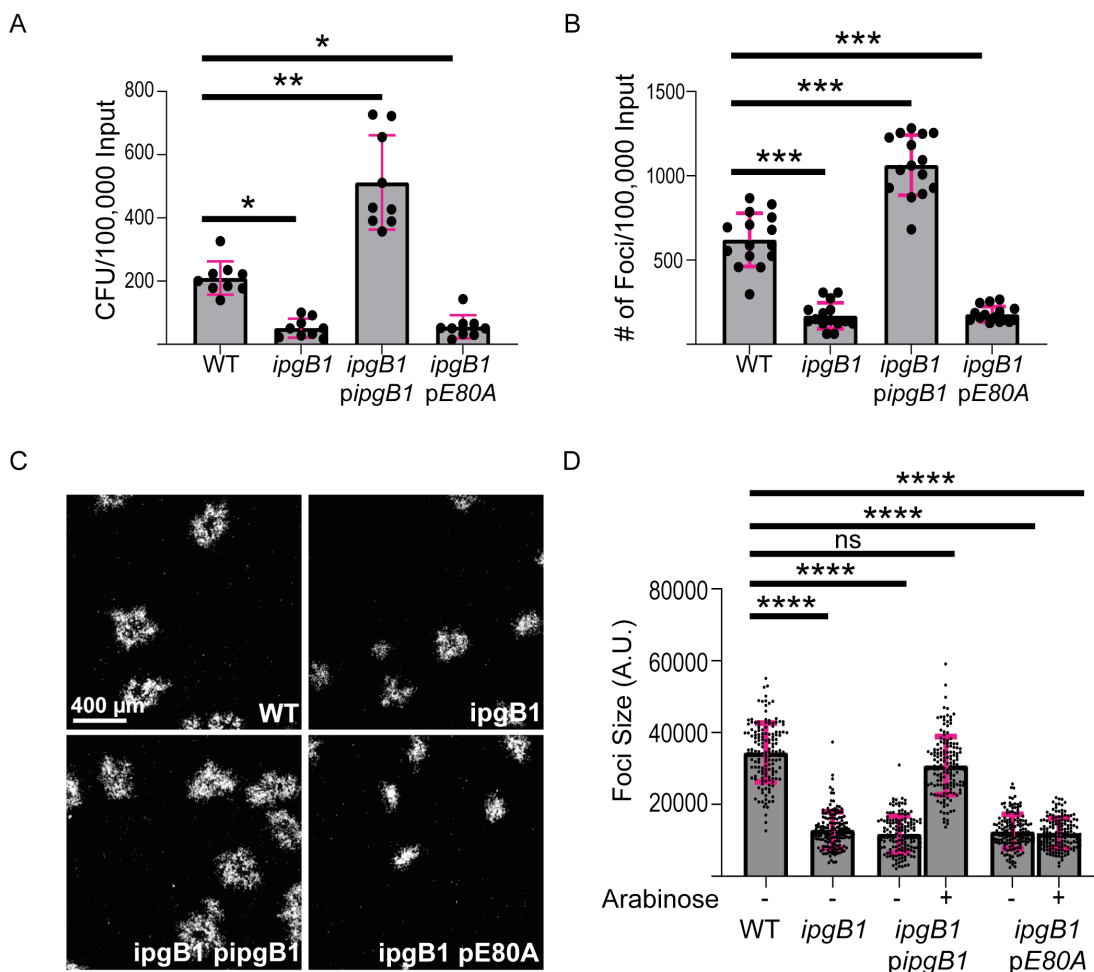


**Figure 3.1: IpgB1 is required for efficient invasion and cell-to-cell spread in HT-29 cells** (A) Intracellular CFUs from HT-29 cells at 2 hr postinfection normalized to inoculum. Three independent biological replicates were performed, each containing three technical replicates. Each point represents one technical replicate and the grey bars represent the mean number of CFU. (B) Number of infection foci formed at 8 hr postinfection normalized to inoculum. Three independent biological replicates were performed, each containing five technical replicates. Each point represents one technical replicate and the grey bars represent the mean number of foci. For *ipgB1 pipgB1* and *ipgB1 pE80A*, arabinose was added at a final concentration of 0.5% during exponential growth and invasion. (C) Representative images showing infection foci formed in HT-29 cells at 16 hr postinfection. The scale bar is 400  $\mu\text{m}$ . (D) Quantification of foci size (area) in arbitrary units at 16 hr postinfection. Three independent biological replicates were performed, each containing at least 50 foci. Each point represents one focus and the grey bars represent the mean foci size. For *ipgB1 pipgB1* and *ipgB1 pE80A*, arabinose was added at a final concentration of 1% at 1 hr postinfection. Error bars represent the standard deviations; one-way ANOVA was performed with Dunnett's multiple comparisons test; ns, not significant; \*,  $p < 0.05$ ; \*\*,  $p < 0.005$ ; \*\*\*,  $p < 0.001$ ; \*\*\*\*,  $p < 0.0001$

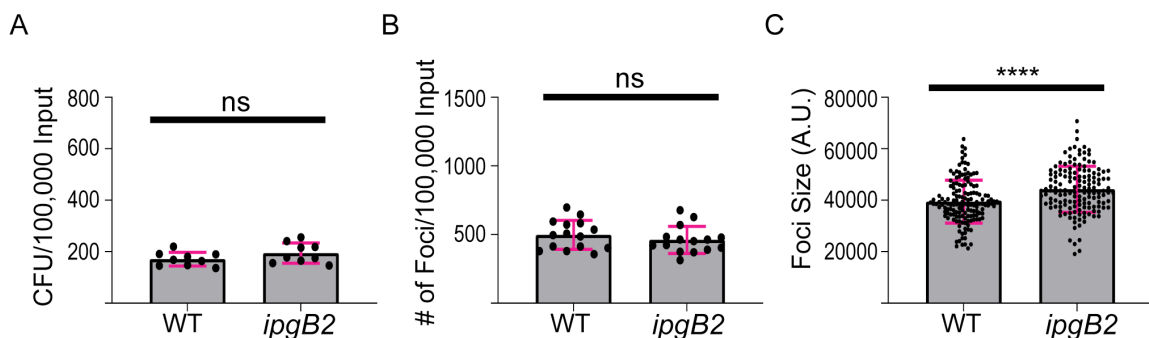


**Figure 3.2: IpgB2 is not required for invasion or cell-to-cell spread in HT-29 cells (A)** Intracellular CFUs from HT-29 cells at 2 hr postinfection normalized to inoculum. Three independent biological replicates were performed, each containing three technical replicates. Each point represents one technical replicate and the grey bars represent the mean number of CFU. **(B)** Number of infection foci formed at 8 hr postinfection normalized to inoculum. Three independent biological replicates were performed, each containing five technical replicates. Each point represents one technical replicate and the grey bars represent the mean number of foci. **(C)** Quantification of foci size (area) in arbitrary units at 16 hr postinfection. Three independent biological replicates were performed, each containing at least 50 foci. Each point represents one focus and the grey bars represent the mean foci size. Error bars represent the standard deviations; unpaired two-tailed t-test; ns, not significant; \*\*\*\*,  $p < 0.0001$

### 3.4.2 IpgB1 is required for efficient dissemination in HT-29 cells

We next sought to determine whether IpgB1 played a role in the dissemination of *S. flexneri*. The *ipgB1* mutant formed smaller infection foci compared to wild type bacteria in HT-29 cells at 16 hr postinfection (Figure 3.1C, WT vs. *ipgB1*). Expression of the wild type, but not the E80A allele of *ipgB1* under the control of an arabinose-inducible promoter restored *ipgB1* spreading, indicating that the GEF activity of IpgB1 was required for efficient dissemination (Figure 3.1C, *ipgB1 pipgB1* vs. *ipgB1 pE80A*). We quantified the area of the infection foci as a measure of cell-to-cell spread and found that the *ipgB1* mutant had a 62% reduction in foci size compared to wild type bacteria, which is fully rescued by *in trans* expression of wild type IpgB1, but not the E80A allele (Figure 3.1D). The *ipgB2* mutant formed similarly sized infection foci (Figure 3.2C, WT vs. *ipgB2*) compared to wild type bacteria, indicating that IpgB2 is dispensable for both invasion and cell-to-cell spread in HT-29 cells. To investigate a potential genetic interaction between IpgB1 and IpgB2, we created a double *ipgB1; ipgB2* mutant and assessed its ability to spread from cell to cell. We found that the *ipgB1; ipgB2* double mutant formed smaller foci compared to wild type and the *ipgB2* mutant, but was not significantly different than the *ipgB1* mutant (Figure 3.3A). Taken together, these results show that IpgB1 functions as a GEF during cell-to-cell spread in HT-29 cells.

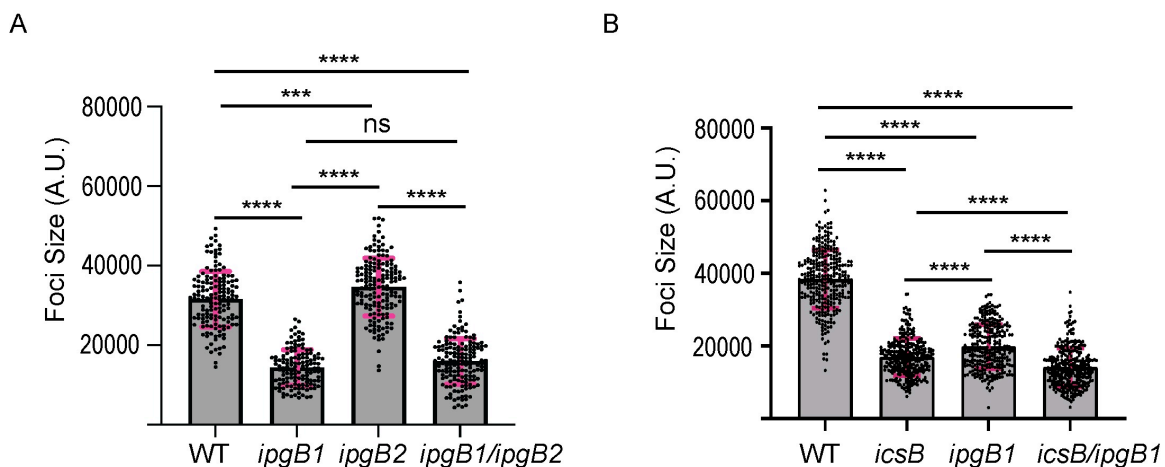


**Figure 3.3: The phenotypes of *ipgB1/ipgB2* and *icsB/ipgB1* double mutants**

Quantification of foci size (area) in arbitrary units at 16 hr postinfection for either (A) *ipgB1/ipgB2* or (B) *icsB/ipgB1* double mutants. Three-six independent biological replicates were performed, each containing at least 50 foci. Each point represents one focus and the grey bars represent the mean foci size. Error bars represent the standard deviations; one-way ANOVA was performed with Dunnett's multiple comparisons test; ns, not significant; \*\*\*,  $p < 0.001$ ; \*\*\*\*,  $p < 0.0001$

### 3.4.3 IpgB1 is required for prompt and efficient DMV escape

To determine at which stage of intracellular dissemination the *ipgB1* mutant is defective, we employed time-lapse confocal microscopy and tracking of individual bacteria during cell-to-cell spread (74, 76, 111). HT-29 cells stably expressing plasma membrane-targeted yellow fluorescent protein (YFP) (mbYFP) were infected with wild type or *ipgB1 S. flexneri* expressing cyan fluorescent protein (CFP). Motile bacteria were tracked from the point at which they protruded into a neighboring cell (Figure 3.4A, light blue, protrusion), through the intermediate stage of vacuole-like protrusion (VLP) (Figure 3.4A, purple, VLP) (23) to the formation of double membrane vacuoles (DMV) (Figure 3.4A, yellow). Subsequent escape from DMVs was marked by the disappearance of mbYFP and the reacquisition of actin-based motility in the adjacent cell (Figure 3.4A, green, escape). Tracking of individual bacteria revealed that *ipgB1* bacteria had a decrease in successfully spreading bacteria (Figure 3.4B and 3.4C, green bars) and an increase in bacteria remaining trapped in DMVs (Figure 3.4B and 3.4C, yellow bars). Quantification of these outcomes revealed that only 58% of the *ipgB1* mutant successfully escaped DMVs, compared to 76% of wild type bacteria (Figure 3.4D, DMV escape). The *ipgB1* mutant had a significant increase in DMV escape failure (35%) compared to wild type bacteria (8%) (Figure 3.4D, DMV escape failure). The proportion of bacteria that failed in protrusions was

not significantly different between wild type and the *ipgB1* mutant (Figure 3.4D, protrusion failure). Additionally, the time spent in protrusions was similar between wild type and *ipgB1* bacteria (Figure 3.4E). Even when spreading was successful, the *ipgB1* mutant spent significantly more time in VLPs (Figure 3.4F) and in DMVs (Figure 3.4G) compared to wild type bacteria. These results indicate a role for IpgB1 in prompt and efficient DMV escape. Given our previous work demonstrating that another *S. flexneri* T3SS effector, IcsB, is involved in DMV escape (111), we investigated whether IcsB and IpgB1 could be contributing cooperatively to DMV escape. We created a *S. flexneri* mutant lacking both *icsB* and *ipgB1* and characterized its capability for cell-to-cell spread. We found that the *icsB; ipgB1* double mutant formed significantly smaller foci than the *icsB* and *ipgB1* single mutants (Figure 3.3B). This compounded spreading defect of the double mutant suggests that IcsB and IpgB1 play non-redundant roles in cell-to-cell spread.

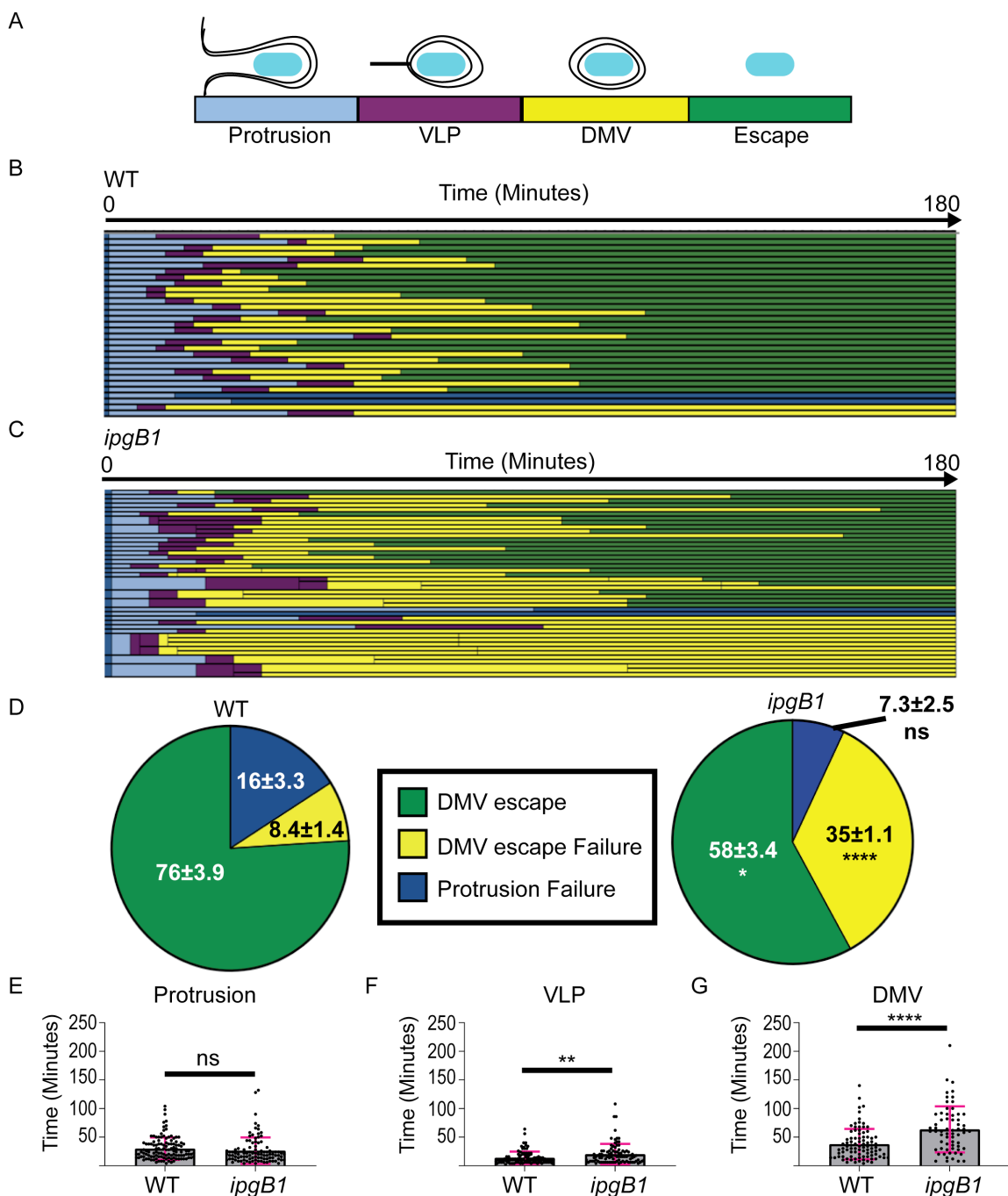


**Figure 3.4: IpqB1 is required for efficient DMV escape** (A) Schematic depicting the stage and corresponding color code of spread progression (B and C) Representative tracking analysis of (B) wild type or (C) *ipqB1* CFP-expressing *S. flexneri* in HT-29 cells expressing plasma membrane-targeted YFP. Each bar represents the tracking of a single bacterium over 180 minutes. For *ipqB1*, the thicker bars indicate when bacteria divided and branched during spreading. At least 30 bacteria were tracked for each strain per biological replicate. (D) Graphs showing the proportions of fates of tracked bacteria from 4 biological replicates. Standard deviations of the means are indicated. Two-way ANOVA with Sidak's multiple comparisons was performed; ns, not significant; \*,

$p < 0.05$ ; \*\*\*\*,  $p < 0.0001$ . Time spent in protrusions (**E**), VLPs (**F**), or DMVs (**G**) is shown for all tracked bacteria. Each dot represents a single bacterium and the grey bars show the mean of all tracked bacteria from four biological replicates. Error bars indicate standard deviation. Unpaired two-tailed t-tests were performed; ns, not significant; \*\*,  $p < 0.005$ ; \*\*\*\*,  $p < 0.0001$

### 3.4.4 The *ipgB1* mutant displays a protrusion branching phenotype

In addition to the canonical dissemination process involving the sequential formation of protrusions, VLPs and DMVs (Figure 3.5A), we found that the *ipgB1* mutant had a tendency to divide and resume ABM in VLPs, leading to a protrusion “branching” phenotype (Figure 3.5B). We found that about 25% of *ipgB1* mutants underwent protrusion branching, whereas none of the wild type bacteria displayed this phenotype (Figure 3.5C). To determine if protrusion branching contributed to the cell-to-cell spreading defect of *ipgB1*, we compared the total time spent in membrane (protrusions, VLPs, and DMVs) (Figure 3.5D), time spent in protrusions and VLPs (Figure 3.5E), and the time spent in DMVs (Figure 3.5F) between non-branching and branching *ipgB1* bacteria. We found no significant differences in the timing of non-branching and branching bacteria, indicating that there is no delay in cell-to-cell spread. Furthermore, when we compared the proportions of bacteria that failed to resolve protrusions, remained trapped in DMVs, or successfully escaped DMVs, we found no major differences between non-branching and branching bacteria (Figure 3.5G). Therefore, we conclude that the branching phenotype observed with the *ipgB1* mutant does not significantly contribute to the observed cell-to-cell spreading defects and that the main phenotype characterized by tracking that contributes to defective *ipgB1* spreading is DMV escape failure.

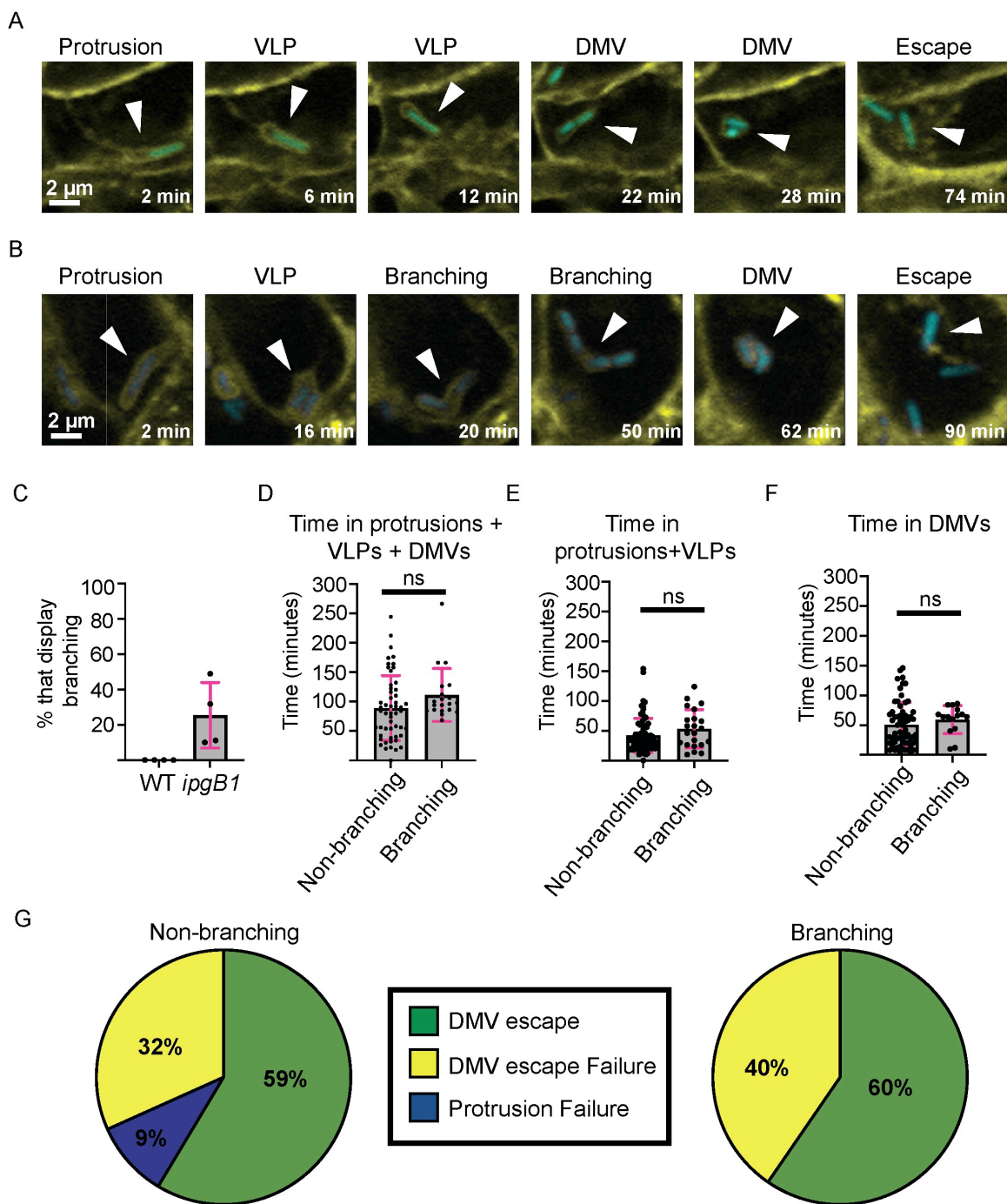


**Figure 3.5: The protrusion branching phenotype**

(A-B) Still images from (A) non-branching or (B) branching cell-to-cell spread example. White arrowheads indicate which bacteria to follow as examples. The time in minutes corresponding to each image is shown in bottom right corner. Each example begins at 2 min, the first frame at which the bacterium is in a protrusion. At 0 min, the bacterium is in the primary infected cell. Scale bar, 2  $\mu$ m (C) Graph depicting the percentage of wild type or *ipgB1* bacteria that display protrusion branching during spreading. Each dot

represents percentage from one biological replicate and grey bars show average of 4 biological replicates. Error bar indicates standard deviation. (D-F) Graphs depicting (D) time spent in membrane compartments (protrusions, VLPs, DMVs), (E) time spent in protrusions and VLPs, or (F) time spent in DMVs by *ipgB1* bacteria displaying non-branching or branching protrusions. Each dot represents one bacterium and the grey bars represent the average of all tracked bacteria per category. Error bars indicate standard deviations. Unpaired two-tailed t-test; ns, not significant. (G) Graphs showing the proportions of fates of all tracked *ipgB1* bacteria from 4 biological replicates.

### 3.4.5 Rac1 promotes cell-to-cell spread

Given that IpgB1 was previously found to function as a GEF with specificity for the small GTPase Rac1 (114), we decided to investigate the contribution of Rac1 to cell-to-cell spread. We depleted HT-29 cells of Rac1 using four independent siRNA duplexes and assessed the effect on foci size. We found that three out of four of the tested siRNA duplexes significantly decreased the spreading of wild type *S. flexneri* (Figure 3.6A and 3B). Additionally, we found that pharmacological inhibition of Rac1 using the inhibitor EHT 1864 decreased wild type spreading to a foci size similar to the size of the foci formed by *ipgB1* (Figure 3.6C). Importantly, we did not observe any decrease in *ipgB1* foci size upon genetic (Figure 3.6B) or chemical (Figure 3.6C) interference with Rac1 activity. These results reveal that Rac1 supports cell to cell spread through a mechanism that depends on IpgB1 expression.

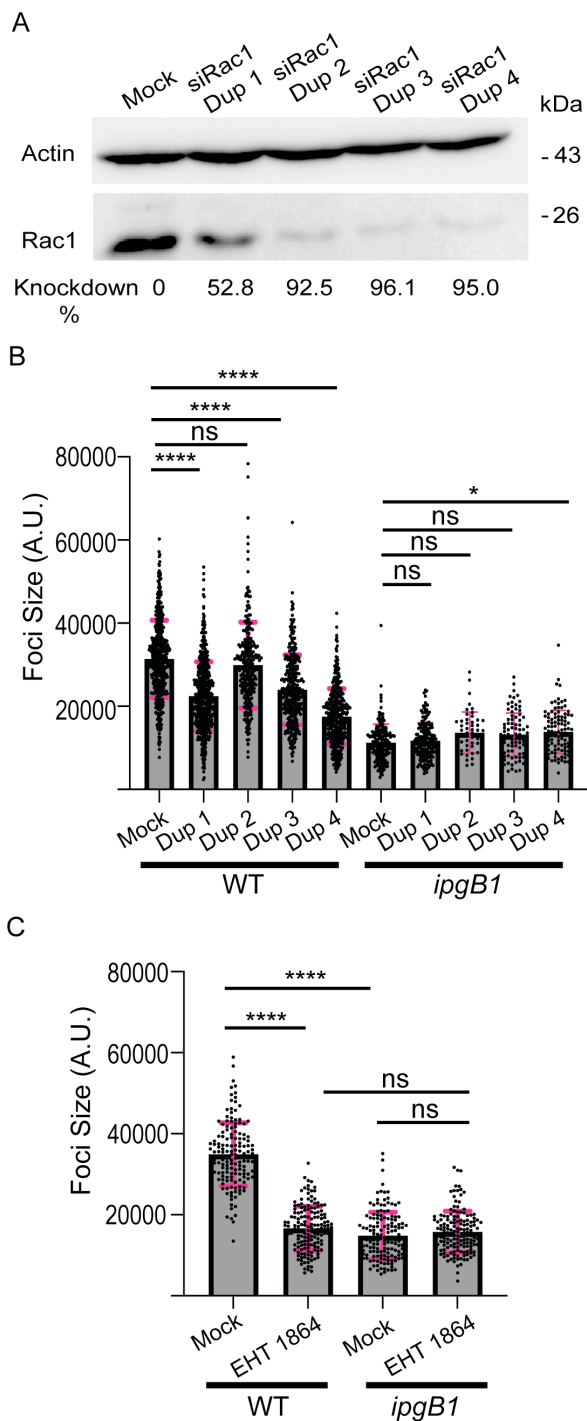


**Figure 3.6: Rac1 signaling is required for efficient cell-to-cell spread (A)** Western blot showing knockdown efficiency of four siRNA duplexes targeting Rac1. Rac1 (bottom panel) was normalized to loading control (actin, top panel) and knockdown efficiency was calculated relative to mock treated cells. **(B)** Quantification of foci size at 16 hr postinfection of wild type or *ipgB1* bacteria in mock treated cells or upon Rac1 depletion with four siRNA duplexes. **(C)** Quantification of wild type or *ipgB1* foci size at 16 hr postinfection in either cells treated with DMSO control or with 20  $\mu$ M EHT 1864. For **(B)**

**and C)**, at least three independent biological replicates were performed, each containing at least 50 foci. Each point represents one focus and the grey bars represent the mean foci size. Error bars represent the standard deviations; one-way ANOVA was performed with Dunnett's multiple comparisons test; ns, not significant; \*,  $p < 0.05$ ; \*\*\*,  $p < 0.0001$

### 3.4.6 Rac1 promotes DMV escape

We next determined whether Rac1 depletion phenocopied the DMV escape defect observed in cells infected with the *ipgB1* mutant. To this end, we used live confocal microscopy to track the spreading of wild type *S. flexneri* in either mock-treated (Figure 3.7A) or Rac1-depleted (Figure 3.7B) HT-29 cells expressing mbYFP. We found that depletion of Rac1 led to an increase in the proportion of wild type bacteria that remained trapped in DMVs (Figure 3.7A and 3.7B, yellow bars). Unexpectedly, we also found an increase in protrusion resolution failure upon Rac1 depletion (Figure 3.7A and 3.7B, dark blue bars). Given that we did not observe this increase in protrusion failure with the *ipgB1* mutant, we reasoned that this could be the result of an additional, IpgB1-independent role of Rac1 in cell-to-cell spread, such as the specification of proper cell-cell contacts (116), which is required for efficient protrusion resolution into vacuoles in polarized cells (75). Quantification of our tracking results revealed that only 26% of bacteria successfully escaped DMVs in Rac1-depleted cells, compared to 74% of bacteria in mock-treated cells (Figure 3.7C, DMV escape). Rac1 depletion significantly increased DMV escape failure (38%) compared to mock-treated cells (12%) (Figure 3.7C, DMV escape failure). As described above, the proportion of bacteria that failed to resolve protrusions was significantly higher in Rac1-depleted cells compared to mock-treated cells (Figure 3.7C,

protrusion failure), but the time spent in protrusions (Figure 3.7D), VLPs (Figure 3.7E) or DMVs (Figure 3.7F) did not significantly differ. Taken together, these data indicate that genetic or chemical interference with Rac1 phenocopies the *ipgB1* mutant in terms of cell-to-cell spread and DMV escape.

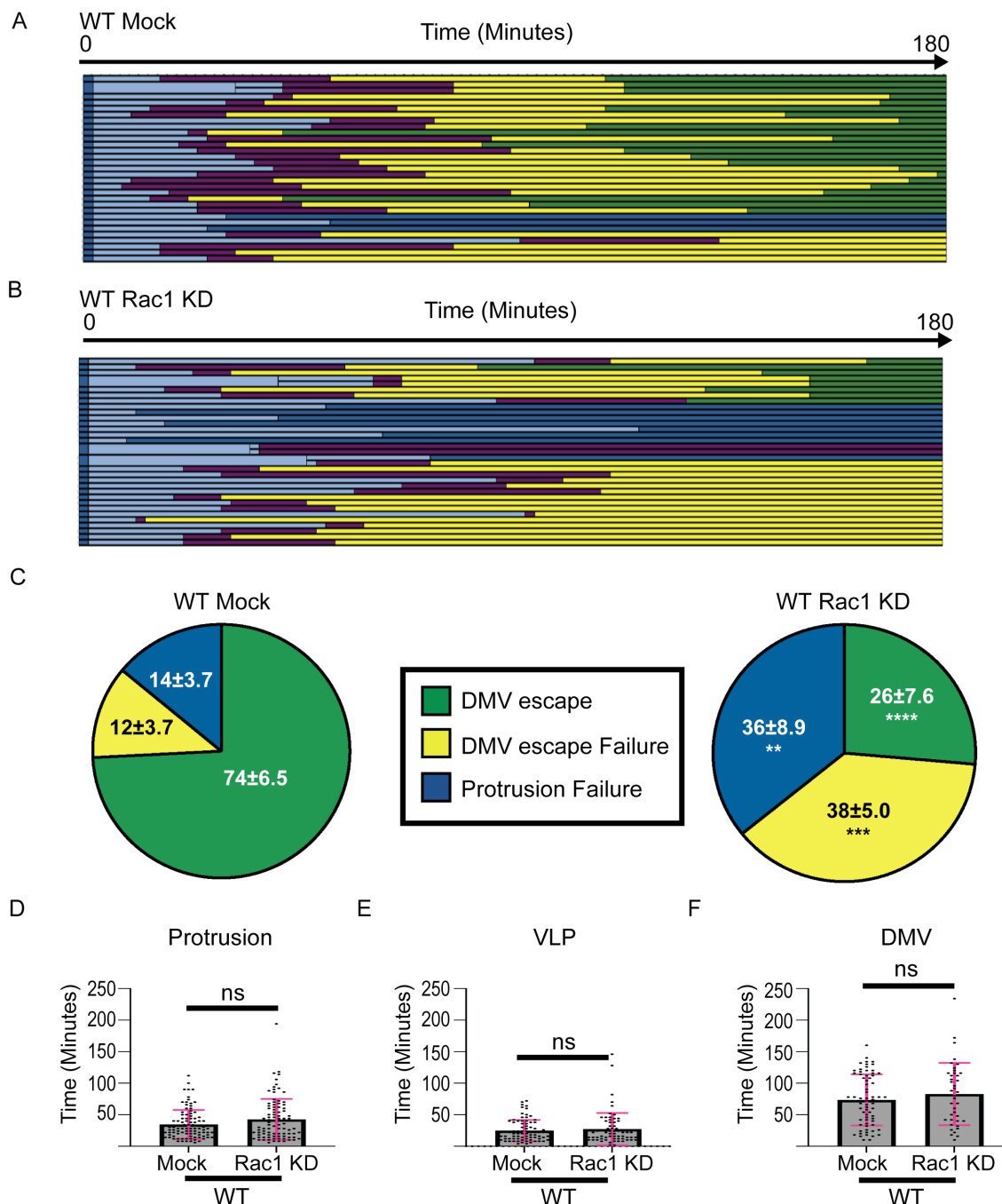


**Figure 3.7: Rac1 depletion decreases DMV escape (A and B)** Representative tracking analysis of CFP-expressing wild type bacteria in (A) mock-treated or (B) Rac1-depleted HT-29 cells expressing plasma membrane-targeted YFP. Each bar represents the tracking of a single bacterium over 180 minutes. Thicker bars indicate instances when bacteria divided and branched during spreading. At least 30 bacteria were tracked for condition per biological replicate. (C) Graphs showing the proportions of fates of tracked bacteria from three biological replicates. Standard deviations of the means are indicated. Two-way ANOVA with Sidak's multiple comparisons was performed; \*\*,  $p < 0.005$ ; \*\*\*,  $p < 0.001$ ; \*\*\*\*,  $p < 0.0001$ . Time spent in (D) protrusions, (E) VLPs, or (F) DMVs is shown

for all tracked bacteria. Each dot represents a single bacterium and the grey bars show the mean of all tracked bacteria from three biological replicates. Error bars indicate standard deviation. Unpaired two-tailed t-tests were performed; ns, not significant

### 3.4.7 RhoA depletion rescues the *ipgB1* cell-to-cell spread defect

To identify any potentially novel relationships between IpgB1 and Rho family small GTPases that could be contributing to *S. flexneri* cell-to-cell spread downstream of IpgB1, we performed a targeted siRNA screen of common Rho family members and related proteins (Table 3.1). HT-29 cells were transfected with four single siRNA duplexes targeting each gene of interest and were then infected with either wild type bacteria or the *ipgB1* mutant. We considered genes as potential “hits” if knockdown with at least two of the four duplexes influenced the size of the infection foci (spreading) by 1.5 or more standard deviations in at least three of the four replicates that we performed. Our siRNA screen results revealed that knockdown of RhoA led to an increase in *ipgB1*, but not wild type, cell-to-cell spread (Table 3.1). We confirmed the efficiency of knockdown of RhoA with four siRNA duplexes using a RhoA antibody and found that all four duplexes resulted in 70-90% depletion of RhoA (Figure 3.8A). To confirm our screening results, we measured the size of wild type or *ipgB1* infection foci formed in mock-treated or RhoA-depleted HT-29 cells at 16 hrs postinfection. All four duplexes significantly restored *ipgB1* cell-to-cell spread to near wild type levels (Figure 3.8B, *ipgB1*). Two duplexes caused a modest increase in wild type cell-to-cell spread (Figure 3.8B, WT). To determine whether the restoration of *ipgB1* cell-to-cell spread was specifically due to RhoA

depletion, we created an HT-29 cell line that stably overexpressed an allele of RhoA resistant to siRNA treatment with siRNA duplex 2 targeting RhoA. In HT-29 cells, we found that the *ipgB1* mutant displayed attenuated spreading compared to wild type (Figure 3.8C, HT-29, Mock) that was fully restored upon depletion of RhoA by siRNA duplex 2 (Figure 3.8C, HT-29, siRhoA Dup 2). In HT-29 cells overexpressing siRNA-resistant RhoA (HT-29 si-resistant RhoA), we found that *ipgB1* was still defective in cell-to-cell spread compared to wild type *S. flexneri* (Figure 3.8C, HT-29 si-resistant RhoA, Mock). This defect was however no longer restored upon treatment with siRNA duplex 2 (Figure 3.8C, HT-29 si-resistant RhoA, siRhoA Dup 2), indicating that overexpression of siRNA-resistant RhoA prevented restoration of *ipgB1* cell-to-cell spread by RhoA knockdown. These results indicate that the restoration of *ipgB1* cell-to-cell spread is specifically due to RhoA depletion.

Gene	cutoff (2 of 4)		# of duplexes that were hits							
	number of replicates		Decreased Spreading		Increased Spreading		Decreased Spreading		Increased Spreading	
	WT	<i>ipgB1</i>	R1 WT	R1 <i>ipgB1</i>	R2 WT	R2 <i>ipgB1</i>	R3 WT	R3 <i>ipgB1</i>	R4 WT	R4 <i>ipgB1</i>
RHOA	0	0	0	0	1	0	0	0	0	1
RHOB	1	0	2	0	0	0	0	0	0	0
RHOC	1	0	0	0	0	0	0	0	2	0
RHOD	0	0	0	0	0	0	1	0	0	1
RHOE	0	1	0	0	0	0	1	1	0	2
RHOF	0	0	0	0	1	1	0	0	0	0
RAC1	0	1	1	1	0	2	2	0	3	0
RAC2	0	0	0	0	1	0	0	0	1	0
CDCA2	1	1	0	0	0	0	0	0	0	2
FLJ22056	0	0	0	0	1	0	0	0	0	0
PFN1	2	0	3	0	3	0	0	0	0	0
SSH1	0	0	0	0	0	0	0	0	0	0
SRC	0	0	0	0	0	0	1	0	0	0
FYN	0	0	0	1	0	0	0	1	1	0
WASL	4	4	4	4	4	4	4	4	4	3
WT	0	3	0	1	0	0	0	0	0	2
<i>ipgB1</i>	0	0	0	0	0	3	3	3	0	1
RHOA	0	0	0	0	0	1	0	0	1	0
RHOB	0	0	0	0	0	0	0	0	0	0
RHOC	0	0	0	0	0	0	0	0	0	0
RHOD	0	0	0	0	0	0	0	0	0	0
RHOE	0	0	0	0	0	0	0	0	0	0
RHOF	0	0	0	1	0	1	0	1	0	0
RAC1	0	0	0	0	1	0	0	1	0	1
RAC2	0	0	0	1	0	0	0	0	0	0
CDCA2	0	0	0	0	0	0	0	0	0	0
FLJ22056	0	0	0	0	0	0	0	0	0	0
PFN1	0	1	0	0	0	0	1	0	0	0
SSH1	0	0	0	0	0	0	0	0	0	0
SRC	0	0	0	1	0	0	0	0	0	1
FYN	0	0	0	0	0	0	0	0	0	1
WASL	0	0	0	0	0	0	0	0	0	1

**Table 3.1: Rho family siRNA screen** Overview of screening data. Each gene name is displayed in column C. The “hit” criteria of how many duplexes were found (out of 4) per replicate and the number of replicates in which this result must repeat (out of 4) are indicated in red and orange text, respectively. For wild type and *ipgB1*, the # of duplexes that resulted in decreased spreading below lower cutoff or increased spreading above upper cutoff for each replicate are shown. Columns A and B indicate the number of replicates in which the “hit”

was found. Values for “hits” that decreased or increased spreading are highlighted in green and red, respectively.

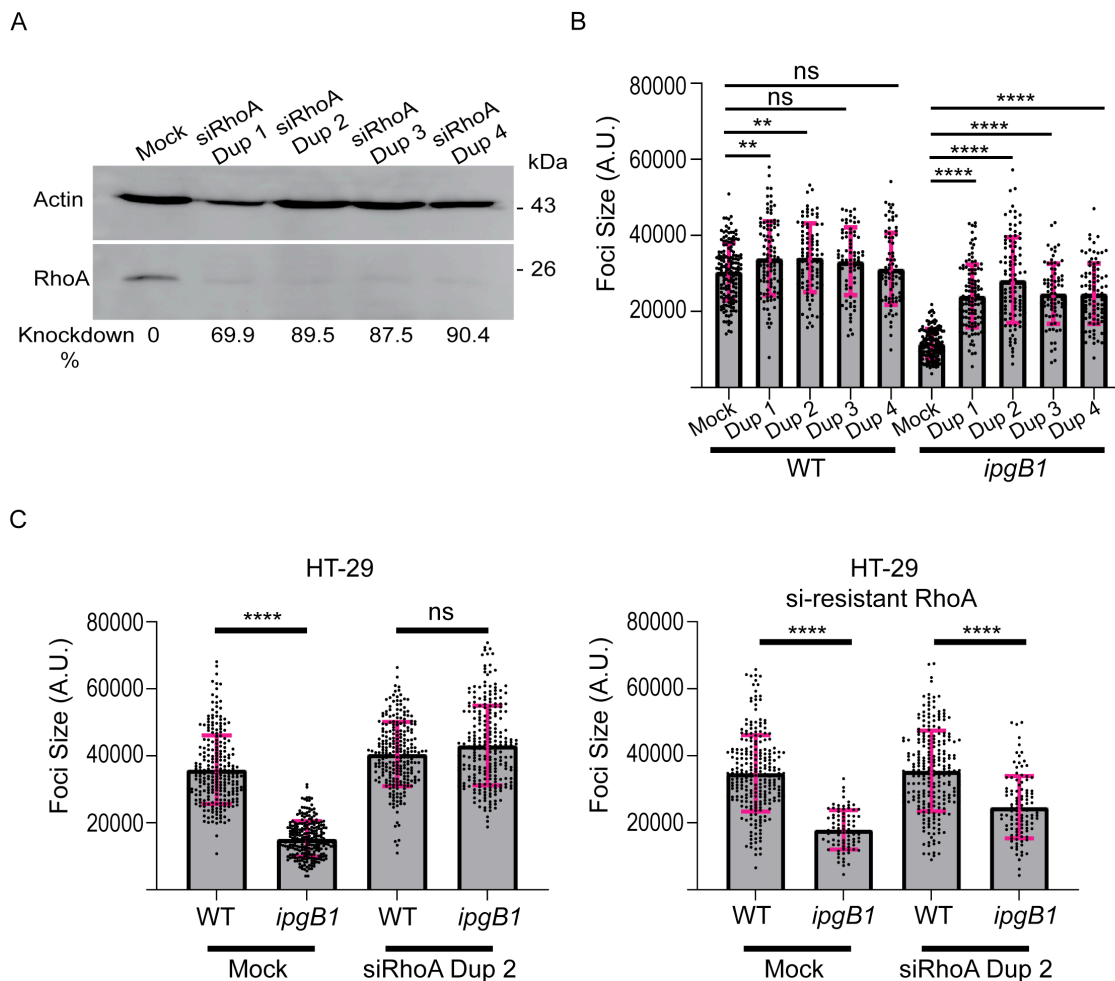


**Figure 3.8: RhoA depletion restores *ipgB1* cell-to-cell spread** (A) Western blot showing knockdown efficiency of four siRNA duplexes targeting RhoA. RhoA (bottom panel) was normalized to loading control (actin, top panel) and knockdown efficiency was calculated relative to mock treated cells. (B) Quantification of wild type or *ipgB1* foci size at 16 hr postinfection in mock treated cells or cells transfected with four RhoA-targeting siRNA duplexes. (C) Quantification of wild type or *ipgB1* foci size at 16 hr postinfection in HT-29 cells (left graph, HT-29) or HT-29 cells stably expressing siRNA duplex 2-resistant mCherry RhoA (right graph, HT-29 si-resistant RhoA) under mock-treated conditions or upon knockdown of RhoA with siRNA duplex 2. For (B and C), at least three independent biological replicates were performed, each containing at least 50 foci. Each point represents one focus and the grey bars represent the mean foci size. Error bars represent the standard deviations; one-way ANOVA was performed with Dunnett's multiple comparisons test; ns, not significant; \*\*,  $p < 0.005$ ; \*\*\*\*,  $p < 0.0001$

### 3.4.8 RhoA restricts DMV escape

We next investigated the mechanism of *ipgB1* spreading restoration upon RhoA knockdown by tracking of *ipgB1* cell-to-cell spread in either mock-treated (Figure 3.9A) or RhoA-depleted (Figure 3.9B) HT-29 cells. Consistent with our previous results, we found that a substantial proportion (~25%) of *ipgB1* bacteria remained trapped in DMVs (Figure 3.9C, *ipgB1* Mock, yellow) and this proportion was significantly decreased (~7%) upon depletion of RhoA (Figure 3.9C, *ipgB1* RhoA KD, yellow). Consistently, the proportion of *ipgB1* bacteria that successfully spread to neighboring cells was significantly increased from 68% to 86% upon RhoA knockdown (Figure 3.9C, green). We did not observe a difference in the proportion of bacteria that failed to transition from protrusions to VLPs (Figure 3.9C, blue). We found a very small, but statistically significant increase in the time that *ipgB1* bacteria spent in protrusions upon RhoA knockdown (Figure 3.9D). There was no difference in time spent in VLPs between mock-treated and RhoA-depleted conditions (Figure 3.9E). Finally, we found that *ipgB1* bacteria spent significantly less time in DMVs in RhoA-depleted cells compared to mock-treated cells (Figure 3.9F). These data indicate that siRNA-mediated depletion of RhoA rescued *ipgB1* cell-to-cell spread to wild type levels by restoring prompt and efficient DMV escape. Taken together, our results

indicate that IpgB1 expression is required to antagonize the restriction on DMV escape mediated by RhoA.

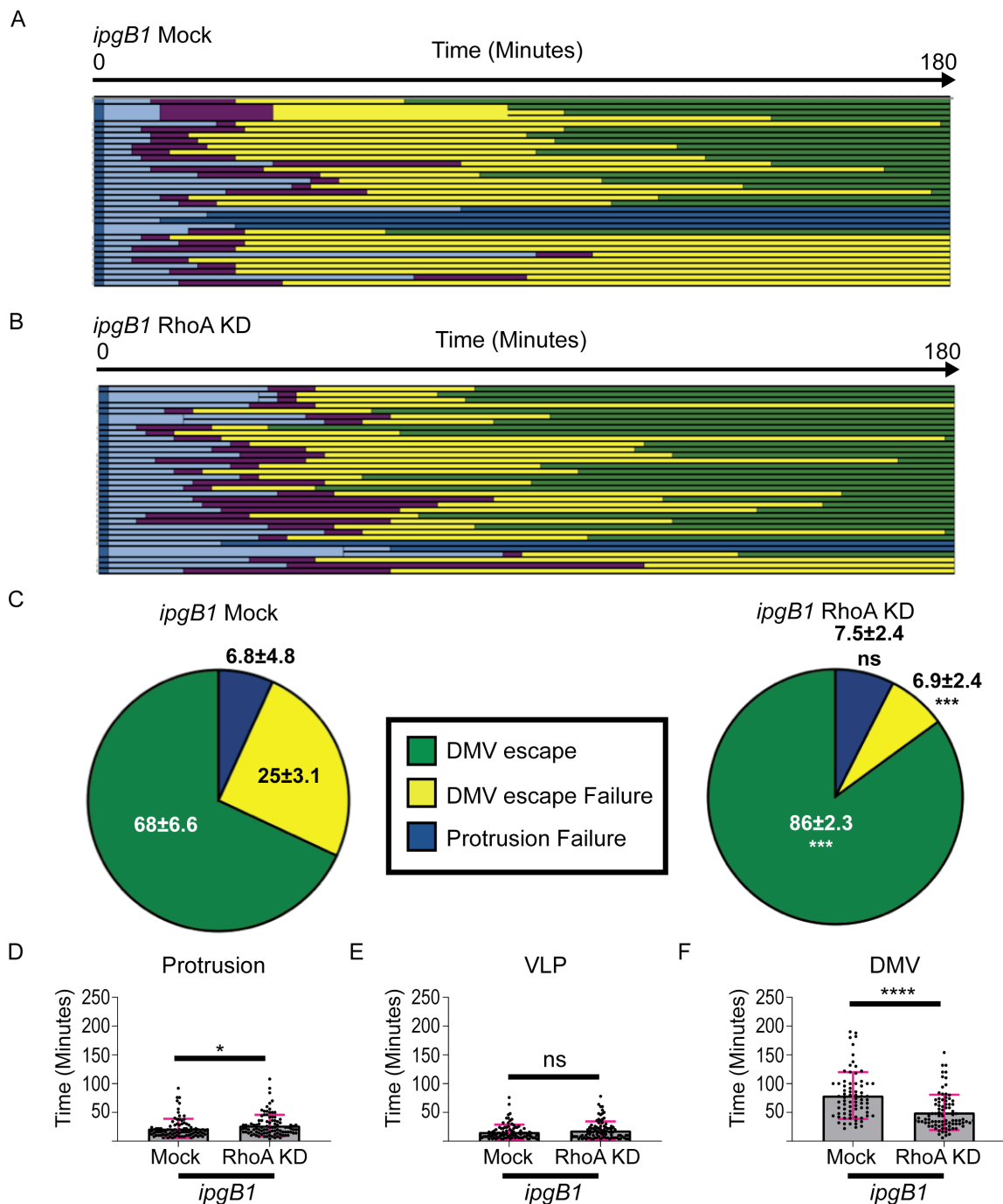


**Figure 3.9: RhoA depletion restores *ipgB1* DMV escape (A and B)**

Representative tracking analysis of CFP-expressing *ipgB1* bacteria in (A) mock-treated or (B) RhoA duplex2-depleted HT-29 cells expressing plasma membrane-targeted YFP. Each bar represents the tracking of a single bacterium over 180 minutes. Thicker bars indicate instances when bacteria divided and branched during spreading. At least 30 bacteria were tracked for condition per biological replicate. (C) Graphs showing the proportions of fates of tracked bacteria from three biological replicates. Standard deviations of the means are indicated. Two-

way ANOVA with Sidak's multiple comparisons was performed; ns, not significant; \*\*\*,  $p < 0.001$ . Time spent in protrusions (**D**), VLPs (**E**), or DMVs (**F**) is shown for all tracked bacteria. Each dot represents a single bacterium and the grey bars show the mean of all tracked bacteria from three biological replicates. Error bars indicate standard deviation. Unpaired two-tailed t-tests were performed; ns, not significant; \*,  $p < 0.05$ ; \*\*\*,  $p < 0.0001$

### 3.4.9 IpgB1 enhances Rac1 recruitment and antagonizes RhoA recruitment to DMVs

Given the IpgB1-dependent role of Rac1 in cell-to-cell spread, we tested whether IpgB1 enhanced the recruitment of Rac1 to DMVs. We infected mbYFP-expressing HT-29 cells with CFP-expressing wild type or *ipgB1* *S. flexneri* for 5 hrs and then imaged endogenous Rac1 recruitment by immunofluorescence microscopy. We observed DMVs displaying substantial recruitment of Rac1 (Figure 3.10A) or lacking Rac1 recruitment (Figure 3.10B). Around 70% of wild type DMVs were positive for Rac1, while only 30% of *ipgB1* DMVs recruited Rac1 (Figure 3.10C), demonstrating that IpgB1 increases Rac1 recruitment to DMVs.

Because RhoA depletion restored DMV escape and cell-to-cell spread of the *ipgB1* mutant, we next wondered whether IpgB1 expression was antagonizing RhoA recruitment to DMVs. To investigate this, we infected mbYFP-expressing HT-29 cells with CFP-expressing wild type or *ipgB1* *S. flexneri* for 5 hr and then visualized endogenous RhoA using immunofluorescence and confocal microscopy. We observed examples of massive recruitment of RhoA to DMVs (Figure 3.10D) as well as DMVs that were devoid of RhoA recruitment (Figure 3.10E). About 25% of wild type DMVs were RhoA-positive (Figure 3.10F, WT, mock). Strikingly, we observed a dramatic increase in the percentage of RhoA-positive DMVs in cells infected with the *ipgB1* mutant (Figure 3.10F, *ipgB1*,

mock). RhoA knockdown significantly decreased the percentage of RhoA-positive DMVs observed in cells infected with the *ipgB1* mutant to wild type levels (Figure 3.10F, siRhoA). These results are in agreement with the notion that IpgB1 supports DMV escape by antagonizing RhoA recruitment to DMVs.

Additionally, we investigated the interplay between Rac1 and RhoA recruitment on DMVs by probing the effect of Rac1 depletion on the recruitment of RhoA to DMVs. We found that Rac1 depletion led to an increase in RhoA-positive DMVs in cells infected with wild type bacteria (Figure 3.11A, WT). Consistent with IpgB1 and Rac1 functioning in the same pathway, we found no significant difference in the percentage of RhoA-positive DMVs upon Rac1 depletion in cells infected with the *ipgB1* mutant (Figure 3.11A, *ipgB1*). We also examined the proportion of Rac1-positive DMVs upon RhoA depletion. There was no difference in the percentage of Rac1-positive DMVs in RhoA-depleted cells infected with wild type bacteria (Figure 3.11B, WT). As expected, the percentage of Rac1-positive DMVs was decreased in cells infected with the *ipgB1* mutant (Figure 3.11B, *ipgB1*). However, upon RhoA depletion, the percentage of Rac1-positive DMVs was restored to wild type level (Figure 3.11B, *ipgB1*). These data further support the notion that IpgB1 modulates Rac1 and RhoA recruitment to DMVs.

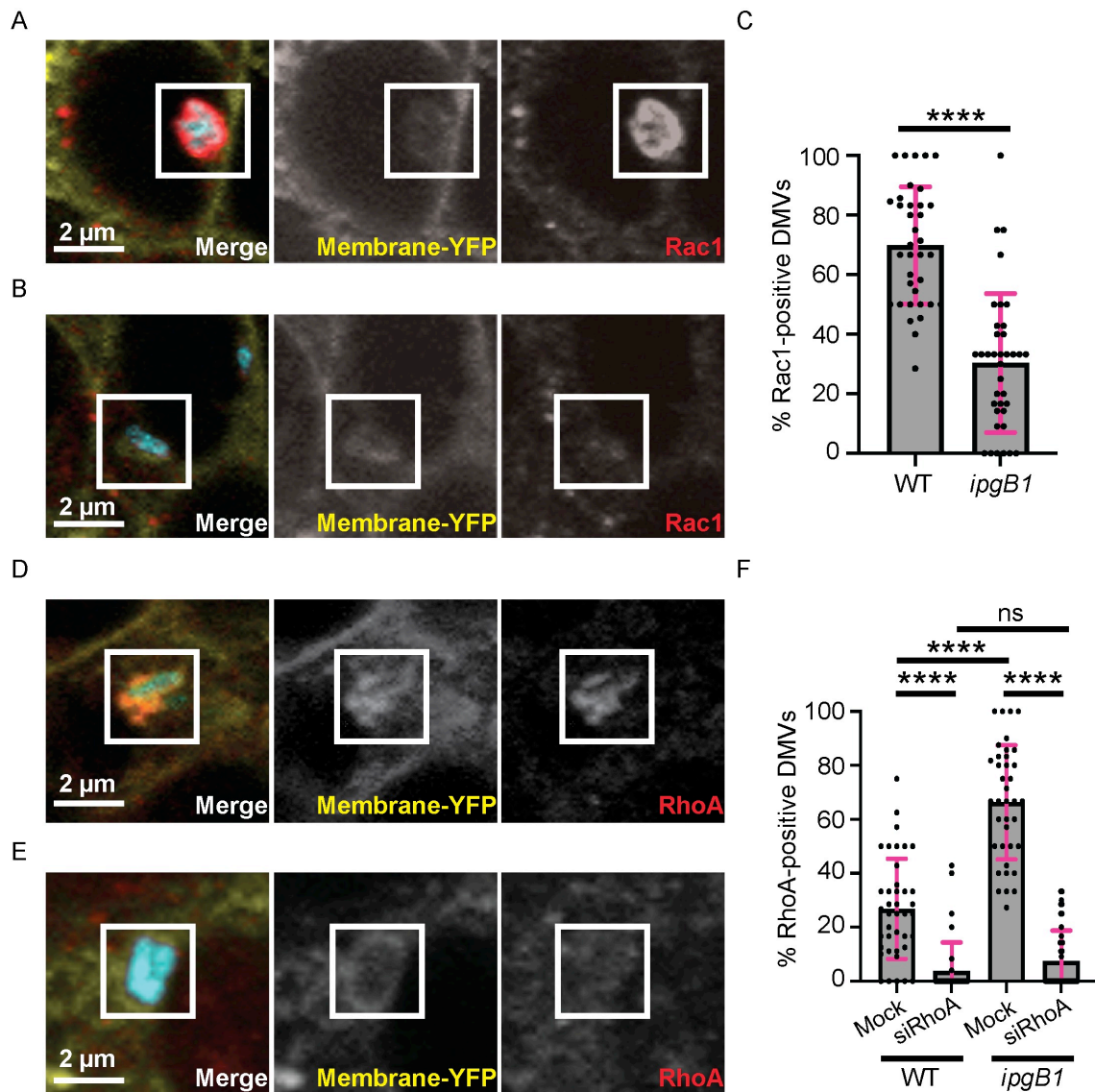


**Figure 3.10: IpgB1 enhances Rac1 and antagonizes RhoA recruitment to DMVs**  
 (A and B) Confocal images of HT-29 cells stably expressing plasma membrane-targeted YFP and infected for 5 hr with CFP-expressing *S. flexneri* and stained using an anti-Rac1 antibody followed by AlexFluor 594-conjugated anti-mouse secondary antibody. Merged images are shown on the left, single YFP channel in middle, and single mCherry channel on the right. Scale bar, 2 μm. (A) Representative example of a DMV that is positive for Rac1 recruitment. (B) Representative example of a DMV that is negative for Rac1 recruitment. (C) Quantification of the percentage of wild type or *ipgB1* DMVs per foci associated with Rac1 HT-29 cells. Each dot represents the percent Rac1-positive DMVs in an infection focus and the grey bars show the mean percentage of Rac1-positive DMVs from all foci measured in three biological replicates. (D and E) Confocal

images of HT-29 cells stably expressing plasma membrane-targeted YFP and infected for 5 hr with CFP-expressing *S. flexneri* and stained using an anti-RhoA antibody followed by AlexFluor 594-conjugated anti-mouse secondary antibody. Merged images are shown on the left, single YFP channel in middle, and single mCherry channel on the right. Scale bar, 2  $\mu\text{m}$ . (D) Representative example of a DMV that is positive for RhoA recruitment. (E) Representative example of a DMV that is negative for RhoA recruitment. (F) Quantification of the percentage of wild type or *ipgB1* DMVs per foci associated with RhoA in either mock-treated or RhoA duplex 2-depleted HT-29 cells. Each dot represents the percent RhoA-positive DMVs in a focus and the grey bars show the mean percentage of RhoA-positive DMVs from all foci measured in three biological replicates. At least twelve foci per condition were analyzed in each biological replicate. Error bars indicate standard deviation. One-way ANOVA with Tukey's multiple comparisons; ns, not significant; \*\*\*\*,  $p < 0.0001$

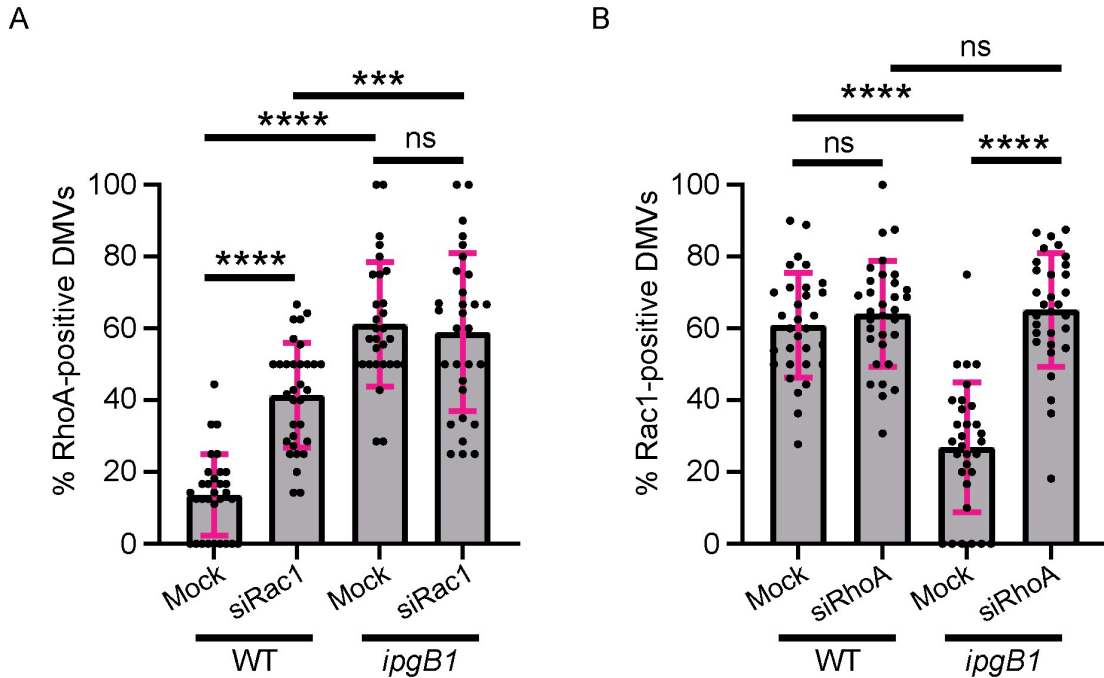


**Figure 3.11: IpgB1 modulates levels of Rac1 and RhoA DMVs**

(A) Quantification of the percentage of RhoA-positive DMVs per foci in mock-treated or Rac1 duplex 3-depleted HT-29 cells infected with wild type or *ipgB1* bacteria. Each dot represents the percent RhoA-positive DMVs in a focus and the grey bars show the mean percentage of RhoA-positive DMVs from all foci measured in three biological replicates. (B) Quantification of the percentage of Rac1-positive DMVs in mock-treated or RhoA duplex 2-depleted HT-29 cells infected with wild type or *ipgB1* bacteria. Each dot represents the percent Rac1-positive DMVs in a focus and the grey bars show the mean percentage of Rac1-positive DMVs from all foci measured in three biological replicates. At least ten foci per condition were analyzed in each biological replicate. Error bars indicate standard deviation. One-way ANOVA with Tukey's multiple comparisons; ns, not significant; \*\*\*,  $p < 0.001$ ; \*\*\*\*,  $p < 0.0001$

### 3.4.10 RhoA does not promote actin polymerization around DMVs

One of the most well studied functions of RhoA in cellular biology is regulation of the actin cytoskeleton. Several vacuole-residing pathogens stimulate the formation of actin structures around their vacuoles. Furthermore, the polymerization of actin around pathogen-containing vacuoles (actin cage) has been shown to be regulated by RhoA modulation (52). To determine whether the formation of RhoA-mediated actin cage could interfere with DMV escape, we investigated the percentage of *S. flexneri* DMVs that were surrounded by F-actin during infection of mbYFP-expressing HT-29 cells infected with CFP-expressing bacteria. Upon quantification of actin-positive (Figure 3.12A) and actin-negative (Figure 3.12B) DMVs, we found no difference between wild type and the *ipgB1* mutant (Figure 3.12C). These data suggest that the DMV escape defect of *ipgB1*, which is restored by RhoA depletion, is probably not due to differences in actin cage formation around DMVs.

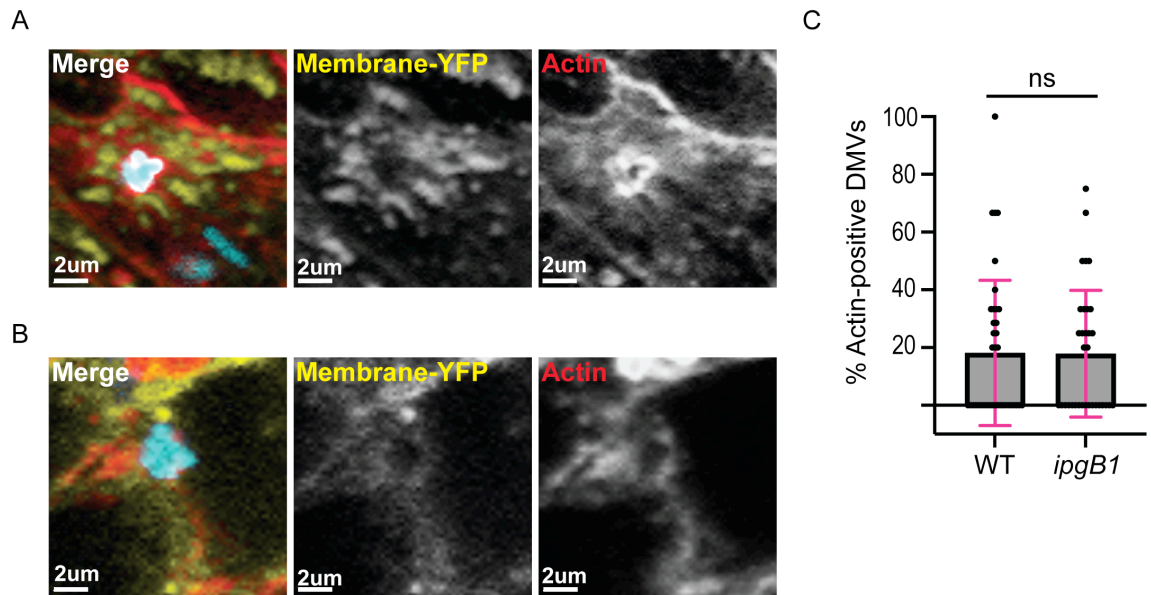


**Figure 3.12: IpgB1 does not affect actin accumulation around DMVs (A and B)**

Confocal images of HT-29 cells stably expressing plasma membrane-targeted YFP and infected for 5 hr with CFP-expressing *S. flexneri* and stained using AlexaFluor 594-conjugated phalloidin. Merged images are shown on the left, single YFP channel in middle, and single mCherry channel on the right. Scale bar, 2  $\mu$ m. (A) Representative example of a DMVs that is positive for actin recruitment. (B) Representative example of a DMV that is negative for actin recruitment. (C) Quantification of the percentage of wild type or *ipgB1* DMVs per focus associated with actin at 5 hr postinfection. Each dot represents the percent positive DMVs in a focus and the grey bars show the mean percentage of actin-positive DMVs from all foci measured in three biological replicates. At least twelve foci per condition were analyzed in each biological replicate. Error bars indicate standard deviation. Unpaired two-tailed t-test; ns, not significant

### 3.4.11 IpgB1 contributes to *S. flexneri* invasion and cell-to-cell spread *in vivo*

In order to correlate our findings in HT-29 cells to *in vivo* infection, we used the recently developed infant rabbit model of shigellosis (23). We infected animals with wild type or *ipgB1* bacteria and harvested colons 4 hr or 8 hr postinfection to measure invasion (foci number) and cell-to-cell spread (foci size), respectively. Colons were immunostained with antibodies against E-cadherin to visualize epithelial cells (Figure 3.13A, green) and *S. flexneri* (Figure 3.13A, red), and imaged using epifluorescence microscopy. To measure invasion, we enumerated foci along the entire colon. We found the colons infected with the *ipgB1* mutant contained significantly fewer foci than those infected with wild type bacteria (Figure 3.13B), indicating that IpgB1 is required for efficient invasion of colonic epithelial cells *in vivo*. As with our foci size experiments in HT-29 cells, we used the Metamorph software to delineate the borders of individual foci along the colons (Figure 3.13A, yellow lines) and derive the corresponding areas as a measure of cell-to-cell spread efficiency. Infection foci formed in animals infected by the *ipgB1* mutant were significantly smaller than those infected by wild type bacteria (Figure 3.13C), demonstrating a role for IpgB1 in cell-to-cell spread *in vivo*. Taken together, these results validate our work in HT-29 cells by unveiling a role for IpgB1 during invasion and intracellular dissemination *in vivo*.

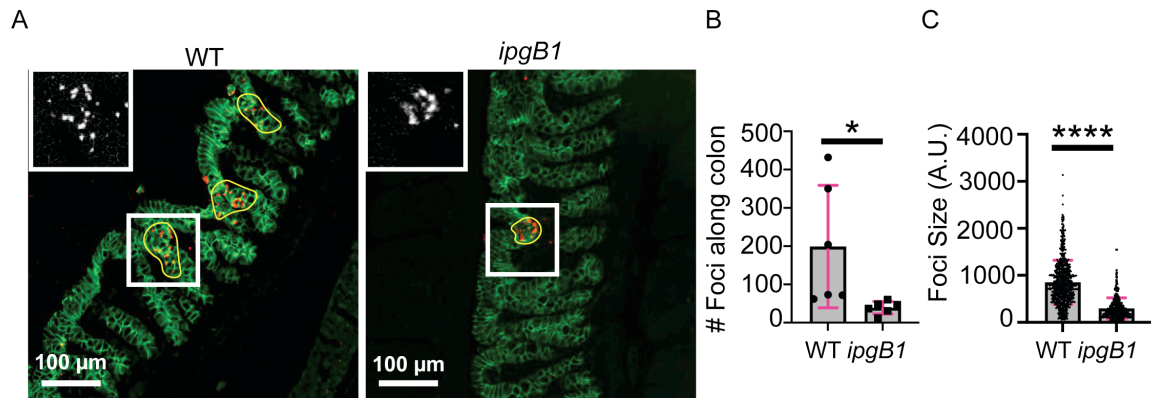


**Figure 3.13: IpgB1 contributes to *S. flexneri* invasion and cell-to-cell spread *in vivo*** (A) Representative images of colon sections infected with wild type or *ipgB1* *S. flexneri* at 8 hr postinfection. Yellow lines delineate individual infection foci and demonstrate how foci size is quantified. Insets in the top left show a zoom-in of the area outlined by the white box and displays single channel image corresponding to *S. flexneri* in an infection foci. E-cadherin, green; *S. flexneri*, red. Scale bar, 100 μm (B) Graph depicting total number of foci measured along entire colon at 4 hr postinfection. Each dot represents one animal and grey bars show average of six biological replicates. Error bars indicate standard deviation. Unpaired two-tailed t-test; \*,  $p < 0.05$  (C) Graph depicting foci size in infected colons at 8 hr postinfection. Each dot represents one focus and grey bars show average foci size across six biological replicates. Error bars indicate standard deviation. Unpaired two-tailed t-test; \*\*\*\*,  $p < 0.0001$

Data in this figure were collected by Köseoğlu, VK and Agaisse, HF. Colon sections were stained and imaged by DeVasure, BA. Foci size and number analyses were performed by Weddle, EA.

### 3.4.12 IpgB1 contributes to *S. flexneri* pathogenesis

We have recently demonstrated the critical importance of cell-to-cell spread in *S. flexneri* pathogenesis (23). To determine how the defects observed with the *ipgB1* mutant would relate to pathogenesis, we infected infant rabbits with either wild type bacteria or the *ipgB1* mutant. At 24 hr postinfection, animals infected with wild type bacteria displayed characteristic bloody diarrhea, while animals infected with *ipgB1* bacteria had attenuated symptoms (Figure 3.14A). Scoring for severity of symptoms for blood in stool (Figure 3.14B) and severity of diarrhea (Figure 3.14C) revealed that infection with the *ipgB1* mutant resulted in less blood and less severe diarrhea compared to infection with wild type. The animals were dissected at 24 hr postinfection and the colons were harvested and hematoxylin- and eosin-stained to score histopathology. For each infected animal, the entire colon was measured and scored for intact epithelium (Figure 3.14D, blue dashed lines) or fenestrated epithelium (Figure 3.14D, yellow dashed lines). The % fenestration along entire colon was calculated by dividing the length of colon with fenestrated epithelium by the total length of the colon. Colons from animals infected with the *ipgB1* mutant had significantly less epithelial fenestration compared to colons from infected with wild type bacteria (Figure 3.14E). These data indicate that IpgB1 significantly contributes to epithelial fenestration and bloody diarrhea during *in vivo* infection.

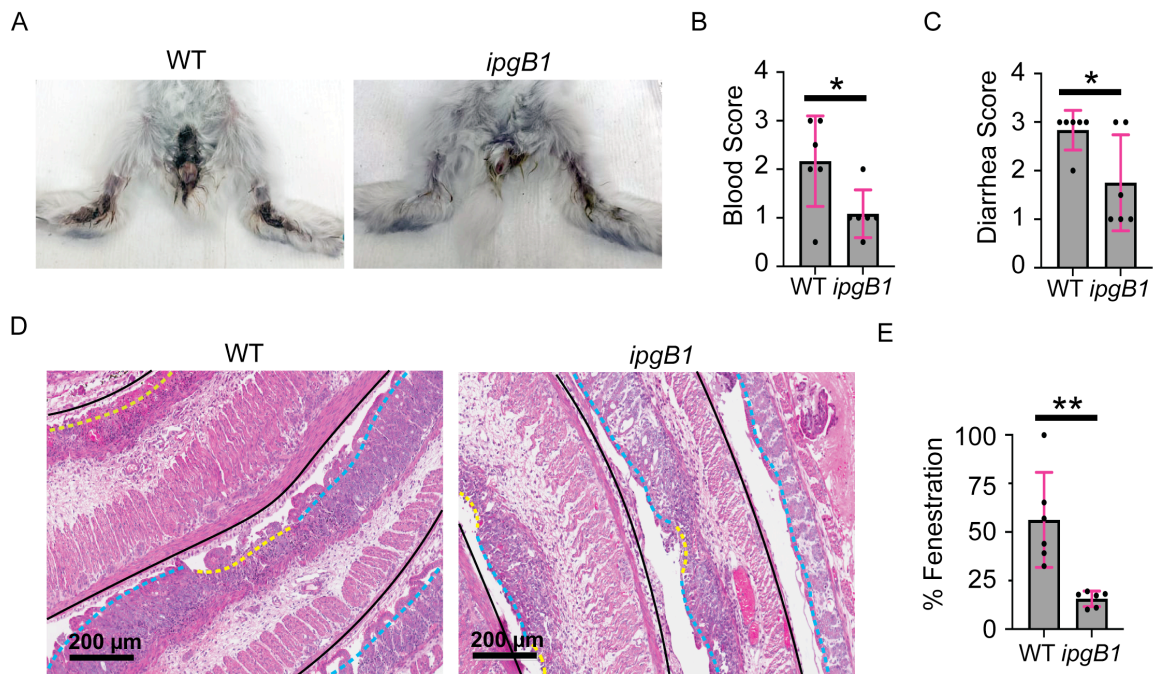


**Figure 3.14: IpgB1 contributes to *S. flexneri* pathogenesis (A)** Representative images of animals infected with wild type or *ipgB1* *S. flexneri* 24 hr postinfection. **(B and C)** Histopathology scores for blood in stool **(B)** or diarrhea **(C)** of animals at 24 hr postinfection with wild type or *ipgB1* strains. Each dot represents one animal and grey bars show average of six biological replicates. Error bars indicate standard deviation. Unpaired two-tailed t-test; \*,  $p < 0.05$  **(D)** Representative images of hematoxylin- and eosin-stained colon sections from animals infected with wild type or *ipgB1* at 24 hr postinfection. Black lines delineate the colon. Blue dashed lines indicate areas of intact epithelium and yellow dashed lines indicate areas with epithelial fenestration. Scale bar, 200  $\mu\text{m}$ . **(E)** Graph depicting the percentage of epithelial fenestration along entire colon. Each dot represents one animal and grey bars show average of six biological replicates. Error bars indicate standard deviation. Unpaired two-tailed t-test; \*\*,  $p < 0.005$

Data in this figure were collected by Köseoğlu, VK and Agaisse, HF. Fenestration analysis was performed by Weddle, EA.

### 3.5 Discussion

*S. flexneri* invasion and ABM have been well studied over several decades, but how the bacteria achieve intercellular dissemination (cell-to-cell spread) is still poorly understood. For instance, the *Shigella* GEFs protein IpgB1 and IpgB2 are known to play a role during invasion of epithelial cells ((117) and Figure 3.1 and 3.2). However, their potential role during later stages of infection is unclear. Here we characterized the role of IpgB1 and IpgB2 during *S. flexneri* dissemination in epithelial cells. We found that, similar to previously published results (71), IpgB2 is not required for cell-to-cell spread. However, we report a novel role for IpgB1 during cell-to-cell spread through DMV escape. As discussed below and summarized in Figure 3.15, our results suggest a model of DMV escape in which IpgB1 and Rac1 facilitate DMV escape by antagonizing the recruitment of RhoA to DMVs.

#### 3.5.1 How does IpgB1 antagonize the recruitment of RhoA?

Our results show that IpgB1 mediates *S. flexneri* dissemination by modulating host cell Rho GTPases. IpgB1 was found to have GEF specificity for Rac1 *in vitro*, with little activity on Cdc42, and no activity on RhoA (114). Consistently, we found that the role of IpgB1 in cell-to-cell spread relied on its GEF activity. Moreover, similar to IpgB1, we found that Rac1 supported cell-to-

cell spread through DMV escape. Our results are therefore in agreement with the notion that, similar to the invasion process, IpgB1 functions as a positive regulator of Rac1 during *S. flexneri* dissemination. Interestingly, we uncovered that depletion of RhoA restored *ipgB1* cell-to-cell spread and DMV escape to wild type levels. In addition, we found that IpgB1 expression antagonized the recruitment of RhoA to DMVs. Altogether these results suggest that the role of IpgB1 during cell-to-cell spread is to activate Rac1 to antagonize the recruitment of RhoA (Figure 3.15, Wild Type). The spatial and temporal antagonism between Rac1 and RhoA has been well documented in the cell biology field (118–123). During cell migration, Rac1 and RhoA are found predominantly at the leading and trailing edges of the cell, respectively (122). Recent studies also elegantly demonstrated the spatiotemporal oscillating waves of Rac1 and RhoA activity coordinate cell protrusion and edge dynamics (119, 123). Rac1/RhoA antagonism has also been found to drive cell shape, invagination, and heterogeneity during epithelial cell morphogenesis (120, 121). Mechanistically, Rac1 counteracts RhoA through activation or inactivation of signaling components displaying RhoGAP or RhoGEF activity, respectively (124, 125). The exact mechanism supporting Rac1/RhoA antagonism in the context of cell-to-cell spread remains to be determined. Our results however reveal that *S. flexneri* has evolved the IpgB1-dependent ability to take advantage of the cell intrinsic antagonism between

Rac1 and RhoA in order to block RhoA-mediated restriction of DMV escape (Figure 3.15, *ipgB1*).

### 3.5.2 How does RhoA restrict DMV escape?

**The actin cytoskeleton hypothesis.** The most studied role of Rho family GTPases, including RhoA, is regulation of the actin cytoskeleton. RhoA-dependent actin polymerization has been implicated in the stabilization of the pathogen-containing vacuole during *Chlamydia trachomatis* infection (52). *C. trachomatis* induces the recruitment of RhoA and the formation of actin filaments around its pathogen-containing vacuole (aka the inclusion). The formation of these actin structures is required for maintaining the integrity of the growing inclusion (52). It is thus tempting to speculate that, in contrast to *Chlamydia*, which uses the RhoA-dependent actin cytoskeleton to stabilize its vacuolar niche, *S. flexneri* antagonizes RhoA recruitment to suppress actin-dependent stabilization of DMVs, thereby promoting DMV escape. However, while our results do not exclude a role for dynamic actin polymerization in the process of *S. flexneri* DMV escape, the dramatic difference we observed in RhoA recruitment on *ipgB1* DMVs compared to wild type DMVs did not translate into differences in polymerized actin around the DMV (Figure S4). Therefore, we do

not favor a model in which RhoA restricts DMV escape through its role in regulation of the actin cytoskeleton.

**The membrane trafficking hypothesis.** Membrane trafficking, which is becoming increasingly recognized as being regulated by Rho GTPases (126, 127) is emerging as a key influencer of pathogen vacuolar stability in the field of host-pathogen interactions (128). There are several examples that involve RhoA as a membrane-bound compartment stabilizer in this context. For instance, the formation of the *Coxiella*-containing vacuole (CCV) relies on endosomal/lysosomal fusion events that are required for delivering membrane to expand the CCV. The *Coxiella* type IV secretion system effector, CirA, recruits and stimulates the activity of RhoA, which regulates the size of CCV (129, 130), possibly by incorporating membrane from favorable trafficking events. Similarly, the *Salmonella* effectors, SseJ and SseL, contribute to vacuole stability by rerouting the host lipid transporter OSBP1 to the *Salmonella*-containing vacuole (SCV)(131). Interestingly, this stabilization process relies on RhoA through SseJ recruitment and activation on SCVs (132–134). Thus, RhoA emerges as an important factor in the modulation of membrane trafficking events critical for the stability of pathogen-containing vacuoles. In the context of *S. flexneri* DMV escape, it is therefore tempting to speculate that IpgB1 antagonizes RhoA recruitment in order to block membrane trafficking events, that would otherwise

lead to vacuole stabilization. Combined with the tension applied to the vacuole as a consequence of bacterial growth, antagonizing RhoA recruitment may thus lead to membrane rupture and promote *S. flexneri* DMV escape.

### 3.5.3 How does IpgB1 contribute to pathogenesis?

We provide the first demonstration in a relevant animal model that a *S. flexneri* mutant lacking the T3SS effector IpgB1 is attenuated *in vivo*. Consistent with our experiments in HT-29 cells, *ipgB1* was less invasive (fewer infection foci) and less efficient at cell-to-cell spread (smaller infection foci). Animals infected with *ipgB1* had attenuated symptoms of illness, including epithelial fenestration and bloody diarrhea. We have previously shown that infection with a non-invasive *mxiG* mutant (76) does not cause epithelial fenestration or diarrhea, demonstrating that T3SS-dependent invasion of epithelial cells is necessary for pathogenesis in our infant rabbit model (23). However, invasion alone is not sufficient for causing symptoms as a mutant lacking *icsA*, which is equally as invasive as wild type but deficient in cell-to-cell spread, does not cause fenestration or bloody diarrhea (23). The *ipgB1* mutant produced fewer foci than wild type, but unlike *mxiG* still retained some ability to invade. The *ipgB1* mutant also produced smaller foci than wild type bacteria, but unlike *icsA*, maintained some level of cell-to-cell spread. It is therefore likely that the attenuated

symptoms of illness caused by the *ipgB1* mutant are the combined result of decreased epithelial invasion, leading to fewer potential sites of fenestration, and diminished cell-to-cell spread, resulting in decreased fenestration and less severe bloody diarrhea. These *in vivo* studies validated our findings in tissue culture and provide evidence that IpgB1 is required for severe *S. flexneri* pathogenesis.

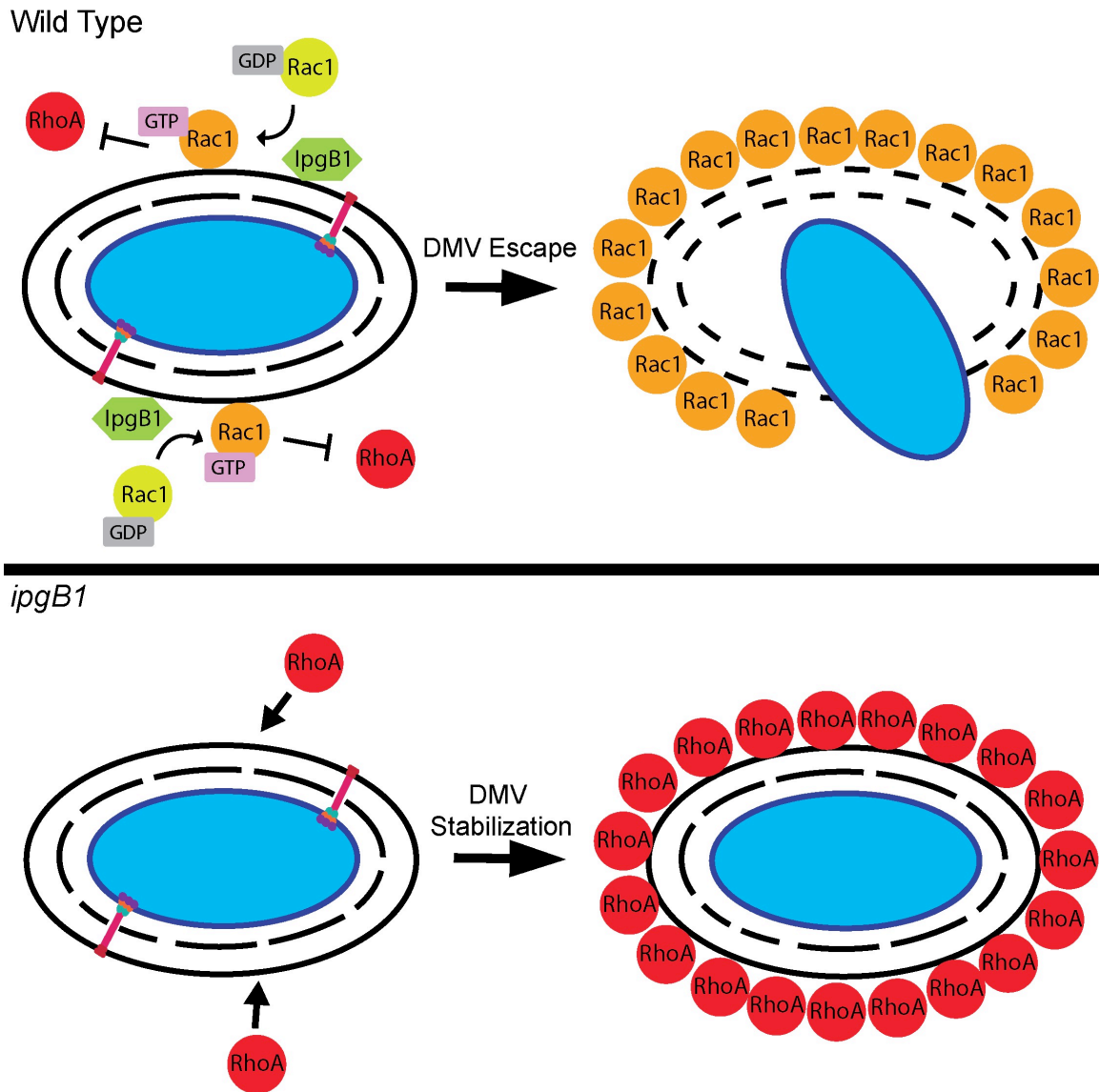


**Figure 3.15: Model for the role of IpgB1 in DMV escape during *S. flexneri* cell-to-cell spread**

In wild type *S. flexneri*, the type three secretion bacterial GEF, IpgB1, recruits Rac1 to DMVs. The IpgB1-Rac1 pathway antagonizes RhoA recruitment to the DMVs to promote DMV escape. The *ipgB1* mutant has diminished ability to recruit Rac1 to the DMV, which allows for the accumulation of RhoA and initiation of RhoA-mediated DMV stabilization, which impedes DMV escape.

**4. Chapter 4: The host lysophospholipase 2 (Lypla2) as a novel player in *S. flexneri* cell-to-cell spread**

This information in the chapter is unpublished.

Experimental Contributions: Weddle, EA designed and performed all experiments, analyzed all data, wrote and edited the chapter, and created all figures. Agaisse, HF supported all aspects of the work.

## 4.1 Summary

To provide further mechanistic insight into the process of *S. flexneri* DMV escape, we performed an siRNA screen for Rho family GTPase-related genes required for cell-to-cell spread. We found several hits that decreased wild type *S. flexneri* foci size, including lysophospholipase II (LYPLA2). LYPLA2, which is also called acyl protein thioesterase II (APT2), is a serine hydrolase that removes acyl chains from lysophospholipids (LysoPLs) in the cell membrane, contributing to membrane structure and lipid homeostasis. The hydrolase activity of LYPLA2/APT2 can also de-palmitoylate membrane-anchored proteins. Here, we show that LYPLA2/APT2 is required for efficient cell-to-cell spread of *S. flexneri* through DMV escape. Depletion of LYPLA2/APT2 did not further reduce *ipgB1* foci size, suggesting that LYPLA2/APT2 could be functioning downstream of IpgB1/Rac1. Future studies should aim to determine the exact role of LYPLA2/APT2 in DMV escape and whether its activity is regulated by a bacterial effector.

## 4.2 Introduction

Cell-to-cell spread of *S. flexneri* results in the formation of double-membrane vacuoles (DMVs), comprised of an inner membrane from the primary infected cell and an outer membrane from the newly infected cell. Rupture of

these DMVs and escape to the cytosol of the newly infected cell is a key step in the process of cell-to-cell spread; however, DMV escape is poorly understood. My thesis identifies two *S. flexneri* effector proteins, IcsB (chapter 2) and IpgB1 (chapter 3) as central players in DMV escape. Further, host factors belonging to the Rho family of small GTPases have emerged as being important for DMV escape. However, additional host factors involved and the mechanism of membrane rupture remain to be determined.

Work presented in this thesis (chapter 3) indicates that the small GTPase RhoA plays a negative role in DMV escape during *S. flexneri* cell-to-cell spread. We show that this negative pressure is relieved by the T3SS effector IpgB1, which functions as a GEF for Rac1, to counteract RhoA and facilitate efficient DMV escape. We sought to better understand the mechanism of this pathway supporting DMV escape. Rac1 and RhoA have been shown to play antagonistic roles in a variety of physiological process, including cell migration, cell morphogenesis, and blood pressure regulation (120, 121, 123, 135). Some of the intermediate factors that facilitate Rac1-RhoA antagonism have been identified and could be potentially implicated in DMV escape. Additionally, Rho family small GTPases have a plethora of targets and regulate numerous cellular targets. Therefore, we reasoned that the best way to gain additional mechanistic insight

into the IpgB1-Rac1-RhoA pathway contributing to DMV escape was to conduct an siRNA screen.

### 4.3 Materials and Methods

#### 4.3.1 Cell lines and bacterial strains

HT-29 cells (ATCC HTB-38) were cultured at 37°C with 5% CO<sub>2</sub> in McCoy's 5A medium (Gibco) supplemented with 10% heat-inactivated fetal bovine serum (FBS) (Invitrogen). The wild-type *Shigella flexneri* strain used in this study is serotype 2a 2457T and the *ipgB1* mutant (chapter 3) was made by replacing the coding region with a kanamycin resistance cassette. HT-29 cell lines stably expressing yellow fluorescent protein (YFP) membrane markers were generated using the pMX-Mb-YFP vector. Lypla2-citrine was amplified by PCR and cloned into the pMX plasmid via Pac1 and Not1 sites. The corresponding lentiviruses were generated in 293T cells co-transfected with the packaging constructs pCMVΔ8.2Δvpr (HIV helix packaging system) and pMD2.G (a vesicular stomatitis virus glycoprotein) as previously described (100).

### 4.3.2 Bacterial Infection

*S. flexneri* was grown as previously described in chapters 2 and 3. For time-lapse microscopy, imaging began 2 hr postinfection. For *S. flexneri* focus size analysis, infected cells were incubated at 37°C for 16 hr.

### 4.3.3 siRNA Transfection

Cells were transfected by reverse transfection with four Dharmafect1 individual small interfering RNAs (siRNAs) (50 nM total final concentration) targeting LYPLA2 or siRNA buffer alone (mock) 96 h in a 96-well format (Corning 3904). For live microscopy and tracking experiment, duplex 1 targeting LYPLA2 was used at 50 nM concentration. Knockdown efficiency was determined by Western blotting. Cells were infected or collected for western blot on day four of knockdown.

### 4.3.4 Antibodies

The following antibodies were used for western blot (WB) and/or immunofluorescence (IF): mouse monoclonal anti-Lypla2 (Santa Cruz sc-515061; WB 1:200), rabbit polyclonal anti-Actin (Sigma WB 1:10,000), HRP-conjugated goat anti-rabbit IgG (Jackson WB 1:10,000), HRP-conjugated goat anti-mouse IgG (Jackson WB 1:10,000)

#### 4.3.5 Size of infection foci

The size of infection foci formed in HT-29 cells and infected with CFP-expressing *S. flexneri* strains was determined in a 96-well plate format. After fixation with 4% paraformaldehyde for 20 minutes at room temperature, the plates were imaged using the ImageXpress Micro imaging system (Molecular Devices). Margins of individual foci were defined manually, and image analysis for foci size (area) was performed using the region measurement function in the ImageXpress imaging software (Molecular Devices) as previously described. Image analyses were conducted on at least 50 infection foci in each biological replicate (n) and for at least three biological replicates (N).

#### 4.3.6 Live Imaging

Bacterial dissemination was monitored using time-lapse confocal microscopy. Plasma membrane YFP-expressing HT-29 cells were grown in collagen-coated (Sigma C3867, 1:100) eight-well chambers (Lab-Tek II (Thermo Fisher Scientific catalog no. 155409) at 37°C in 5% CO<sub>2</sub>. Cells were infected with CFP-expressing *S. flexneri* strains and centrifuged at 800 rpm for 4 min. Bacteria were then allowed to invade for 1 hr before gentamicin (50 µg/ml) and IPTG (10 mM final concentration) were added to kill the extracellular bacteria and induce

CFP expression, respectively. Starting 2 hrs postinfection, cells were imaged and tracking was performed as previously described ((23) and chapters 2 and 3).

## 4.4 Results

### 4.4.1 LYPLA2/APT2 facilitates *S. flexneri* cell-to-cell spread

We built a screening library of ~200 Rho family small GTPase-associated genes based on literature search and recent proteomic insights (136). HT-29 cells were transfected with four single siRNA duplexes targeting each gene in this library and were then infected with either wild type or *ipgB1 S. flexneri*. Genes were considered as potential “hits” if knockdown with at least two of the four duplexes influenced the size of the infection foci (spreading) in at least two of the three replicates that we performed. We found four genes (LYPLA2, Lysophospholipase 2; ACBD5, acyl-CoA binding domain containing 5; CFL1, cofilin 1; PFN1, profilin 1) that resulted in decreased wild type, but not *ipgB1*, spreading (Figure 4.1A, green, WT). As expected, our positive control for decreased spreading, WASL, decreased spreading of both wild type and *ipgB1* bacteria (Figure 4.1A, green, middle). We did not find any genes that exclusively decreased *ipgB1* spreading. RhoA, our positive control for increased *ipgB1* spreading, was found as a hit that exclusively increased *ipgB1* foci size (Figure

4.1A, red, *ipgB1*). However, we did not find any other genes that increased spreading of wild type or *ipgB1* bacteria (Figure 4.1A, red).

Cofilin 1 and Profilin 1 are actin remodeling proteins that have been previously implicated in *Shigella* infection during epithelial cell entry and actin-based motility, respectively (64, 137). ACBD5 is a peroxisome membrane protein that mediates peroxisome- endoplasmic reticulum membrane contact sites and functions in lipid transport and homeostasis (138). LYPLA2 is a serine hydrolase that contributes to the maintenance of the shape, structure, and fluidity of cellular membranes. Specifically, LYPLA2 is responsible for the conversion of lysophospholipids to free fatty acid and glycerophosphate (139). Additionally, LYPLA2 removes thioester-linked long chain fatty acids from membrane-anchored proteins, regulating their sublocalization, and is therefore also named acyl protein thioesterase 2 (APT2) (140). Given that LYPLA2/APT2 is a known modulator of membrane structure, we decide to follow-up this hit from our siRNA screen as a potential contributor to DMV escape.

We confirmed the efficiency of LYPLA2 knockdown with four siRNA duplexes by western blot using a LYPLA2 antibody and found that three of the four duplexes resulted in over 80% depletion of LYPLA2, while the fourth resulted in ~40% reduction in protein level (Figure 4.2A). To confirm our screening results, we measured the size of wild type or *ipgB1* infection foci

formed in mock-treated or LYPLA2-depleted HT-29 cells at 16 hrs postinfection. All four LYPLA2 duplexes significantly decreased wild type cell-to-cell spread (Figure 4.2B, wild type). However, depletion of LYPLA2 did not further decrease *ipgB1* spreading (Figure 4.2B, *ipgB1*). This trend is similar to what we observed with knockdown of the target of IpgB1, Rac1, and suggests that IpgB1-Rac1 could be functioning in the same pathway as LYPLA2.

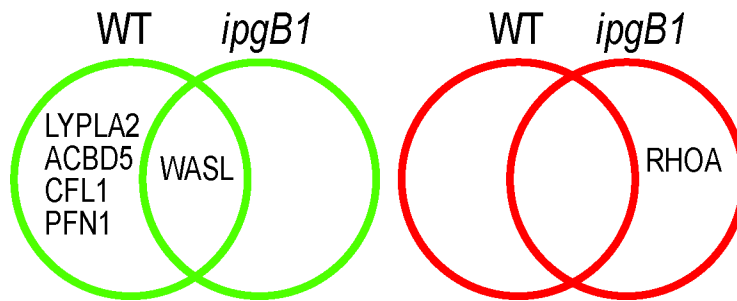


**Figure 4.1: Rho family-related siRNA screen** Overview of hits from siRNA screen. Green circles indicate genes that decreased foci size of wild type, *ipgB1*, or both. Red circles indicate genes that increased foci size of wild type, *ipgB1*, or both.

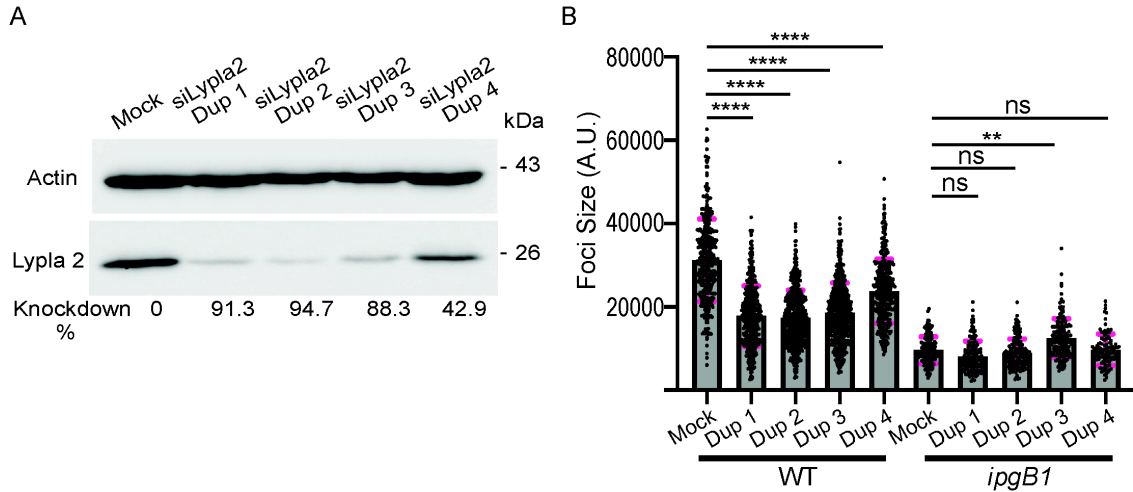


**Figure 4.2: LYPLA2 depletion reduces cell-to-cell spread (A)** Western blot showing knockdown efficiency of four siRNA duplexes targeting LYPLA2. LYPLA2 (bottom panel) was normalized to loading control (actin, top panel) and knockdown efficiency was calculated relative to mock-treated cells. **(B)** Quantification of wild type or *ipgB1* foci size at 16 hr postinfection in mock-treated cells or cells transfected with four LYPLA2-targeting siRNA duplexes. Three independent biological replicates were performed, each containing at least 50 foci. Each point represents one focus and the grey bars represent the mean foci size. Error bars shown in pink represent the standard deviations; One-way ANOVA was performed with Dunnett's multiple comparisons test; ns, not significant; \*\*,  $p < 0.005$ ; \*\*\*\*,  $p < 0.0001$

#### 4.4.2 LYPLA2/APT2 promotes *S. flexneri* DMV escape

To determine if LYPLA2 played a role in DMV escape, we performed live confocal microscopy and tracking of spreading of wild type bacteria in mock-treated (Figure 4.3A) or LYPLA2-depleted (Figure 4.3B) HT-29 cells expressing mbYFP. The majority of bacteria (77%) in mock-treated cells successfully escaped DMVs in the adjacent cell (Figure 4.3C, wild type mock, green), while a small proportion remained trapped in DMVs (12%)(Figure 4.3C, wild type mock, yellow) or failed to resolve protrusions into DMVs (11%)(Figure 4.3C, wild type mock, blue). In contrast, only 34% of wild type bacteria successfully escaped DMVs in LYPLA2-depleted cells (Figure 4.3C, wild type Lypla2 KD, green) and the majority (51%) remained trapped in DMVs (Figure 4.3C, wild type, Lypla2 KD, yellow). In LYPLA2-depleted cells, 16% of bacteria failed to resolve from protrusions into DMVs (Figure 4.3C, wild type Lypla2 KD, blue). This increase was not statistically significant compared to mock-treated cells. There was a significant increase in the time that bacteria spent in protrusions (Figure 4.3D) and DMVs (Figure 4.3F) in LYPLA2-depleted cells compared to the mock-treated cells. There was no difference in the time spent in VLPs between mock and LYPLA2 knockdown conditions (Figure 4.3E). These data support the notion the LYPLA2 is required for efficient DMV escape of *S. flexneri*.

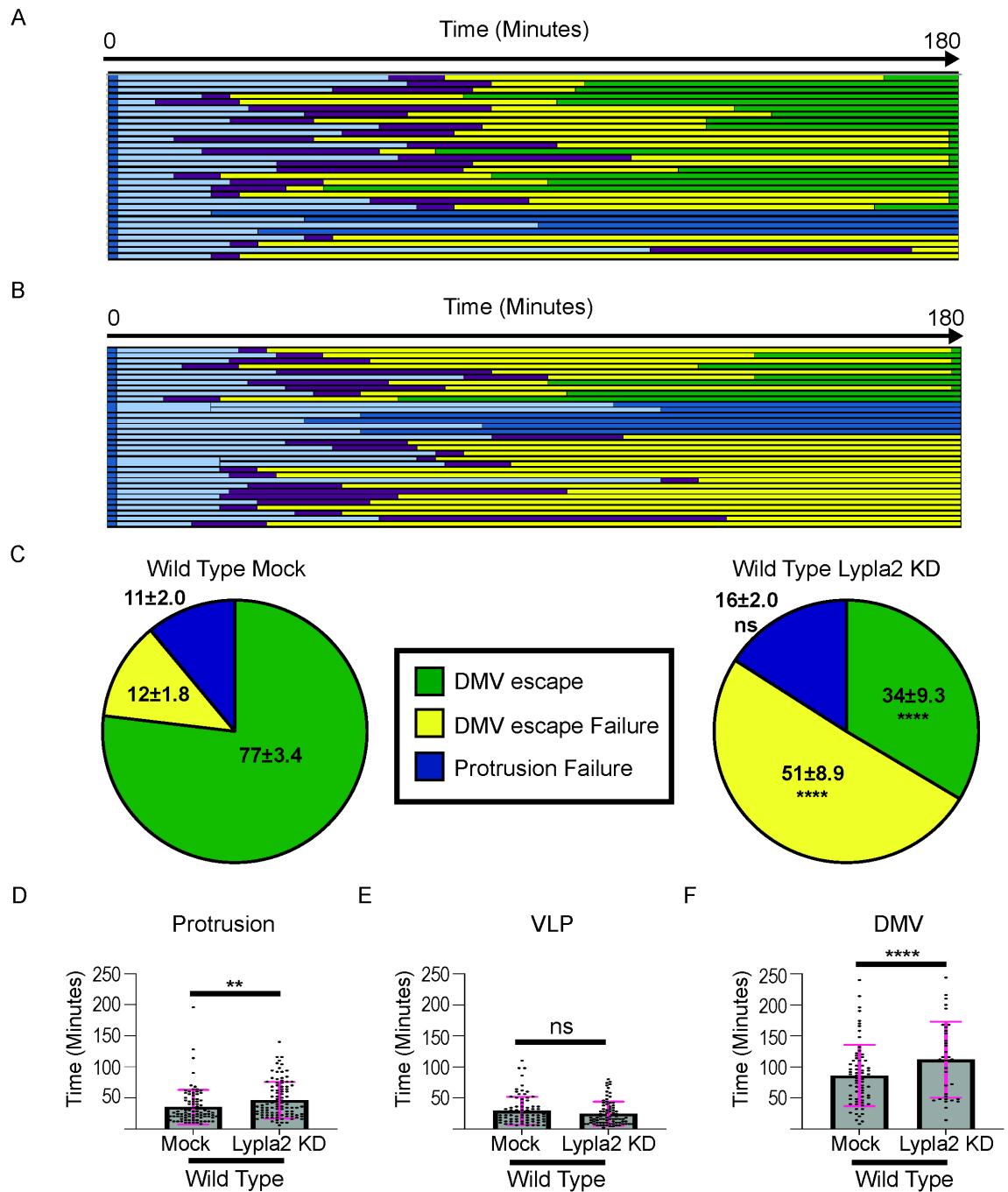


### Figure 4.3: LYPLA2/APT2 is required for efficient DMV escape (A)

Representative tracking analysis of wild type CFP-expressing *S. flexneri* in (A) mock-treated or (B) LYPLA2-depleted HT-29 cells expressing plasma membrane-targeted YFP. Each bar represents the tracking of a single bacterium over 180 minutes. The thicker bars indicate when bacteria divided and branched during spreading. At least 30 bacteria were tracked for each strain per biological replicate. (C) Graphs showing the proportions of fates of tracked bacteria from 4

biological replicates. Standard deviations of the means are indicated. Two-way ANOVA with Sidak's multiple comparisons was performed; ns, not significant; \*\*\*\*,  $p < 0.0001$ . Time spent in protrusions (**D**), VLPs (**E**), or DMVs (**F**) is shown for all tracked bacteria. Each dot represents a single bacterium and the grey bars show the mean of all tracked bacteria from four biological replicates. Error bars indicate standard deviation. Unpaired two-tailed t-tests were performed; ns, not significant; \*\*,  $p < 0.005$ ; \*\*\*\*,  $p < 0.0001$

## 4.5 Discussion

These data indicate that the host lysophospholipase LYPLA2/APT2 is a novel factor involved in *S. flexneri* DMV escape during cell-to-cell spread. LYPLA2/APT2 is a cytosolic serine hydrolase with thioesterase activity that catalyzes the removal of long-chain fatty acids (depalmitolation) from membrane-associated proteins (Figure 4.4, APT2 activity) or membrane components lysophospholipids (LysoPLs)(Figure 4.4, LYPLA2 activity) (139, 140). LYPLA2/APT2 possesses a catalytic triad of Asp176, His210, and Ser122 and is able to hydrolyze both 16 and 18 chain fatty acids, with specificity for sn1-lysoPLs (139). The function of LYPLA2/APT2, along with its homolog LYPLA1/APT1, in LysoPL hydrolysis is important for lipid homeostasis and proper cell membrane composition (139, 141, 142). Interestingly, in neuronal cells, depletion of both LYPLA1/APT1 and LYPLA2/APT2 was required for substantial cellular effects on LysoPL levels, suggesting some redundancy in function (143). Although HT-29 cells express both LYPLA1/APT1 and LYPLA2/APT2, we did not observe an effect of LYPLA1/APT1 depletion on *S. flexneri* cell-to-cell spread in our siRNA screen, suggesting that *S. flexneri* may have evolved to specifically co-opt LYPLA2/APT2 for DMV escape.

LYPLA2/APT2 is also an important enzyme for the depalmitolation of several membrane-anchored proteins, including cell differentiation signaling

proteins and cell junction scaffolding proteins small GTPases (144). Interestingly, proper localization and function of LYPLA2/APT2 relies on a palmitoylation/depalmitoylation cycle of the enzyme, which may be achieved by LYPLA1/APT1 or LYPLA2/APT2 itself (143). The homologous LYPLA1/APT1 protein can also be regulated by the Rho family small GTPase CDC42 (144), suggesting LYPLAs/APTs undergo further spatiotemporal regulation. We have shown that the Rho family GTPases RhoA and Rac1 are important for DMV escape of *S. flexneri*; therefore, the question remains as to whether they could be involved in LYPLA2/APT2 regulation. It is also unclear whether the role of LYPLA2/APT2 in DMV escape relies on the T3SS effector IpgB1. Depletion of LYPLA2/APT2 decreased wild type, but not *ipgB1* foci size, suggesting that LYPLA2/APT2 could function in the same pathway; however, future studies are necessary to determine if these factors act cooperatively or in distinct manners.

The activity of LYPLA2/APT2 that contributes to DMV escape also remains unknown. LYPLA2/APT2 could directly disrupt the vacuolar membrane by hydrolysis of lysophospholipids. Consistently, the extraction of acyl chains is predicted to deform the membrane (145), which could be exacerbated by additional host or bacterial factors that drive DMV escape. Alternatively, LYPLA2/APT2 could release protein(s) from the vacuole membrane to challenge its integrity, perhaps by relief of steric hindrance or prevention of downstream

trafficking events that would lead to the expansion and/or stabilization of the vacuolar membrane. Future studies are needed to determine whether LYPLA2/APT2 is localized to the DMV and whether its localization and/or activity are facilitated by IcsB, IpgB1, or another T3SS effector protein.

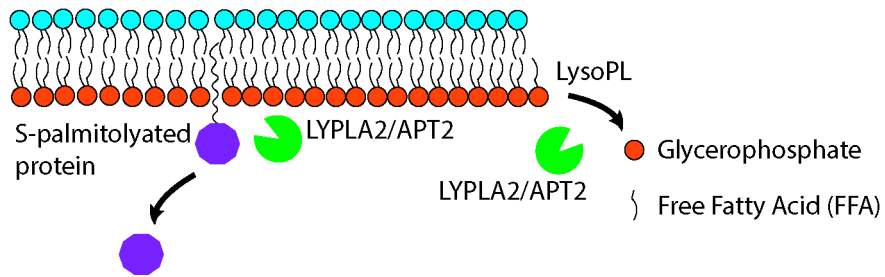


**Figure 4.4: The activities of LYPLA2/APT2.** LYPLA2/APT2 is a serine hydrolase with esterase and thioesterase activity that can cleave long chain fatty acids from the sn1 position of lysophospholipids (LysoPLs) in the membrane to form free fatty acid (FFA) and glycerophosphate (**LYPLA2 activity**). LYPLA2/APT2 can also cleave long chain fatty acids from proteins (depalmitolation), altering their subcellular locations (for example, removal from membranes) (**APT2 activity**).

**5. Chapter 5: Perspectives and Future Directions**

## 5.1 Summary of work

My thesis work has uncovered multiple factors, both host and bacterial, that contribute to *S. flexneri* DMV escape (Figure 5.1). We characterized two T3SS effectors, IcsB (Chapter 2) and IpgB1 (Chapter 3), during cell-to-cell spread. IcsB, via its acyltransferase activity, is required for efficient DMV escape and cell-to-cell spread through an unknown mechanism that does not involve host autophagy, a process that IcsB was proposed to modulate. IpgB1, via its GEF activity, facilitates cell-to-cell spread through its target small GTPases, Rac1, to antagonize RhoA-mediated restriction of DMV escape. We also found a novel host factor, Lypla2 that plays a role in DMV escape (Chapter 4). In this chapter, I will further discuss the implications of our work in the context of *Shigella* infection.

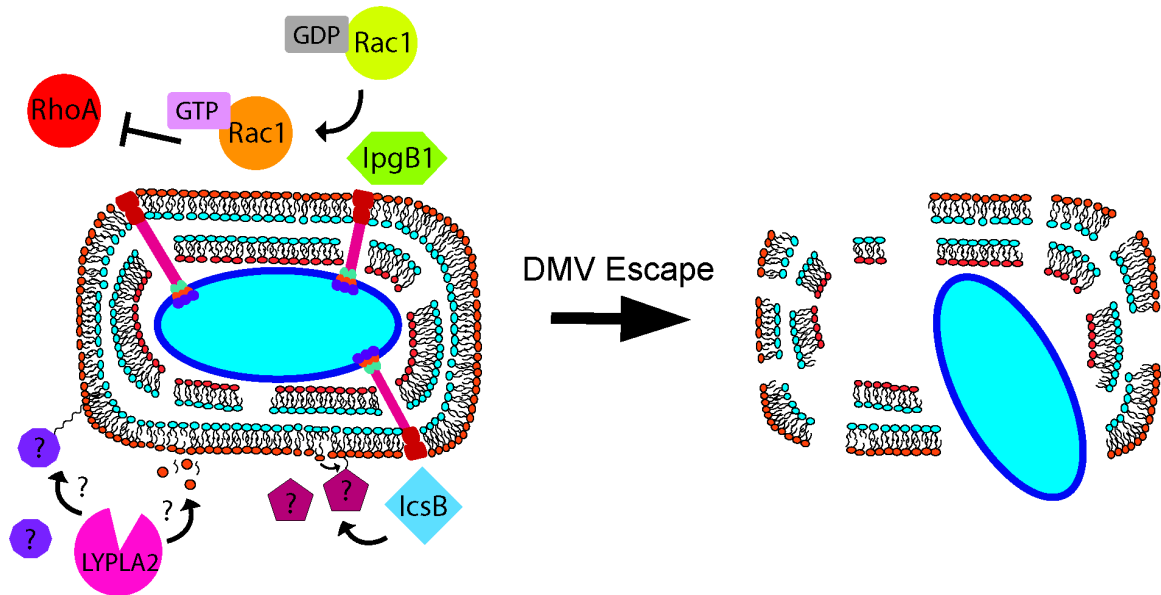


**Figure 5.1: Current Model of DMV escape.** The T3SS effector IcsB functions as an acyltransferase, which could recruit an unidentified host protein to the DMV through lipid modification or could directly disrupt the vacuole membrane by altering the fatty acid composition. The T3SS effector IpgB1 functions as a GEF for Rac1 to antagonize RhoA-mediated stabilization of the DMV. The host LYPLA2/APT2 could directly disrupt the vacuole membrane through its serine hydrolase activity by cleaving LysoPLs in the vacuole membrane. LYPLA2/APT2 could also function as an acyl protein thioesterase to remove membrane-anchored proteins from the vacuole membrane. The concerted efforts of IcsB, IpgB1, and LYPLA2/APT2 lead to the global destruction of the DMV membrane and DMV escape.

## 5.2 DMV escape as a process driven by T3SS effectors

Before my thesis research, the process of DMV escape by *S. flexneri* was poorly characterized. *S. flexneri* does not possess obvious candidates for driving DMV escape, such as phospholipases. Early electron microscopy studies showed that inactivation of the T3SS led to bacteria being trapped in double membrane vacuoles (47). Live imaging later unambiguously demonstrated that the T3SS is required for DMV escape (76). The T3SS translocases IpaC and IpaB form a translocon pore, which contributes to vacuole escape (36, 38, 47, 146) and is thought to also play a role in DMV escape. However, assessing the potential role of the translocon in challenging the integrity of the membrane was difficult because the translocon is also required for translocation of effector proteins. Our work is the first, to our knowledge, that unambiguously implicates specific bacterial effectors in DMV escape.

### 5.2.1 What is the mechanism of IcsB-dependent DMV escape?

The T3SS effector IcsB was originally proposed to counteract autophagy during *S. flexneri* cell-to-cell spread by preventing the recruitment of LC3 to cytosolic or vacuole-bound bacteria (51, 84). We clarified these results by using live imaging and found that LC3 was not recruited to cytosolic bacteria, but instead was exclusively recruited to a small proportion (~20%) of DMVs during

spread. Further, the function of IcsB is not to counteract the recruitment of LC3, but to facilitate escape from DMVs following cell-to-cell spread.

The mechanism by which IcsB (chapter 2) mediates DMV escape remains unknown. Mutation of one of the catalytic residues (C306) of IcsB abrogated its ability to restore cell-to-cell spread of the *icsB* mutant, implicating the acyltransferase activity of IcsB in its role during cell-to-cell spread. IcsB is an 18-carbon fatty acyltransferase that acylates the lysine residues of more than 60 membrane-associated targets (103, 112). These targets range from small GTPases of the Ras, Rho, and Rab families to SNARE proteins and other components of membrane trafficking pathways (112). Systematic exploration of these targets aiming to uncover the “functional” target of IcsB that leads to DMV escape would be demanding and it is unlikely that a single functional target leads to DMV escape. Given the number of membrane trafficking-associated targets, IcsB could be a central modulator of membrane trafficking. Fatty acylation makes proteins more hydrophobic and can induce stable membrane association (147, 148). This activity could be used to stably recruit proteins to the DMV, decorating the DMV with factors that would lead to favorable trafficking events. Alternatively, this activity could be used to trap proteins on the DMV, sequestering them and disrupting normal membrane trafficking that could lead

to degradation of the bacteria or expansion of the DMV membrane that would mechanically prevent DMV escape.

While several targets of IcsB-dependent acylation were identified, the fatty acid donors remain unclear. IcsB was shown to be able to utilize stearyl-CoA to transfer 16 or 18-carbon fatty acid chains to target proteins (112). However, the source of these long chain fatty chains during infection is unknown. If IcsB could utilize fatty acid chains from membrane lipids, such as sphingolipids or glycerophospholipids, it could directly disrupt the vacuolar membrane. In this regard, the important consideration for the role of IcsB in DMV escape could be the source of fatty acids instead of the modified targets. Interestingly, the most common fatty acids in mammalian membranes contain 18 carbons (147). Furthermore, 18-carbon fatty acid containing phospholipids are enriched in the inner, cytoplasmic leaflet of the plasma membrane (149), which is likely where IcsB is localized following translocation from the T3SS into the adjacent cell cytosol. Another important lipid component of the membrane, cholesterol was also reported to be important for IcsB activity (102), although it is unknown whether cholesterol contributes to proper localization of IcsB or to its catalytic activity.

Future studies should aim to compare the lipid composition of the DMV membrane of wild type and *icsB* DMVs to uncover potential contributions of IcsB

to remodeling of lipid membrane. An siRNA screen for the roles of IcsB-modified targets (112) in *S. flexneri* could reveal potential functional targets for DMV escape during cell-to-cell spread. Given the number of targets, there are likely multiple important targets so there may not be only one single gene whose knockdown leads an effect on cell-to-cell spread. In this case, combinatorial knockdowns or chemical inhibitors that can target multiple proteins or pathways could be used to assess the functionality of these targets in cell-to-cell spread.

### **5.2.2 What is the mechanism of IpgB1-dependent DMV escape?**

Our work revealed that another T3SS effector, IpgB1, is involved in DMV escape. IpgB1 was previously characterized as a guanine nucleotide exchange factor (GEF) that specifically activates the host Rho family small GTPase Rac1, with slight activity toward Cdc42 (41). In chapter 3, we showed that the functional role of IpgB1/Rac1 during DMV escape is to antagonize RhoA localization to DMV. This demonstrates an indirect mechanism of DMV escape, whereby the role of IpgB1 is not to directly disrupt the vacuolar membrane, but to influence host proteins/processes that can lead to membrane disruption.

### 5.2.3 How are IcsB and IpgB1 localized during infection?

Our work shows that IcsB and IpgB1 contribute to DMV escape. Evidence from our lab and others suggests that IcsB is localized to DMV and functions locally. Furthermore, Rac1 and RhoA localize differently to *ipgB1* DMVs, suggesting that IpgB1 exerts its effects locally, on the DMV. However, the localization IcsB and IpgB1 during infection requires further investigation.

Tagging of T3SS effectors to allow for their visualization has been challenging as many tags affect secretion, translocation, or function of the effector (150, 151). IcsB binds cholesterol, a major component of cell membranes and modifies membrane-associated targets (102, 112). A tagging system that involves fusion of several repeats of a linear peptide (Suntag) to the protein has been used to localize IcsB to *Shigella*-containing vacuoles (112). The Suntag peptide is recognized by a single chain antibody (scFV), which can be expressed in cells fused to a fluorescent protein for visualization (152). The Suntag-scFV system can uniquely be used to visualize T3SS effectors once they have been translocated into the host cytosol and are accessible by scFV. We have created an HT-29 cell line that stably expresses mCherry-scFv and have used it to confirm that IcsB-Suntag localizes to DMVs following cell-to-cell spread. This approach could be used to study the localization of IpgB1-Suntag during infection. Excitingly, since the Suntag-scFV system does not rely on fixation and staining,

this approach could be used to detect the translocation of IcsB-Suntag and IpgB1-Suntag from *S. flexneri* in DMVs in real-time during cell-to-cell spread.

### **5.3 Host factors as contributors to *S. flexneri* DMV escape**

In the field of vacuolar stability of vacuole-residing bacteria, it is proposed that the bacteria actively block cellular processes aimed at disrupting vacuole integrity through the activity of microbial proteins termed “vacuole guards” (128). It has been proposed in the context of primary vacuoles, that *S. flexneri*, which lacks canonical membrane disruption proteins (i.e. phospholipases) and vacuole guard proteins, may rely on the innate ability of the host cell to disrupt the vacuole. The potential utilization of host processes by *S. flexneri* to drive primary vacuole escape is discussed in chapter 1. Our data support the notion that hijacking of host factors and processes may also promote *S. flexneri* DMV escape.

#### **5.3.1 Host membrane trafficking as a regulator of vacuole escape**

We speculate that host membrane trafficking plays a significant role in DMV escape. There is a plethora of evidence that modulation of membrane trafficking supports the formation and stabilization of pathogen-containing vacuoles. On the other hand, there is also increasing evidence that membrane

trafficking influences primary vacuole escape of the cytosolic pathogens *S. flexneri* and *L. monocytogenes*. Therefore, subtle differences in bacterial-driven membrane trafficking to the vacuole could influence whether intravacuolar or cytosolic pathogens maintain or destabilize vacuoles, respectively.

### 5.3.1.1 Modulation of membrane trafficking to remain inside vacuole

Vacuole-residing bacteria are masters at manipulating host membrane trafficking pathways for their own benefit. One goal of modulation of membrane trafficking by vacuole-residing bacteria is to prevent degradation by the endocytic pathway. Endosomal maturation is marked by differential recruitment of Rab-family small GTPases, modification of phosphoinositide lipids, decreasing pH of the endosomal compartments, and the eventual degradation of vacuolar contents by lysosomal hydrolases. Some bacteria, such as *Salmonella* and *Coxiella* enable endosomal maturation to a point, but diverge from the pathway before they are degraded. Other bacteria, such as *Legionella*, *Chlamydia*, and *Mycobacteria*, diverge early from the endocytic pathway by avoiding the recruitment of canonical endocytic Rab proteins (153–159). Modulation of membrane trafficking is also important for acquiring membrane to allow for the expansion of the pathogen-containing vacuole and many bacteria hijack vesicular trafficking pathways for this purpose. Examples of how vacuole-residing bacteria modulate

host membrane trafficking are presented in table 5.1. Surprisingly, in chapter 2 we found a previously unappreciated role for vATPase-dependent endo/lysosomal acidification in *S. flexneri* cell-to-cell spread (Figure 2.12). Future studies will determine whether this role is related to DMV escape, but this finding suggests that membrane trafficking could also be harnessed by bacteria to promote DMV escape.

Pathogen	Virulence factor	Host target	Effect on Trafficking/Role in infection	Reference
<i>Salmonella</i>	SopB	Rab5/VPS34	PI3P enrichment on SCV/endosomal maturation of SCV	(160, 161)
	?	EEA1	Endosomal maturation of SCV	(162)
	?	Rab7/LAMP1/LAMP2	SCV biogenesis/endosomal maturation of SCV	(163)
	SopD2	Rab7	Disruption of endocytic trafficking	(164, 165)
	SifA	SKIP/PHLEKHM2, Rab9; kinesin-1; HOPS Complex	Subvert retrograde trafficking of mannose-6-phosphate receptors to misroute lysosomal hydrolases; Provide membrane for formation of Sifs	(166–169)
<i>Coxiella</i>	CirA	RhoA	Recruit Rab5 and Rab7 to CCV, Modulation of endosomal/lysosomal trafficking	(170, 171)
	?	v-ATPASE, LAMP1, LAMP2, LAMP3	Endosomal maturation of CCV	(157)

<i>Mycobacteria</i>	LAM	Block PI3P	Prevent endosomal maturation of MCV	(159)
	SapM	Hydrolyze PI3P	Prevent endosomal maturation of MCV	(172)
	?	Rab22a	Prevent transition from Rab5 recruitment to Rab7	(173)
<i>Legionella</i>	VipD	PI3P	Removes PI3P from LCV to prevent Rab5 and EEA1 recruitment and LCV maturation	(154)
	DrrA and LepB	Rab1	Trafficking of ER and Golgi-derived vesicles to LCV	(158)
<i>Chlamydia</i>	IncE/CT 116	SNX5	Modulation of endosomal membrane trafficking	(174, 175)
	?	Rab1, Rab4, Rab 11	Regulate favorable trafficking events	(156)

**Table 5.1: Mechanisms of membrane trafficking modulation by vacuole-residing bacterial pathogens** For each bacteria, the virulence factor, its targeted host factor or process, the effect on trafficking, and the reference(s) are displayed. Abbreviations: SCV, *Salmonella*-containing vacuole; CCV, *Coxiella*-containing vacuole; MCV, *Mycobacteria*-containing vacuole; LCV, *Legionella*-containing vacuole

### 5.3.1.2 Modulation of host membrane trafficking and vacuole escape

Modulation of membrane trafficking to prevent bacterial degradation and allow for vacuolar expansion is important for the establishment of a vacuolar niche. For cytosolic pathogens like *Shigella* and *Listeria*, primary vacuole escape is rapid (within minutes) and thus, the contributions of host cell trafficking events have been under appreciated. However, it is becoming increasingly evident that modulation of membrane trafficking is important for vacuole escape. Early studies showed that *Listeria* inhibited phagosome maturation and lysosomal fusion to prevent bacterial degradation prior to vacuole escape (176–178). Specifically, *Listeria* promotes the recruitment of the host small GTPase Rab5a to its vacuole and prevents its GDP exchange activity through an unknown mechanism to prevent lysosomal fusion (178). Silencing of one downstream effector of Rab5, Rabaptin-5, decreased vacuole maturation and allowed for increased LLO-independent *Listeria* vacuole escape (79), suggesting that delayed endosome maturation is advantageous for vacuole escape. Additional host endocytic and vesicular trafficking proteins were identified in a screen as being involved in the vacuole escape of *Listeria*; however, their exact roles remain to be determined (79). Interesting, the same study found that blocking several complexes involved in the later stages of vesicular trafficking, such as Class E/ESCRT complexes and Class C/B vacuolar sorting complexes involved in

lysosomal tethering, circumvented the requirement of LLO for vacuole escape (179). These results highlight an underappreciated role for host vesicular trafficking in *Listeria* vacuole escape and could suggest modulation of host membrane trafficking as a general requirement for vacuole escape of cytosolic pathogens.

Several host membrane trafficking-related proteins were identified as contributing factors to *Shigella* primary vacuole escape, including early endosomal markers (EEA1 and Rab5), sorting nexins, and endosomal markers Rab4 and Rab11 (105, 180, 181). Furthermore, Rab11-positive vesicles, which arise from infection-associated macropinosome (IAM) formation during *Shigella* invasion, were recruited to the *Shigella* primary vacuole in a manner dependent on the T3SS effector IpgD, which possesses PI(4,5)P2 phosphatase activity (105, 180). Mass-spectrometry analysis of IAMs revealed that they were enriched in several host cell small GTPases, tethering proteins, and vesicular trafficking-associated proteins (180). The authors of this study also showed that several components (Exo70, Rab8a, Rab11a, Sec5) of the exocyst complex, which facilitates the tethering of proximal vesicles during trafficking (180), are recruited to IAMs. They propose that the exocyst-mediated tethering of IAMs to the primary vacuole is required for the complete disassembly of the membrane during vacuole escape (180).

Most of what is known about modulation of membrane trafficking by cytosolic pathogens is in the context of primary vacuole escape; this concept is novel in the context of *S. flexneri* DMVs. We identified RhoA as a restrictor of IpgB1-dependent DMV escape. How RhoA restricts DMV escape remains unknown. RhoA is a well known regulator of the actin cytoskeleton, but is also emerging as a regulator of membrane trafficking (182–184). We did not see differences in actin polymerization on DMVs between wild type and *ipgB1* bacteria (Figure 3.12) and, unlike what we observed with RhoA, we did not find restoration in *ipgB1* spreading upon depletion of the major actin regulators downstream of RhoA (Figure 4.1). Therefore, we favor a model in which RhoA restricts DMV escape through membrane trafficking.

While we suggest that modulation of membrane trafficking could be a mechanism by which *S. flexneri* escapes from DMVs, many questions remain to be answered. For example, what is the nature of trafficking to DMVs? One way to address this question would be to determine if DMVs are enriched in canonical endocytic proteins, such as Rab5, Rab7, and Rab8, or with transport and recycling associated Rab proteins, including Rab1, Rab4, and Rab11. Given that RhoA pathways have been previously reported to have crosstalk with Rab proteins (184), it would also be interesting to determine if RhoA regulates the recruitment of any of these Rabs to DMVs. This could also functionally be

investigated by conducting an siRNA screen for trafficking-associated factors (Rabs, Sorting nexins, EEA1) whose depletion affects *S. flexneri* cell-to-cell spread.

### 5.3.2 LYPLA2, a host lipid-modifying enzyme exploited for DMV escape?

One of the most exciting findings of my thesis work is that host lysophospholipase II is required for efficient cell-to-cell spread through DMV escape. This is the first report of a host protein with known lipid-modifying activity being co-opted by intracellular bacteria to disrupt the vacuole membrane. LYPLA2/APT2 may directly challenge the integrity of the vacuolar membrane by removing acyl chains from either membrane lipids or lipid-modified membrane proteins. While we favor the hypothesis that LYPLA2/APT2 contributes to DMV escape through the local alteration in lipid moieties in the DMV membrane, it will be important in future studies to determine whether LYPLA2/APT2 localizes to the DMV during infection. Preliminary experiments indicate that commercially available antibodies for LYPLA2/APT2 may not be useful for visualizing LYPLA2/APT2 by immunofluorescence (data not shown). Previous studies demonstrated that, upon overexpression, LYPLA2/APT2 C-terminally tagged with fluorescent proteins localized to the Golgi (145). This fusion protein could be helpful for future studies to localize LYPLA2/APT2 during *S. flexneri* infection.

Another important question that remains is whether LYPLA2/APT2 is linked to the function of either of the T3SS effectors that we have characterized during DMV escape (IcsB, IpgB1) or whether its contributions are distinct from T3SS activity. Tracking of *icsB* and *ipgB1* mutants in either mock or LYPLA2-depleted cells as well, as localization of LYPLA2/APT2, will help to address this outstanding question.

#### **5.4 How are the inner and outer membrane dissolved? Which goes first?**

DMV escape is a complex process that requires that destabilization of two host-derived membranes (inner from the primary infected cell and outer from the newly infected cell) surrounding the bacteria (Figure 1.3). Interestingly, the two membranes of the DMV differ in their topologies with respect to the cytoplasmic-facing and extracellular-facing leaflets (Figure 1.3). The cytoplasmic-facing and extracellular-facing leaflets differ in their lipid compositions, in terms of the phospholipid fatty acid tail lengths and head group identities, as well as the distribution of cholesterol, sphingomyelin, and gangliosides (185, 186). Given these differences, disruption of the inner and outer membranes could require distinct mechanisms. Consistently, *L. monocytogenes* escape from primary (single membrane) vacuoles can be achieved in the absence of LLO through the

activity of bacterial phospholipases, while escape from DMVs following cell-to-cell spread requires the activity of LLO (82).

In *S. flexneri*, the T3SS is required for escape from both primary vacuoles and DMVs. Interestingly, IcsB is required for DMV escape, but seems to be dispensable for invasion and primary vacuole escape, as the *icsB* mutant was fully invasive (111). IpgB1 is required for invasion and/or primary vacuole escape as well DMV escape (42, 187). Uncoupling invasion and primary vacuole escape to determine if IpgB1 plays a role in primary vacuole escape would require a more sensitive assay, such as live imaging to compare differences in frequency and timing of primary vacuole escape. Nevertheless, our data suggest that at least one bacterial factor (IcsB) is uniquely required for DMV escape. However, the exact mechanism of disruption of each membrane and the respective contributions of the T3SS and IcsB and IpgB1 will require further investigation. This question could be addressed using electron microscopy to distinguish the integrity the inner and outer membranes of DMVs containing wild type, *icsB*, or *ipgB1* bacteria. Fluorescence microscopy could also potentially address this question by infecting a mixed monolayer of mb-YFP and mb-mCherry expressing cells with wild type, *icsB*, or *ipgB1* bacteria. For instance, bacteria that spread from mb-YFP to mb-mCherry cells would be encased in a DMV with a yellow inner membrane and red outer membrane and differences in

inner versus outer membrane could be measured between strains. Correlative light-electron microscopy (CLEM) could also be employed using this experimental setup and would allow for the spatial identification of DMVs by fluorescence microscopy followed by higher resolution imaging to visualize the inner and outer membranes of specific DMVs.

The T3SS has only been reported to span three membranes: two bacterial membranes and the host plasma membrane. Therefore, the T3SS would only be able to access the outer membrane of the DMV once the inner membrane is disrupted. Live imaging and tracking of cell-to-cell spread of bacteria from mb-YFP cells to mb-mCherry cells could also be used to characterize the dynamics of inner and outer membrane disruption and could provide the first experimental evidence that disruption of the inner and outer membranes of DMVs occurs sequentially. The sequential disruption of the inner and outer membranes could also be investigated using IcsB-Suntag and IpgB1-Suntag as tools to visualize translocation of effectors. Using a CLEM approach, DMVs that are enriched in or devoid of IcsB-Suntag and/or IpgB1-Suntag could be spatially identified using fluorescence microscopy, then imaged with EM to compare the states of the inner and outer membranes at the time of effector translocation.

## 5.5 Novel targets for therapeutic interventions

The ability of *S. flexneri* to spread from cell to cell is critical for its pathogenesis (23) and therefore, disruption of cell-to-cell is promising avenue for therapeutic intervention. Our work has identified multiple novel targets for potential therapeutic interventions aimed at attenuating *Shigella* infection. We have uncovered that the T3SS effector IpgB1 co-opts host protein Rac1 to antagonize RhoA during DMV escape and cell-to-cell spread. In chapter 3, we show that chemical inhibition of Rac1 using EHT 1864 lead to decreased cell-to-cell spread in HT-29 cells (Figure 3.6C). EHT 1864 could be used to limit *S. flexneri* dissemination and attenuate bacillary dysentery symptoms *in vivo*. However, given the diverse functions of Rac1 (122), global interference of Rac1 in the host is likely to lead many adverse effects. Instead, a strategy that specifically disrupts the interaction between IpgB1 and Rac1 would likely be more successful.

Another potentially targetable protein that has emerged from my studies is the host protein LYPLA2/APT2. *S. flexneri* seems to specifically target LYPLA2/APT2, as the homolog LYPLA1/APT1 was not identified as a hit in our siRNA screen. Some pharmacological inhibitors of LYPLA2/APT2 have been developed, including the specific inhibitor ML349, which potently inhibits LYPLA2/APT2 with little effect on LYPLA1/APT1 (141). Following

intraperitoneal injection in mice, ML349 was active and specific for LYPLA2/APT2 across all major tissues (141). Altering the route of administration of ML349 could mitigate potential adverse effects from global LYPLA2/APT2 inhibition. Oral administration of this compound could result in effect local LYPLA2/APT2 inhibition in colonic epithelial cells and decreased *S. flexneri* cell-to-cell spread, without widespread whole-body effects. Additional research would be required to determine the feasibility of targeting either Rac1 or LYPLA2/APT2 *in vivo* to attenuate symptoms of bacillary dysentery caused by *S. flexneri* cell-to-cell spread, but the identification of these potential therapeutic targets represents a significant advancement in the understanding of *Shigella* infection.

## 5.6 Conclusions and significance of work

The work presented here contributes significant advancements to the understanding of *S. flexneri* escape from DMVs during cell-to-cell spread. We have shown that DMV escape is a bacteria-driven process that involves the actions of two T3SS effectors, IcsB and IpgB1. Furthermore, we have implicated multiple host proteins, Rac1, RhoA, and LYPLA2/APT2 in DMV escape. Using our infant rabbit model, we demonstrated that IpgB1-mediated DMV escape is important for *S. flexneri* pathogenesis. Future studies will characterize the

contribution of IcsB-mediated DMV escape to pathogenesis. DMV escape is a critical step of cell-to-cell spread, which is essential for pathogenesis (23). Our work has identified novel targets for future therapeutic interventions aimed at attenuating *Shigella* infection. On a larger scale, this work further defines the requirements for vacuole stability versus vacuole disruption and how bacterial pathogens coopt their hosts to establish their ideal niches.

## Appendix 1: Primers pairs (name and sequence) and corresponding templates

### Primers used in Chapter 2

Cloning of pSB890-upIcsB-kan-downIcsB (to create <i>icsB</i> mutant)			
Constructed by overlapping PCR			
	Primers		Template
PCR A1	5IcsB	ACGCTTACACCTTTGTGCTTTCCGG	Wild type <i>S. flexneri</i> genomic DNA
	3IcsB-Km	CAATCCGGTGATATTCTCATTTTAGCCATACTTTAT TAACTCTCCACTTACTGG	
PCR A2	5Km-IcsB	ATTATATTTTACTGGATGAATTGTTTAGAAGGCCAT AGAAATGTGTCGCAAAC	pSB890-kan
	3Km-IcsB	GTTTGC GACACATTTCTATGGCCTTCTAAAACAATTC ATCCAGTAAAATATAAT	
PCR A3	5IcsB-Km	CCAAGTAATGGAGAGTTAATAAAGTATGGCTAAAA TGAGAATATCACCGGAATTG	Wild type <i>S. flexneri</i> genomic DNA
	3IcsB	GATGAGTATCAGGGAGAAGACAG	
PCR B	5IcsB	ACGCTTACACCTTTGTGCTTTCCGG	PCR A1+A2
	3Km-IcsB	GTTTGC GACACATTTCTATGGCCTTCTAAAACAATTC ATCCAGTAAAATATAAT	
PCR C	5IcsB	ACGCTTACACCTTTGTGCTTTCCGG	PCR B+A3
	3IcsB	GATGAGTATCAGGGAGAAGACAG	
Cloning of pBAD_IcsB			
	Primers		Template
	5IcsBEcoR1nopromoter	AATTGAATTCCACAATCACCAAGTAATGGAGAG	Wild type <i>S. flexneri</i> genomic DNA
	3IpgA Not1	AATTGCGGCCGCTTAGTTCACCTTCTGAAGTG	

### Primers used in Chapter 3

Primers pairs (name and sequence) and corresponding templates used in this study			
Cloning of pSB890-upIpgB1-kan-downIpgB1 (to create <i>ipgB1</i> mutant)			
Constructed by overlapping PCR			
	Primers		Template
PCR A1	5IpgB1_Not1	AATTGCGGCCGCTGAAAAGTGTGCTGGTATGGCAC	Wild type <i>S. flexneri</i> genomic DNA
	3IpgB1-KmR	CAATCCGGTGATATTCTCATTTTAGCCATGATACCC	

		CCTATATGTTAGTTCAC	DNA
PCR A2	5IpgB1-KmR	GTGAACTAACATATAGGGGGTATCATGGCTAAAAT GAGAATATCACCGGAATTG	pSB890-kan
	3KmR-IpgB1	TAAGTATAAGATTTAATATAAAAAGATCTAAAACAA TTCATCCAGTAAAATATAAT	
PCR A3	5KmR_IpgB1	ATTATATTTTACTGGATGAATTGTTTTAG ATCTTTTA TATTAATCTTATACTTA	Wild type <i>S. flexneri</i> genomic DNA
	3IpgB1_Blunt	CTAGGTCTTTTATTTTAGAATCTGCG	
PCR B	5IpgB1_Not1	AATTGCGGCCGCCTGAAAACCTGTGCTGGTATGGCAC	PCR A1+A2
	3KmR-IpgB1	TAAGTATAAGATTTAATATAAAAAGATCTAAAACAA TTCATCCAGTAAAATATAAT	
PCR C	5IpgB1_Not1	AATTGCGGCCGCCTGAAAACCTGTGCTGGTATGGCAC	PCR B+A3
	3IpgB1_Blunt	CTAGGTCTTTTATTTTAGAATCTGCG	
<b>Cloning of pSB890-upIpgB2-cat-downIpgB2 (to create <i>ipgB2</i> mutant)</b>			
Constructed by overlapping PCR			
	<b>Primers</b>		<b>Template</b>
PCR A1	5IpgB2up_Not 1	AATTGCGGCCGCTACTTTTATAGAAGCTGTCAGCGG C	Wild type <i>S. flexneri</i> genomic DNA
	3IpgB2-CAT prm	CTAAGGAGGATATTCATATGTATAATCACCTTGTCATG	
PCR A2	5CAT prm IpgB2	ACATGACAAGGTGATTATACATATGAATATCCTCCT TAG	pSB890- CAT
	3KmR-IpgB1	CTGTGTTCTGCACAAAACCTTATCGTGTAGGCTGGAG CTGCTTCG	
PCR A3	5IpgB2 dwn CAT	CGAAGCAGCTCCAGCCTACACGATAAGTTTTGTGCA GAACACAG	Wild type <i>S. flexneri</i> genomic DNA
	3IpgB2dwn	CTGTGTTCTGCACAAAACCTTATCGTGTAGGCTGGAG CTGCTTCG	
PCR B	5IpgB2up_Not 1	AATTGCGGCCGCTACTTTTATAGAAGCTGTCAGCGG C	PCR A1+A2
	3KmR-IpgB1	CTGTGTTCTGCACAAAACCTTATCGTGTAGGCTGGAG CTGCTTCG	
PCR C	5IpgB2up_Not 1	AATTGCGGCCGCTACTTTTATAGAAGCTGTCAGCGG C	PCR B+A3

	3IpgB2down	CTGTGTTCTGCACAAAACCTATCGTGTAGGCTGGAG CTGCTTCG	
<b>Cloning of pBAD_IpgB1</b>			
	<b>Primers</b>		<b>Template</b>
	Nhe1 IpgB1 close to start	AATTGCTAGCGTGAACATAACATATAGGGGGT	Wild type <i>S. flexneri</i> genomic DNA
	IpgB1 Rev Xba1	AATTTGTAGATTAATTTGTATTGCTTTGACGG	
<b>Cloning of pBAD_IpgB1 E80A</b>			
Constructed by overlapping PCR			
	<b>Primers</b>		<b>Template</b>
PCR A1	Nhe1 IpgB1 close to start	AATTGCTAGCGTGAACATAACATATAGGGGGT	Wild type <i>S. flexneri</i> genomic DNA
	IpgB1 E80A new rev	CATAAGTGGTTCGCGCTTGGCTC	
PCR A2	IpgB1 E80A new fwd	GAGCCAAGCGCGAACCACTTATG	Wild type <i>S. flexneri</i> genomic DNA
	IpgB1 Rev Xba1	AATTTGTAGATTAATTTGTATTGCTTTGACGG	
PCR B	Nhe1 IpgB1 close to start	AATTGCTAGCGTGAACATAACATATAGGGGGT	PCR A1+A2
	IpgB1 Rev Xba1	AATTTGTAGATTAATTTGTATTGCTTTGACGG	
<b>Cloning of pMX_RhoA-mCherry siRNA resistant (for creating stable HT-29 cell line)</b>			
Constructed by overlapping PCR			
	<b>Primers</b>		<b>Template</b>
PCR A1	Xho1 RhoA Fwd	AATTCTCGAGGGGCTGCCATCCGGAAGAACTG	pMX_GFP RhoA
	RhoA duplex 2-res rev	CTGCTTCCATCCACCTCAATATCGGCAACGTAGT TTCAAACACTGTGGGCAC	
PCR A2	RhoA duplex 2-res fwd	GTGCCACAGTGTGGAAACTACGTTGCCGATA TTGAGGTGGATGGAAAGCAG	pMX_GFP RhoA
	RhoA Not1 rev	TTAAGCGCCGCTCACAAGACAAGGCACCCAG	
PCR B	Xho1 RhoA Fwd	AATTCTCGAGGGGCTGCCATCCGGAAGAACTG	PCR A1+A2
	RhoA Not1 rev	TTAAGCGCCGCTCACAAGACAAGGCACCCAG	

## References

1. Musher DM, Musher BL. 2004. Contagious acute gastrointestinal infections. *N Engl J Med* 351:2417–2427.
2. Khalil IA, Troeger C, Blacker BF, Rao PC, Brown A, Atherly DE, Brewer TG, Engmann CM, Houpt ER, Kang G, Kotloff KL, Levine MM, Luby SP, MacLennan CA, Pan WK, Pavlinac PB, Platts-Mills JA, Qadri F, Riddle MS, Ryan ET, Shoultz DA, Steele AD, Walson JL, Sanders JW, Mokdad AH, Murray CJL, Hay SI, Reiner Jr RC. 2018. Morbidity and mortality due to shigella and enterotoxigenic *Escherichia coli* diarrhoea: the Global Burden of Disease Study 1990–2016. *Lancet Infect Dis.* 18:1229–1240.
3. Kotloff KL, Blackwelder WC, Nasrin D, Nataro JP, Farag TH, van Eijk A, Adegbola RA, Alonso PL, Breiman RF, Faruque ASG, Saha D, Sow SO, Sur D, Zaidi AKM, Biswas K, Panchalingam S, Clemens JD, Cohen D, Glass RI, Mintz ED, Sommerfelt H, Levine MM. 2012. The Global Enteric Multicenter Study (GEMS) of diarrheal disease in infants and young children in developing countries: epidemiologic and clinical methods of the case/control study. *Clin Infect Dis.* 4:S232-45.
4. Kotloff KL, Nataro JP, Blackwelder WC, Nasrin D, Farag TH, Panchalingam S, Wu Y, Sow SO, Sur D, Breiman RF, Faruque AS, Zaidi AK, Saha D, Alonso PL, Tamboura B, Sanogo D, Onwuchekwa U, Manna B, Ramamurthy T, Kanungo S, Ochieng JB, Omoro R, Oundo JO, Hossain A, Das SK, Ahmed S, Qureshi S, Quadri F, Adegbola RA, Antonio M, Hossain MJ, Akinsola A, Mandomando I, Nhampossa T, Acácio S, Biswas K, O'Reilly CE, Mintz ED, Berkeley LY, Muhsen K, Sommerfelt H, Robins-Browne RM, Levine MM. 2013. Burden and aetiology of diarrhoeal disease in infants and young children in developing countries (the Global Enteric Multicenter Study, GEMS): a prospective, case-control study. *Lancet* 382:209–222.
5. Liu J, Platts-Mills JA, Juma J, Kabir F, Nkeze J, Okoi C, Operario DJ, Uddin J, Ahmed S, Alonso PL, Antonio M, Becker SM, Blackwelder WC, Breiman RF, Faruque ASG, Fields B, Gratz J, Haque R, Hossain A, Hossain MJ, Jarju S, Qamar F, Iqbal NT, Kwambana B, Mandomando I, McMurry TL, Ochieng C, Ochieng JB, Ochieng M, Onyango C, Panchalingam S, Kalam A, Aziz F, Qureshi S, Ramamurthy T, Roberts JH, Saha D, Sow SO, Stroup SE, Sur D, Tamboura B, Taniuchi M, Tennant SM, Toema D, Wu Y, Zaidi A, Nataro JP, Kotloff KL, Levine MM, Houpt ER. 2016. Use of quantitative molecular diagnostic methods to identify causes of diarrhoea in children: a reanalysis of the GEMS case-control study. *Lancet* 388:1291–1301.
6. Kotloff KL, Riddle MS, Platts-Mills JA, Pavlinac P, Zaidi AKM. 2018.

- Shigellosis. *Lancet* 391:801–812.
7. Connor TR, Barker CR, Baker KS, Weill F-X, Talukder KA, Smith AM, Baker S, Gouali M, Thanh DP, Azmi IJ. 2015. Species-wide whole genome sequencing reveals historical global spread and recent local persistence in *Shigella flexneri*. *Elife* 4:e07335.
  8. Agaisse H. 2015. *Shigella flexneri* serotype 3a: the rise of a superbug. *Lancet Infect Dis* 15:867–868.
  9. Mani S, Wierzba T, Walker RI. 2016. Status of vaccine research and development for *Shigella*. *Vaccine* 34:2887–2894.
  10. Shaughnessy HJ, Olsson RC. 1946. Experimental human bacillary dysentery; polyvalent dysentery vaccine in its prevention. *J Am Med Assoc* 132:362–368.
  11. Kotloff KL, Nataro JP, Losonsky GA, Wasserman SS, Hale TL, Taylor DN, Sadoff JC, Levine MM. 1995. A modified *Shigella* volunteer challenge model in which the inoculum is administered with bicarbonate buffer: clinical experience and implications for *Shigella* infectivity. *Vaccine* 13:1488–1494.
  12. Porter CK, Thura N, Ranallo RT, Riddle MS. 2013. The *Shigella* human challenge model. *Epidemiol Infect* 141:223–232.
  13. Takeuchi A, Sprinz H, LaBrec E, Formal S. 1968. Experimental bacillary dysentery. An electron microscopic study of the response of the intestinal mucosa to bacterial invasion. *Am J Pathol* 52:503–529.
  14. Freter R. 1956. Experimental enteric *Shigella* and *Vibrio* infections in mice and guinea pigs. *J Exp Med* 104:411–418.
  15. Sereny B. 1957. Experimental keratoconjunctivitis shigellosa. *Acta Microbiol Acad Sci Hung* 4:367–376.
  16. Voino-Yasenetsky M V, Voino-Yasenetskaya MK. 1962. Experimental pneumonia caused by bacteria of the *Shigella* group. *Acta Morphol Acad Sci Hung* 11:439–454.
  17. Perdomo OJ, Cavaillon JM, Huerre M, Ohayon H, Gounon P, Sansonetti PJ. 1994. Acute inflammation causes epithelial invasion and mucosal destruction in experimental shigellosis. *J Exp Med* 180:1307–1319.
  18. Sansonetti PJ, Arondel J, Huerre M, Harada A, Matsushima K. 1999. Interleukin-8 controls bacterial transepithelial translocation at the cost of epithelial destruction in experimental shigellosis. *Infect Immun* 67:1471–1480.
  19. Sansonetti PJ, Arondel J, Cavaillon JM, Huerre M. 1995. Role of interleukin-1 in the pathogenesis of experimental shigellosis. *J Clin Invest* 96:884–892.
  20. Shim D-H, Suzuki T, Chang S-Y, Park S-M, Sansonetti PJ, Sasakawa C, Kweon M-N. 2007. New animal model of shigellosis in the Guinea pig: its

- usefulness for protective efficacy studies. *J Immunol* 178:2476–2482.
21. Mitchell PS, Roncaioli JL, Turcotte EA, Goers L, Chavez RA, Lee AY, Lesser CF, Rauch I, Vance RE. 2020. NAIP-NLRC4-deficient mice are susceptible to shigellosis. *Elife* 9.
  22. Kuehl CJ, D’Gama JD, Warr AR, Waldor MK, Sperandio V. 2020. An Oral Inoculation Infant Rabbit Model for *Shigella* Infection. *MBio* 11:e03105-19.
  23. Yum LK, Byndloss MX, Feldman SH, Agaisse H. 2019. Critical role of bacterial dissemination in an infant rabbit model of bacillary dysentery. *Nat Commun* 10:1826.
  24. Labrec EH, Schneider H, Magnani TJ, Formal SB. 1964. Epithelial cell penetration as an essential step in the pathogenesis of bacillary dysentery. *J Bacteriol* 88:1503–18.
  25. Jin Q, Yuan Z, Xu J, Wang Y, Shen Y, Lu W, Wang J, Liu H, Yang J, Yang F, Zhang X, Zhang J, Yang G, Wu H, Qu D, Dong J, Sun L, Xue Y, Zhao A, Gao Y, Zhu J, Kan B, Ding K, Chen S, Cheng H, Yao Z, He B, Chen R, Ma D, Qiang B, Wen Y, Hou Y, Yu J. 2002. Genome sequence of *Shigella flexneri* 2a: insights into pathogenicity through comparison with genomes of *Escherichia coli* K12 and O157. *Nucleic Acids Res* 30:4432–4441.
  26. Mattock E, Blocker AJ. 2017. How Do the Virulence Factors of *Shigella* Work Together to Cause Disease? *Front Cell Infect Microbiol* 7:64.
  27. Muthuramalingam M, Whittier SK, Picking WL, Picking WD. 2021. The *Shigella* Type III Secretion System: An Overview from Top to Bottom. *Microorganisms* 9.
  28. Ogawa M, Handa Y, Ashida H, Suzuki M, Sasakawa C. 2008. The versatility of *Shigella* effectors. *Nat Rev Microbiol* 6:11–16.
  29. Henderson IR, Czczulin J, Eslava C, Noriega F, Nataro JP. 1999. Characterization of pic, a secreted protease of *Shigella flexneri* and enteroaggregative *Escherichia coli*. *Infect Immun* 67:5587–5596.
  30. Navarro-Garcia F, Gutierrez-Jimenez J, Garcia-Tovar C, Castro LA, Salazar-Gonzalez H, Cordova V. 2010. Pic, an autotransporter protein secreted by different pathogens in the Enterobacteriaceae family, is a potent mucus secretagogue. *Infect Immun*. 78:4101–4109.
  31. Haider K, Hossain A, Wanke C, Qadri F, Ali S, Nahar S. 1993. Production of mucinase and neuraminidase and binding of *Shigella* to intestinal mucin. *J Diarrhoeal Dis Res* 11:88–92.
  32. Sansonetti PJ, Phalipon A. 1999. M cells as ports of entry for enteroinvasive pathogens: mechanisms of interaction, consequences for the disease process. *Semin Immunol* 11:193–203.
  33. Carayol N, Tran Van Nhieu G. 2013. The inside story of *Shigella* invasion of intestinal epithelial cells. *Cold Spring Harb Perspect Med* 3:a016717.

34. Sakaguchi T, Köhler H, Gu X, McCormick BA, Reinecker H-C. 2002. *Shigella flexneri* regulates tight junction-associated proteins in human intestinal epithelial cells. *Cell Microbiol* 4:367–381.
35. Cossart P, Sansonetti PJ. 2004. Bacterial invasion: the paradigms of enteroinvasive pathogens. *Science* 304:242–248.
36. Blocker A, Gounon P, Larquet E, Niebuhr K, Cabiaux V, Parsot C, Sansonetti P. 1999. The tripartite type III secretin of *Shigella flexneri* inserts IpaB and IpaC into host membranes. *J Cell Biol* 147:683–693.
37. Russo BC, Stamm LM, Raaben M, Kim CM, Kahoud E, Robinson LR, Bose S, Queiroz AL, Herrera BB, Baxt LA, Mor-Vaknin N, Fu Y, Molina G, Markovitz DM, Whelan SP, Goldberg MB. 2016. Intermediate filaments enable pathogen docking to trigger type 3 effector translocation. *Nat Microbiol* 1:16025.
38. Chen P, Russo BC, Duncan-Lowey JK, Bitar N, Egger KT, Goldberg MB. 2021. Topology and Contribution to the Pore Channel Lining of Plasma Membrane-Embedded *Shigella flexneri* Type 3 Secretion Translocase IpaB. *MBio* 12:e0302121.
39. Russo BC, Duncan JK, Wiscovitch AL, Hachey AC, Goldberg MB. 2019. Activation of *Shigella flexneri* type 3 secretion requires a host-induced conformational change to the translocon pore. *PLoS Pathog* 15:e1007928.
40. Russo BC, Duncan-Lowey JK, Chen P, Goldberg MB. 2021. The type 3 secretion system requires actin polymerization to open translocon pores. *PLoS Pathog* 17:e1009932.
41. Alto NM, Shao F, Lazar CS, Brost RL, Chua G, Mattoo S, McMahon SA, Ghosh P, Hughes TR, Boone C, Dixon JE. 2006. Identification of a bacterial type III effector family with G protein mimicry functions. *Cell* 124:133–145.
42. Ohya K, Handa Y, Ogawa M, Suzuki M, Sasakawa C. 2005. IpgB1 is a novel *Shigella* effector protein involved in bacterial invasion of host cells: Its activity to promote membrane ruffling via Rac1 and Cdc42 activation. *J Biol Chem* 280:24022–24034.
43. Hachani A, Biskri L, Rossi G, Marty A, Ménard R, Sansonetti P, Parsot C, Van Nhieu GT, Bernardini ML, Allaoui A. 2008. IpgB1 and IpgB2, two homologous effectors secreted via the Mxi-Spa type III secretion apparatus, cooperate to mediate polarized cell invasion and inflammatory potential of *Shigella flexneri*. *Microbes Infect* 10:260–268.
44. Handa Y, Suzuki M, Ohya K, Iwai H, Ishijima N, Koleske AJ, Fukui Y, Sasakawa C. 2007. *Shigella* IpgB1 promotes bacterial entry through the ELMO-Dock180 machinery. *Nat Cell Biol* 9:121–128.
45. Izard T, Tran Van Nhieu G, Bois PRJ. 2006. *Shigella* applies molecular mimicry to subvert vinculin and invade host cells. *J Cell Biol* 175:465–475.

46. Niebuhr K, Jouihri N, Allaoui A, Gounon P, Sansonetti PJ, Parsot C. 2000. IpgD, a protein secreted by the type III secretion machinery of *Shigella flexneri*, is chaperoned by IpgE and implicated in entry focus formation. *Mol Microbiol* 38:8–19.
47. Schuch R, Sandlin RC, Maurelli AT. 1999. A system for identifying post-invasion functions of invasion genes: requirements for the Mxi-Spa type III secretion pathway of *Shigella flexneri* in intercellular dissemination. *Mol Microbiol* 34:675–689.
48. Grundling A, Gonzalez MD, Higgins DE. 2003. Requirement of the *Listeria monocytogenes* broad-range phospholipase PC-PLC during infection of human epithelial cells. *J Bacteriol* 185:6295–6307.
49. Dupont N, Lacas-Gervais S, Bertout J, Paz I, Freche B, Van Nhieu GT, van der Goot FG, Sansonetti PJ, Lafont F. 2009. *Shigella* Phagocytic Vacuolar Membrane Remnants Participate in the Cellular Response to Pathogen Invasion and Are Regulated by Autophagy. *Cell Host Microbe* 6:137–149.
50. Kreibich S, Emmenlauer M, Fredlund J, Dehio C, Enninga J, Hardt WD, Rämö P, Münz C, Dehio C, Enninga J, Hardt WD. 2015. Autophagy proteins promote repair of endosomal membranes damaged by the *Salmonella* type three secretion system 1. *Cell Host Microbe* 18:527–537.
51. Campbell-Valois FX, Sachse M, Sansonetti PJ, Parsot C. 2015. Escape of actively secreting *shigella flexneri* from ATG8/LC3-Positive vacuoles formed during cell-to-cell spread is facilitated by IcsB and VirA. *MBio* 6:1–11.
52. Kumar Y, Valdivia RH. 2008. Actin and intermediate filaments stabilize the *Chlamydia trachomatis* vacuole by forming dynamic structural scaffolds. *Cell Host Microbe* 4:159–169.
53. Méresse S, Unsworth KE, Habermann A, Griffiths G, Fang F, Martínez-Lorenzo MJ, Waterman SR, Gorvel JP, Holden DW. 2001. Remodelling of the actin cytoskeleton is essential for replication of intravacuolar *Salmonella*. *Cell Microbiol* 3:567–577.
54. Ehsani S, Santos JC, Rodrigues CD, Henriques R, Audry L, Zimmer C, Sansonetti P, Tran Van Nhieu G, Enninga J. 2012. Hierarchies of host factor dynamics at the entry site of *Shigella flexneri* during host cell invasion. *Infect Immun* 80:2548–2557.
55. Kühn S, Bergqvist J, Gil M, Valenzuela C, Barrio L, Lebreton S, Zurzolo C, Enninga J. 2020. Actin Assembly around the *Shigella*-Containing Vacuole Promotes Successful Infection. *Cell Rep* 31:107638.
56. Makino S, Sasakawa C, Kamata K, Kurata T, Yoshikawa M, Makino, Sasakawa, Kamata, Kurata Y. 1986. A genetic determinant required for continuous reinfection of adjacent cells on large plasmid in *S. flexneri* 2a.

- Cell 46:551–555.
57. Bernardini ML, Mounier J, D'Hauteville H, Coquis-Rondon M, Sansonetti PJ. 1989. Identification of *icsA*, a plasmid locus of *Shigella flexneri* that governs bacterial intra- and intercellular spread through interaction with F-actin. *Proc Natl Acad Sci U S A* 86:3867–3871.
  58. Egile C, Loisel TP, Laurent V, Li R, Pantaloni D, Sansonetti PJ, Carlier M. 1999. Protein Promotes Actin Nucleation by Arp2 / 3 Complex and Bacterial. *J Cell Biol* 146:1319–1332.
  59. Egile C, Loisel TP, Laurent V, Li R, Pantaloni D, Sansonetti PJ, Carlier M-F. 1999. Activation of the Cdc42 Effector N-Wasp by the *Shigella flexneri* Icsa Protein Promotes Actin Nucleation by Arp2/3 Complex and Bacterial Actin-Based Motility. *J Cell Biol* 146:1319–1332.
  60. Mauricio RPM, Jeffries CM, Svergun DI, Deane JE. 2017. The *Shigella* Virulence Factor IcsA Relieves N-WASP Autoinhibition by Displacing the Verprolin Homology/Cofilin/Acidic (VCA) Domain. *J Biol Chem*. 292:134–145.
  61. Leung Y, Ally S, Goldberg MB. 2008. Bacterial Actin Assembly Requires Toca-1 to Relieve N-WASP Autoinhibition. *Cell Host Microbe* 3:39–47.
  62. Dragoi A-M, Talman AM, Agaisse H. 2013. Bruton's tyrosine kinase regulates *Shigella flexneri* dissemination in HT-29 intestinal cells. *Infect Immun* 81:598–607.
  63. Burton EA, Oliver TN, Pendergast AM. 2005. Abl kinases regulate actin comet tail elongation via an N-WASP-dependent pathway. *Mol Cell Biol* 25:8834–8843.
  64. Mimuro H, Suzuki T, Suetsugu S, Miki H, Takenawa T, Sasakawa C. 2000. Profilin Is Required for Sustaining Efficient Intra- and Intercellular Spreading of *Shigella flexneri*. *J Biol Chem* 275:28893–28901.
  65. Michard C, Yum LK, Agaisse H. 2019. WIPF2 promotes *Shigella flexneri* actin-based motility and cell-to-cell spread. *Cell Microbiol* 21:e13098.
  66. Steinhauer J, Agha R, Pham T, Varga AW, Goldberg MB. 1999. The unipolar *Shigella* surface protein IcsA is targeted directly to the bacterial old pole: IcsP cleavage of IcsA occurs over the entire bacterial surface. *Mol Microbiol* 32:367–377.
  67. Fukumatsu M, Ogawa M, Arakawa S, Suzuki M, Nakayama K, Shimizu S, Kim M, Mimuro H, Sasakawa C. 2012. *Shigella* targets epithelial tricellular junctions and uses a noncanonical clathrin-dependent endocytic pathway to spread between cells. *Cell Host Microbe* 11:325–336.
  68. Kim M, Ogawa M, Fujita Y, Yoshikawa Y, Nagai T, Koyama T, Nagai S, Lange A, Fässler R, Sasakawa C. 2009. Bacteria hijack integrin-linked kinase to stabilize focal adhesions and block cell detachment. *Nature*

- 459:578–582.
69. Miura M, Terajima J, Izumiya H, Mitobe J, Komano T, Watanabe H. 2006. OspE2 of *Shigella sonnei* is required for the maintenance of cell architecture of bacterium-infected cells. *Infect Immun* 74:2587–2595.
  70. Fattouh R, Kwon H, Czuczman MA, Copeland JW, Pelletier L, Quinlan ME, Muise AM, Higgins DE, Brumell JH. 2015. The Diaphanous-Related Formins Promote Protrusion Formation and Cell-to-Cell Spread of *Listeria monocytogenes*. *J Infect Dis* 211:1185–1195.
  71. Heindl JE, Saran I, Yi C, Lesser CF, Goldberg MB. 2010. Requirement for Formin-Induced Actin Polymerization during Spread of *Shigella flexneri*. *Infect Immun* 78:193–203.
  72. Bishai EA, Sidhu GS, Li W, Dhillon J, Bohil AB, Cheney RE, Hartwig JH, Southwick FS. 2013. Myosin-X facilitates *Shigella*-induced membrane protrusions and cell-to-cell spread. *Cell Microbiol* 15:353–367.
  73. Duncan-Lowey JK, Wiscovitch AL, Wood TE, Goldberg MB, Russo BC. 2020. *Shigella flexneri* Disruption of Cellular Tension Promotes Intercellular Spread. *Cell Rep* 33:108409.
  74. Dragoi A-MM, Agaisse H. 2015. The class II phosphatidylinositol 3-phosphate kinase PIK3C2A promotes *Shigella flexneri* dissemination through formation of vacuole-like protrusions. *Infect Immun* 83:1695–1704.
  75. Dragoi A-MM, Agaisse H. 2014. The Serine/Threonine Kinase STK11 Promotes *Shigella flexneri* Dissemination through Establishment of Cell-Cell Contacts Competent for Tyrosine Kinase Signaling. *Infect Immun* 82:4447–4457.
  76. Kuehl CJ, Dragoi A-MM, Agaisse HH. 2014. The *shigella flexneri* type 3 secretion system is required for tyrosine kinase-dependent protrusion resolution, and vacuole escape during bacterial dissemination. *PLoS One* 9:e112738.
  77. Köseoğlu VK, Jones MK, Agaisse H. 2022. The type 3 secretion effector IpgD promotes *S. flexneri* dissemination. *PLoS Pathog* 18:e1010324.
  78. Gedde MM, Higgins DE, Tilney LG, Portnoy DA. 2000. Role of Listeriolysin O in Cell-to-Cell Spread of *Listeria monocytogenes*. *Infect Immun* 68:999–1003.
  79. Burrack LS, Harper JW, Higgins DE. 2009. Perturbation of vacuolar maturation promotes listeriolysin O-independent vacuolar escape during *Listeria monocytogenes* infection of human cells. *Cell Microbiol* 11:1382–1398.
  80. Marquis H, Hager EJ. 2000. pH-regulated activation and release of a bacteria-associated phospholipase C during intracellular infection by *Listeria monocytogenes*. *Mol Microbiol* 35:289–298.

81. Alvarez DE, Agaisse H. 2016. The Metalloprotease Mpl Supports *Listeria monocytogenes* Dissemination through Resolution of Membrane Protrusions into Vacuoles. *Infect Immun* 84:1806–1814.
82. Christine A-S, R. GK, E. HD. 2006. Differential function of *Listeria monocytogenes* listeriolysin O and phospholipases C in vacuolar dissolution following cell-to-cell spread. *Cell Microbiol* 9:179–195.
83. Cemma M, Brumell JH. 2012. Interactions of Pathogenic Bacteria with Autophagy Systems. *Curr Biol* 22:R540–R545.
84. Ogawa M, Yoshimori T, Suzuki T, Sagara H, Mizushima N, Sasakawa C. 2005. Escape of intracellular *Shigella* from Autophagy. *Science* 307:727–731.
85. Pankiv S, Clausen TH, Lamark T, Brech A, Bruun JA, Outzen H, Øvervatn A, Bjørkøy G, Johansen T. 2007. p62/SQSTM1 binds directly to Atg8/LC3 to facilitate degradation of ubiquitinated protein aggregates by autophagy. *J Biol Chem* 282:24131–24145.
86. Mostowy S, Sancho-Shimizu V, Hamon MA, Simeone R, Brosch R, Johansen T, Cossart P. 2011. p62 and NDP52 proteins target intracytosolic *Shigella* and *Listeria* to different autophagy pathways. *J Biol Chem* 286:26987–26995.
87. Thurston TLM. 2009. The tbk1 adaptor and autophagy receptor ndp52 restricts the proliferation of ubiquitin-coated bacteria. *Nat Immunol* 10:1215–1222.
88. Kraft C, Peter M, Hofmann K. 2010. Selective autophagy: Ubiquitin-mediated recognition and beyond. *Nat Cell Biol* 12:836–841.
89. He C, Klionsky DJ. 2009. Regulation Mechanisms and Signalling Pathways of Autophagy. *Annu Rev Genet* 43:67.
90. Kabeya Y. 2000. LC3, a mammalian homologue of yeast Apg8p, is localized in autophagosome membranes after processing. *EMBO J* 19:5720–5728.
91. Xie Z, Nair U, Klionsky DJ. 2008. Atg8 controls phagophore expansion during autophagosome formation. *Mol Biol Cell* 19:290–298.
92. Huang J, Brumell JH. 2014. Bacteria–autophagy interplay: a battle for survival. *Nat Rev Microbiol* 12:101.
93. Martinez J, Malireddi RKS, Lu Q, Cunha LD, Pelletier S, Gingras S, Orchard R, Guan J-L, Tan H, Peng J, Kanneganti T-D, Virgin HW, Green DR. 2015. Molecular characterization of LC3-associated phagocytosis (LAP) reveals distinct roles for Rubicon, NOX2, and autophagy proteins. *Nat Cell Biol* 17:893–906.
94. Kageyama S, Omori H, Saitoh T, Sone T, Guan J-L, Akira S, Imamoto F, Noda T, Yoshimori T. 2011. The LC3 recruitment mechanism is separate from Atg9L1-dependent membrane formation in the autophagic response against *Salmonella*. *Mol Biol Cell* 22:2290–2300.

95. Mitchell G, Cheng MI, Chen C, Nguyen BN, Whiteley AT, Kianian S, Cox JS, Green DR, McDonald KL, Portnoy DA. 2017. *Listeria monocytogenes* triggers noncanonical autophagy upon phagocytosis, but avoids subsequent growth-restricting xenophagy. *Proc Natl Acad Sci* 9:115(2):E210-E217.
96. Kubori T, Bui XT, Hubber A, Nagai H. 2017. Legionella RavZ Plays a Role in Preventing Ubiquitin Recruitment to Bacteria-Containing Vacuoles. *Front Cell Infect Microbiol* 7:1–9.
97. Bernal-Bayard J, Ramos-Morales F. 2017. Molecular Mechanisms Used by Salmonella to Evade the Immune System. *Curr Issues Mol Biol* 25:133–168.
98. Ogawa M, Suzuki T, Tatsuno I, Abe H, Sasakawa C. 2003. IcsB, secreted via the type III secretion system, is chaperoned by IpgA and required at the post-invasion stage of Shigella pathogenicity. *Mol Microbiol* 48:913–931.
99. Allaoui A, Mounier J, Prévost MC, Sansonetti PJ, Parsot C. 1992. icsB: a Shigella flexneri virulence gene necessary for the lysis of protrusions during intercellular spread. *Mol Microbiol* 6:1605–1616.
100. Kissler S, Stern P, Takahashi K, Hunter K, Peterson LB, Wicker LS. 2006. In vivo RNA interference demonstrates a role for Nramp1 in modifying susceptibility to type 1 diabetes. *Nat Genet* 38:479.
101. Baxt LA, Goldberg MB. 2014. Host and Bacterial Proteins That Repress Recruitment of LC3 to Shigella Early during Infection. *PLoS One* 9:e94653.
102. Kayath CA, Hussey S, El hajjami N, Nagra K, Philpott D, Allaoui A. 2010. Escape of intracellular Shigella from autophagy requires binding to cholesterol through the type III effector, IcsB. *Microbes Infect* 12:956–966.
103. Pei J, Grishin N V. 2009. The Rho GTPase inactivation domain in Vibrio cholerae MARTX toxin has a circularly permuted papain-like thiol protease fold. *Proteins* 77:413–419.
104. Dong N, Zhu Y, Lu Q, Hu L, Zheng Y, Shao F. 2012. Structurally distinct bacterial TBC-like GAPs link Arf GTPase to Rab1 inactivation to counteract host defenses. *Cell* 150:1029–1041.
105. Mellouk N, Weiner A, Aulner N, Schmitt C, Elbaum M, Shorte SLL, Danckaert A, Enninga J. 2014. Shigella subverts the host recycling compartment to rupture its vacuole. *Cell Host Microbe* 16:517–530.
106. Birmingham CL, Smith AC, Bakowski MA, Yoshimori T, Brumell JH. 2006. Autophagy controls Salmonella infection in response to damage to the Salmonella-containing vacuole. *J Biol Chem* 281:11374–11383.
107. Mansilla Pareja ME, Bongiovanni A, Lafont F, Colombo MI. 2017. Alterations of the Coxiella burnetii Replicative Vacuole Membrane Integrity and Interplay with the Autophagy Pathway. *Front Cell Infect Microbiol* 7:1–17.

108. Ménard R, Prévost MC, Gounon P, Sansonetti P, Dehio C. 1996. The secreted Ipa complex of *Shigella flexneri* promotes entry into mammalian cells. *Proc Natl Acad Sci U S A* 93:1254–1258.
109. Agaisse H. 2016. Molecular and Cellular Mechanisms of *Shigella flexneri* Dissemination. *Front Cell Infect Microbiol* 6:1–10.
110. Weddle E, Agaisse H. 2018. Principles of intracellular bacterial pathogen spread from cell to cell. *PLoS Pathog* 14:e1007380–e1007380.
111. Weddle E, Agaisse H. 2018. Spatial, temporal and functional assessment of LC3-dependent autophagy in *Shigella flexneri* dissemination. *Infect Immun* 86.
112. Liu W, Zhou Y, Peng T, Zhou P, Ding X, Li Z, Zhong H, Xu Y, Chen S, Hang HC, Shao F. 2018. N $\epsilon$ -fatty acylation of multiple membrane-associated proteins by *Shigella* IcsB effector to modulate host function. *Nat Microbiol*.
113. Alto NM, Dixon JEBT-M in E. 2008. Analysis of Rho-GTPase Mimicry by a Family of Bacterial Type III Effector Proteins. *In Small GTPases in Disease, Part B*.
114. Huang Z, Sutton SE, Wallenfang AJ, Orchard RC, Wu X, Feng Y, Chai J, Alto NM. 2009. Structural insights into host GTPase isoform selection by a family of bacterial GEF mimics. *Nat Struct Mol Biol* 16:1922–2013.
115. Weigele BA, Orchard RC, Jimenez A, Cox GW, Alto NM. 2017. A systematic exploration of the interactions between bacterial effector proteins and host cell membranes. *Nat Commun* 8:532.
116. Ehrlich JS, Hansen MDH, Nelson WJ. 2002. Spatio-Temporal Regulation of Rac1 Localization and Lamellipodia Dynamics during Epithelial Cell-Cell Adhesion. *Dev Cell* 3:259–270.
117. Bulgin R, Raymond B, Garnett JA, Frankel G, Crepin VF, Berger CN, Arbeloa A. 2010. Bacterial Guanine Nucleotide Exchange Factors SopE-Like and WxxxE Effectors . *Infect Immun* 78:1417–1425.
118. Short B. 2016. Rac and Rho compete to cooperate. *J Cell Biol* 215:433.
119. Machacek M, Hodgson L, Welch C, Elliott H, Pertz O, Nalbant P, Abell A, Johnson GL, Hahn KM, Danuser G. 2009. Coordination of Rho GTPase activities during cell protrusion. *Nature*. 461:99–103.
120. Martin E, Ouellette M-H, Jenna S. 2016. Rac1/RhoA antagonism defines cell-to-cell heterogeneity during epidermal morphogenesis in nematodes. *J Cell Biol* 215:483–498.
121. Chauhan BK, Lou M, Zheng Y, Lang RA. 2011. Balanced Rac1 and RhoA activities regulate cell shape and drive invagination morphogenesis in epithelia. *Proc Natl Acad Sci U S A* 108:18289–18294.
122. Nguyen LK, Kholodenko BN, von Kriegsheim A. 2018. Rac1 and RhoA:

- Networks, loops and bistability. *Small GTPases*. 9:316–321.
123. Bolado-Carrancio A, Rukhlenko OS, Nikonova E, Tsyganov MA, Wheeler A, Garcia-Munoz A, Kolch W, von Kriegsheim A, Kholodenko BN. 2020. Periodic propagating waves coordinate RhoGTPase network dynamics at the leading and trailing edges during cell migration. *Elife* 9.
  124. Bustos RI, Forget M-A, Settleman JE, Hansen SH. 2008. Coordination of Rho and Rac GTPase function via p190B RhoGAP. *Curr Biol* 18:1606–1611.
  125. Barac A, Basile J, Vázquez-Prado J, Gao Y, Zheng Y, Gutkind JS. 2004. Direct interaction of p21-activated kinase 4 with PDZ-RhoGEF, a G protein-linked Rho guanine exchange factor. *J Biol Chem* 279:6182–6189.
  126. Olayioye MA, Noll B, Hausser A. 2019. Spatiotemporal Control of Intracellular Membrane Trafficking by Rho GTPases. *Cells* 8:1478.
  127. Nishimura Y, Itoh K, Yoshioka K, Ikeda K, Himeno M. 2002. A role for small GTPase RhoA in regulating intracellular membrane traffic of lysosomes in invasive rat hepatoma cells. *Histochem J* 34:189–213.
  128. Anand I, Choi W, Isberg RR. 2020. The vacuole guard hypothesis: how intravacuolar pathogens fight to maintain the integrity of their beloved home. *Curr Opin Microbiol* 54:51–58.
  129. Aguilera M, Salinas R, Rosales E, Carminati S, Colombo MI, Berón W. 2009. Actin dynamics and Rho GTPases regulate the size and formation of parasitophorous vacuoles containing *Coxiella burnetii*. *Infect Immun* 77:4609–4620.
  130. Weber MM, Faris R, van Schaik EJ, McLachlan JT, Wright WU, Tellez A, Roman VA, Rowin K, Case EDR, Luo Z-Q, Samuel JE. 2016. The Type IV Secretion System Effector Protein CirA Stimulates the GTPase Activity of RhoA and Is Required for Virulence in a Mouse Model of *Coxiella burnetii* Infection. *Infect Immun* 84:2524–2533.
  131. Kolodziejek AM, Altura MA, Fan J, Petersen EM, Cook M, Brzovic PS, Miller SI. 2019. Salmonella Translocated Effectors Recruit OSBP1 to the Phagosome to Promote Vacuolar Membrane Integrity. *Cell Rep* 27:2147-2156.e5.
  132. LaRock DL, Brzovic PS, Levin I, Blanc M-P, Miller SI. 2012. A Salmonella typhimurium-translocated Glycerophospholipid:Cholesterol Acyltransferase Promotes Virulence by Binding to the RhoA Protein Switch Regions. *J Biol Chem* 287:29654–29663.
  133. Kolodziejek AM, Miller SI. 2015. Salmonella modulation of the phagosome membrane, role of SseJ. *Cell Microbiol* 17:333–341.
  134. Christen M, Coye LH, Hontz JS, LaRock DL, Pfuetzner RA, Megha, Miller SI. 2009. Activation of a Bacterial Virulence Protein by the GTPase RhoA. *Sci Signal* 2:ra71 LP-ra71.

135. André G, Sandoval JE, Retailleau K, Loufrani L, Toumaniantz G, Offermanns S, Rolli-Derkinderen M, Loirand G, Sauzeau V. 2014. Smooth muscle specific Rac1 deficiency induces hypertension by preventing p116RIP3-dependent RhoA inhibition. *J Am Heart Assoc* 3:e000852.
136. Bagci H, Sriskandarajah N, Robert A, Boulais J, Elkholi IE, Tran V, Lin Z-Y, Thibault M-P, Dubé N, Faubert D, Hipfner DR, Gingras A-C, Côté J-F. 2020. Mapping the proximity interaction network of the Rho-family GTPases reveals signalling pathways and regulatory mechanisms. *Nat Cell Biol* 22:120–134.
137. Maldonado-Contreras A, Birtley JR, Boll E, Zhao Y, Mumy KL, Toscano J, Ayehunie S, Reinecker H-C, Stern LJ, McCormick BA. 2017. *Shigella* depends on SepA to destabilize the intestinal epithelial integrity via cofilin activation. *Gut Microbes*. 8:544–560.
138. Schrader M, Kamoshita M, Islinger M. 2020. Organelle interplay-peroxisome interactions in health and disease. *J Inherit Metab Dis*. 43:71–89.
139. Wepy JA, Galligan JJ, Kingsley PJ, Xu S, Goodman MC, Tallman KA, Rouzer CA, Marnett LJ. 2019. Lysophospholipases cooperate to mediate lipid homeostasis and lysophospholipid signaling. *J Lipid Res*. 60:360–374.
140. Won SJ, Cheung See Kit M, Martin BR. 2018. Protein depalmitoylases. *Crit Rev Biochem Mol Biol*. 53:83–98.
141. Adibekian A, Martin BR, Chang JW, Hsu K-L, Tsuboi K, Bachovchin DA, Speers AE, Brown SJ, Spicer T, Fernandez-Vega V, Ferguson J, Hodder PS, Rosen H, Cravatt BF. 2012. Confirming target engagement for reversible inhibitors in vivo by kinetically tuned activity-based probes. *J Am Chem Soc* 134:10345–10348.
142. Manna JD, Wepy JA, Hsu K-L, Chang JW, Cravatt BF, Marnett LJ. 2014. Identification of the major prostaglandin glycerol ester hydrolase in human cancer cells. *J Biol Chem* 289:33741–33753.
143. Kong E, Peng S, Chandra G, Sarkar C, Zhang Z, Bagh MB, Mukherjee AB. 2013. Dynamic palmitoylation links cytosol-membrane shuttling of acyl-protein thioesterase-1 and acyl-protein thioesterase-2 with that of proto-oncogene H-ras product and growth-associated protein-43. *J Biol Chem* 288:9112–9125.
144. Stypulkowski E, Asangani IA, Witze ES. 2018. The depalmitoylase APT1 directs the asymmetric partitioning of Notch and Wnt signaling during cell division. *Sci Signal* 11.
145. Abrami L, Audagnotto M, Ho S, Marcaida MJ, Mesquita FS, Anwar MU, Sandoz PA, Fonti G, Pojer F, Dal Peraro M, van der Goot FG. 2021. Palmitoylated acyl protein thioesterase APT2 deforms membranes to

- extract substrate acyl chains. *Nat Chem Biol* 17:438–447.
146. Page AL, Ohayon H, Sansonetti PJ, Parsot C. 1999. The secreted IpaB and IpaC invasins and their cytoplasmic chaperone IpgC are required for intercellular dissemination of *Shigella flexneri*. *Cell Microbiol* 1:183–193.
  147. Resh MD. 2016. Fatty acylation of proteins: The long and the short of it. *Prog Lipid Res* 63:120–131.
  148. Tom CTMB, Martin BR. 2013. Fat chance! Getting a grip on a slippery modification. *ACS Chem Biol* 8:46–57.
  149. van Meer G, Voelker DR, Feigenson GW. 2008. Membrane lipids: where they are and how they behave. *Nat Rev Mol Cell Biol* 9:112–124.
  150. Akeda Y, Galán JE. 2005. Chaperone release and unfolding of substrates in type III secretion. *Nature* 437:911–915.
  151. Singh MK, Zangoui P, Yamanaka Y, Kenney LJ. 2021. Genetic code expansion enables visualization of *Salmonella* type three secretion system components and secreted effectors. *Elife* 10:e67789.
  152. Tanenbaum ME, Gilbert LA, Qi LS, Weissman JS, Vale RD. 2014. A protein-tagging system for signal amplification in gene expression and fluorescence imaging. *Cell* 159:635–646.
  153. Anand IS, Choi W, Isberg RR. 2020. Components of the endocytic and recycling trafficking pathways interfere with the integrity of the *Legionella*-containing vacuole. *Cell Microbiol* 22:e13151.
  154. Gaspar AH, Machner MP. 2014. VipD is a Rab5-activated phospholipase A1 that protects *Legionella pneumophila* from endosomal fusion. *Proc Natl Acad Sci* 111:4560 LP – 4565.
  155. Stein M-P, Müller MP, Wandinger-Ness A. 2012. Bacterial pathogens commandeer Rab GTPases to establish intracellular niches. *Traffic* 13:1565–1588.
  156. Rzomp KA, Scholtes LD, Briggs BJ, Whittaker GR, Scidmore MA. 2003. Rab GTPases Are Recruited to Chlamydial Inclusions in Both a Species-Dependent and Species-Independent Manner. *Infect Immun* 71:5855 LP – 5870.
  157. Heinzen RA, Scidmore MA, Rockey DD, Hackstadt T. 1996. Differential interaction with endocytic and exocytic pathways distinguish parasitophorous vacuoles of *Coxiella burnetii* and *Chlamydia trachomatis*. *Infect Immun* 64:796–809.
  158. Mishra AK, Del Campo CM, Collins RE, Roy CR, Lambright DG. 2013. The *Legionella pneumophila* GTPase activating protein LepB accelerates Rab1 deactivation by a non-canonical hydrolytic mechanism. *J Biol Chem* 288:24000–24011.
  159. Vergne I, Chua J, Deretic V. 2003. Tuberculosis Toxin Blocking Phagosome

- Maturation Inhibits a Novel Ca<sup>2+</sup>/Calmodulin-PI3K hVPS34 Cascade . *J Exp Med* 198:653–659.
160. Mallo G V, Espina M, Smith AC, Terebiznik MR, Alemán A, Finlay BB, Rameh LE, Grinstein S, Brumell JH. 2008. SopB promotes phosphatidylinositol 3-phosphate formation on Salmonella vacuoles by recruiting Rab5 and Vps34 . *J Cell Biol* 182:741–752.
  161. Hernandez LD, Hueffer K, Wenk MR, Galán JE. 2004. Salmonella Modulates Vesicular Traffic by Altering Phosphoinositide Metabolism. *Science* 304:1805 LP – 1807.
  162. Steele-Mortimer O, Méresse S, Gorvel JP, Toh BH, Finlay BB. 1999. Biogenesis of Salmonella typhimurium-containing vacuoles in epithelial cells involves interactions with the early endocytic pathway. *Cell Microbiol* 1:33–49.
  163. Méresse S, Steele-Mortimer O, Finlay BB, Gorvel J-P. 1999. The rab7 GTPase controls the maturation of Salmonella typhimurium-containing vacuoles in HeLa cells. *EMBO J* 18:4394–4403.
  164. Brumell JH, Kujat-Choy S, Brown NF, Vallance BA, Knodler LA, Finlay BB. 2003. SopD2 is a Novel Type III Secreted Effector of Salmonella typhimurium That Targets Late Endocytic Compartments Upon Delivery Into Host Cells. *Traffic* 4:36–48.
  165. D’Costa VM, Braun V, Landekic M, Shi R, Proteau A, McDonald L, Cygler M, Grinstein S, Brumell JH. 2015. Salmonella Disrupts Host Endocytic Trafficking by SopD2-Mediated Inhibition of Rab7. *Cell Rep* 12:1508–1518.
  166. McEwan DG, Richter B, Claudi B, Wigge C, Wild P, Farhan H, McGourty K, Coxon FP, Franz-Wachtel M, Perdu B, Akutsu M, Habermann A, Kirchof A, Helfrich MH, Odgren PR, Van Hul W, Frangakis AS, Rajalingam K, Macek B, Holden DW, Bumann D, Dikic I. 2015. PLEKHM1 Regulates Salmonella-Containing Vacuole Biogenesis and Infection. *Cell Host Microbe* 17:58–71.
  167. McGourty K, Thurston TL, Matthews SA, Pinaud L, Mota LJ, Holden DW. 2012. Salmonella Inhibits Retrograde Trafficking of Mannose-6-Phosphate Receptors and Lysosome Function. *Science* 338:963 LP – 967.
  168. Dumont A, Boucrot E, Drevensek S, Daire V, Gorvel J-P, Poüs C, Holden DW, Méresse S. 2010. SKIP, the Host Target of the Salmonella Virulence Factor SifA, Promotes Kinesin-1-Dependent Vacuolar Membrane Exchanges. *Traffic* 11:899–911.
  169. Sindhwani A, Arya SB, Kaur H, Jagga D, Tuli A, Sharma M. 2017. Salmonella exploits the host endolysosomal tethering factor HOPS complex to promote its intravacuolar replication. *PLOS Pathog* 13:e1006700.

170. Weber MM, Faris R, van Schaik EJ, Samuel JE. 2018. Identification and characterization of arginine finger-like motifs, and endosome-lysosome basolateral sorting signals within the *Coxiella burnetii* type IV secreted effector protein CirA. *Microbes Infect* 20:302–307.
171. Romano PS, Gutierrez MG, Berón W, Rabinovitch M, Colombo MI. 2007. The autophagic pathway is actively modulated by phase II *Coxiella burnetii* to efficiently replicate in the host cell. *Cell Microbiol* 9:891–909.
172. Vergne I, Chua J, Lee H-H, Lucas M, Belisle J, Deretic V. 2005. Mechanism of phagolysosome biogenesis block by viable *Mycobacterium tuberculosis*. *Proc Natl Acad Sci U S A* 102:4033 LP – 4038.
173. Roberts EA, Chua J, Kyei GB, Deretic V. 2006. Higher order Rab programming in phagolysosome biogenesis. *J Cell Biol* 174:923–929.
174. Paul B, Kim HS, Kerr MC, Huston WM, Teasdale RD, Collins BM. 2017. Structural basis for the hijacking of endosomal sorting nexin proteins by *Chlamydia trachomatis*. *Elife* 6:e22311.
175. Mirrashidi KM, Elwell CA, Verschueren E, Johnson JR, Frando A, Von Dollen J, Rosenberg O, Gulbahce N, Jang G, Johnson T, Jäger S, Gopalakrishnan AM, Sherry J, Dunn JD, Olive A, Penn B, Shales M, Cox JS, Starnbach MN, Derre I, Valdivia R, Krogan NJ, Engel J. 2015. Global Mapping of the Inc-Human Interactome Reveals that Retromer Restricts *Chlamydia* Infection. *Cell Host Microbe* 18:109–121.
176. Alvarez-Dominguez C, Roberts R, Stahl PD. 1997. Internalized *Listeria monocytogenes* modulates intracellular trafficking and delays maturation of the phagosome. *J Cell Sci* 6:731–743.
177. Alvarez-Dominguez C, Barbieri AM, Berón W, Wandinger-Ness A, Stahl PD. 1996. Phagocytosed live *Listeria monocytogenes* influences Rab5-regulated in vitro phagosome-endosome fusion. *J Biol Chem* 271:13834–13843.
178. Prada-Delgado A, Carrasco-Marín E, Peña-Macarro C, Del Cerro-Vadillo E, Fresno-Escudero M, Leyva-Cobián F, Alvarez-Dominguez C. 2005. Inhibition of Rab5a exchange activity is a key step for *Listeria monocytogenes* survival. *Traffic* 6:252–265.
179. Cheng LW, Viala JPM, Stuurman N, Wiedemann U, Vale RD, Portnoy DA. 2005. Use of RNA interference in *Drosophila* S2 cells to identify host pathways controlling compartmentalization of an intracellular pathogen. *Proc Natl Acad Sci U S A* 102:13646–13651.
180. Chang Y-Y, Stévenin V, Duchateau M, Gai Gianetto Q, Hourdel V, Rodrigues CD, Matondo M, Reiling N, Enninga J. 2020. *Shigella* hijacks the exocyst to cluster macropinosomes for efficient vacuolar escape. *PLoS Pathog* 16:e1008822.

181. Weiner A, Mellouk N, Lopez-Montero N, Chang YY, Souque C, Schmitt C, Enninga J. 2016. Macropinosomes are Key Players in Early *Shigella* Invasion and Vacuolar Escape in Epithelial Cells. *PLoS Pathog* 12:1–24.
182. Ridley AJ. 2001. Rho proteins: linking signaling with membrane trafficking. *Traffic* 2:303–310.
183. Ridley AJ. 2006. Rho GTPases and actin dynamics in membrane protrusions and vesicle trafficking. *Trends Cell Biol* 16:522–529.
184. Shibata S, Teshima Y, Niimi K, Inagaki S. 2019. Involvement of ARHGEF10, GEF for RhoA, in Rab6/Rab8-mediating membrane traffic. *Small GTPases* 10:169–177.
185. Bucci M. 2013. Leaflets out of order. *Nat Chem Biol* 9:67.
186. Ingólfsson HI, Melo MN, van Eerden FJ, Arnarez C, Lopez CA, Wassenaar TA, Periolo X, de Vries AH, Tieleman DP, Marrink SJ. 2014. Lipid Organization of the Plasma Membrane. *J Am Chem Soc* 136:14554–14559.
187. Weddle EA, Köseoğlu VK, DeVasure BA, Agaisse HF. 2022. The type three secretion system effector protein IpgB1 promotes *Shigella flexneri* cell-to-cell spread through double-membrane vacuole escape. *PLoS Pathog* 18:e1010380.